CONFERENCE

Organized by the International University of Sarajevo

INTERNATIONAL CONFERENCE ON ELECTRICAL ENGINEERING AND COMPUTER SCIENCE

May 1-4, 2019

Sarajevo, Bosnia and Herzegovina

Book of Proceedings

INTERNATIONAL UNIVERSITY OF SARAJEVO

INTERNATIONAL CONFERENCE ON ELECTRICAL ENGINEERING AND COMPUTER SCIENCE

INTERNATIONAL
UNIVERSITY OF SARAJEVO

CONFERENCE SPONSORS

Platinium Sponsor

aselsan

"Proven Technology"

ASELSAN A.Ş. is a Turkish Armed Forces Foundation company.

HAVELSAN

INTERNATIONAL UNIVERSITY OF SARAJEVO

2004

IUS

INTERNATIONAL UNIVERSITY OF SARAJEVO

SEDEF

BOSNIA

CONFERENCE ORGANIZERS

General Chair:
Taha Imeci
International University of Sarajevo

Technical Program Chairs:
Tarik Namas
International University of Sarajevo

Finance Chair:
Ibrahim Inal
International University of Sarajevo

Local Arrangements Chair:
Senad Hodzic
International University of Sarajevo

Conference Secretariat:
Adnan Beganovic
International University of Sarajevo

Website Administrator:
Osman Gursoy
International University of Sarajevo

Designer:
Emir Isovic
International University of Sarajevo

Content

Blockchain Based E-Voting

Doğa Barış Çakmak
Applied Informatics
Istanbul Technical University
Istanbul, Turkey
cakmakdo@itu.edu.tr

Ertuğrul Karaçuha
Applied Informatics
Istanbul Technical University
Istanbul, Turkey
karacuhae@itu.edu.tr

***Abstract*—Humanity has used elections as a decision-making mechanism since they began to live as a community. With the development of technology, election system technologies have evolved. It is expected that it will comply with democratic criteria when designing electoral systems. The election systems that are widely used today have disadvantages in various aspects. Blockchain technology, which increases its importance day by day, has the features that will change the processes in many areas. It is generally associated with digital money because of its successful practices in the financial field. But the potential of this technology is far beyond that. In this study, a model suitable for modern and democratic criteria is presented by utilizing the benefits of blockchain technology.**

Keywords-blockchain; e-voting; blockchain based e-voting

I. INTRODUCTION

The election is the way in which a specific community vote by means of voting by the public authorities, or the acceptance or rejection of political proposals. Although elections were held in Ancient Greece and Rome, the origins of the elections in the modern world emerge as the gradual selection of representative governments in Europe and North America, starting in the 17th century (1). The methods used in the modern world are paper ballots, lever voting machines, punched card voting, optical mark-sense voting, direct recording electronic voting, and online voting (2). Traditional methods are used worldwide for many years. On the other hand, electronic-based applications have been implemented in recent years. The first country-wide internet election system, where citizens used their national identity cards over the Internet, was used by Estonia for municipal elections in 2005. Similarly, Norway used the remote electronic electoral system in 2011 in country council elections (3).

Blockchain can be considered as a distributed digital registry, which is constantly updated by countless users, is almost impossible to corrupt, and can be viewed by all users involved in the network, keeping all transactions from past to present. Bitcoin, which can be considered as the first version of the activated blockchain technology, was mentioned by Satoshi Nakamoto on October 31, 2008, in a technical paper titled Bitcoin: A peer-to-peer electronic cash system (4).

In the following part of this paper, the requirements of a democratic and modern electoral system have been revealed. Then, a blockchain based electronic election model has been developed to satisfy the requirements. While creating the model, auxiliary models were used in areas where blockchain technology was inadequate. At the end of the paper, conclusions and recommendations are presented.

II. ELECTION REQUIREMENTS

Election processes are carried out by countries or institutions in a system by determining the laws/rules. These rules determine the requirements of the electoral system be implemented and set the standards for the whole process. Each country or institution sets its own laws/rules for the electoral processes, which makes it difficult to establish a set of universal election standards. However, when the studies of laws, practices and related institutions are examined, generally agreed and universal election standards can be determined.

The Republic of Turkey, 298 on the second article of the law is subject election principles. According to this article (5); elections shall be held in accordance with the principles of free, equal and one suffrage, the voter marks the ballot itself, the vote is given in secrecy, counting, casting, and processing of the votes are made explicitly.

In 2006, the Commonwealth of Independent States, published by the European Commission for Democracy Through Law, Venice Commission, stated the requirements for election standards and electoral processes (6). The items that are relevant and agreed on the electoral systems are universal suffrage, equal voting rights, secret ballot, clear and transparent elections. According to these articles; every citizen has the right to vote and has the right to vote equally. Voters may vote invalid. Voters must have equal access to voting. The votes are hidden and used without any pressure. Elections should be clear and transparent.

The following standards and recommendations regarding the voting are set out in the Using International Election Standards prepared by the Council of Europe (7); confidentiality should be ensured during the entire voting process and in particular during the voting, extra voting and any control over the vote of another elector must be prohibited, voting centers should be accessible to disabled voters and their designs should be appropriate.

As a result, a well-designed electoral system can be considered as follows; ensuring that all voters have equal and one voting right, prevention of voting by proxy, secret

balloting, equality of access to all voters, monitoring of an open and transparent method in counting and processing of votes, the election results cannot be tracked until the voting process is over, finding a backup of the votes and re-counting, no change can be made on ballot papers, be audible and reliable.

III. BLOCKCHAIN BASED E-VOTING MODEL

In developing a blockchain based e-voting model, election requirements, actors in the election process, the duties and responsibilities of the actors and the performance criteria that the blockchain technology should provide are taken into account. The model consists of three stages: Installation, Voting, Counting of Votes and Announcement of Results.

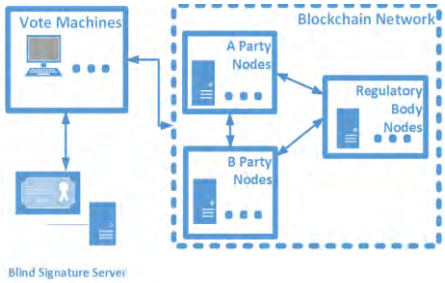

Fig. 1. Blockchain voting topology.

A. Installation

At this stage, the regulatory institution installs the blockchain network. Some of the nodes in the blockchain network will be owned by the regulatory authority, while others will be owned by political parties. In this way, every political party that joins the election will have a say in the approval of the vote together with the regulatory body. At this point, any actor should be careful not to reach the number of nodes that would jeopardize the integrity of the network. For example, if BFT is chosen as a consensus model, it should be ensured that any actor's node ownership rate never exceeds %33 (8).

B. Voting

At this stage, votes are given. First, the voter goes to the ballot box and the officer in charge gives him the public key in a closed envelope that he will use to encrypt the vote. Then he heads to the voting machine. It first reads the identity card and determines whether the voter has the right to vote. When determining the right to vote, whether or not to vote before by reading from the chain. He then re-authenticates himself with biometric data. Two-step verification with biometric data prevents proxy voting. He then marks the vote and machine reads the given public key. At this point, the vote is encrypted with this public key. The voter can check whether the vote is counted after voting with the same public key. The next step is the confirmation with the blind signature.

C. Counting of Votes and Announcement of Results

The last stage is the counting of votes and the announcement of the results. This stage starts after the voting process is over. First, it starts with revealing the corresponding private key pairs of public keys that voters have used to encrypt their votes when voting. These key pairs are held in the blockchain. A rule is added to the smart contract to secure these keys. According to this rule, after the voting process, the relevant keys can be read. The votes that have been encrypted are resolved by the corresponding private key used in the encryption and the actual values are read. At this stage, voters can check whether their votes are counted by a client application provided by the regulatory body. After the actual values of the votes are resolved, the counting of votes begins. After the vote counting process is completed, the candidates / political parties who win the election according to the rules specified by the law are determined and announced. The rules do not need to be executed through smart contracts. According to the values of the votes can be carried out by the regulatory agency. The values of the votes can be provided in a blockchain network because it is clearly visible to all participants.

IV. CONCLUSION AND RECOMMENDATIONS

In this study, a blockchain based electronic election system has been developed. By using the features of blockchain technology, the model that will provide the election requirements has been shown. Cryptographic methods such as blind signature were used in areas where blockchain technology was inadequate. In this way, a reliable and transparent model that provides election requirements has been introduced.

A. Suggestions

The presented model is very safe due to the advantages of blockchain technology. However, this situation involves the processes after the votes are written to the chain. The security of the client machines in the model is the biggest problem. In future studies, standards can be established to ensure that these machines are reliable.

The backup of the votes is available on all nodes that are joined to the network. Therefore, technically no other backup is needed, but it is unlikely for the public and stakeholders to fully understand the blockchain technology. In this case, the confidence in the proposed model may be reduced. In order to prevent this, digitally signed voting papers by the voting machines can also be included in the election process.

Tens of millions of voters vote in the general elections. This number may also rise to hundreds of millions in some countries. It is important to make sure that blockchain technology can handle this heavy throughput load. Performance criteria can be determined in future studies and it can be investigated whether blockchain technology can provide these criteria.

REFERENCES

[1] Eulau, H., Gibbins, R., & Webb, P. D. (22 January 2015). Election. Retrieve 08 November 2018, from https://www.britannica.com/topic/election-political-science.

[2] Jones, D. W. (2003). The evaluation of voting technology. Secure electronic voting (pp. 3-16). Springer, Boston, MA.

[3] Ayed, A. B. (2017). A conceptual secure blockchain-based electronic voting system. International Journal of Network Security & Its Applications, 9(3), 01-09.

[4] Nakamoto, S. (2008). Bitcoin: A peer-to-peer electronic cash system.

[5] Seçimlerin Temel Hükümleri Ve Seçmen Kütükleri Hakkinda Kanun. Retrieved November 10, 2018, from Mevzuat: http://www.mevzuat.gov.tr/MevzuatMetin/1.4.298.pdf.

[6] Strasbourg, (22 January 2007) European Commission for Democracy Through Law (Venice Commission), Opinion No. 399 / 2006.

[7] Council of Europe. (2016). Using international election standards: Council of Europe handbook for civil society organizations. Strasbourg: Council of Europe Publishing. (p.82)

[8] Yu, B., Liu, J. K., Sakzad, A., Nepal, S., Steinfeld, R., Rimba, P., & Au, M. H. (2018, September). Platform-independent secure blockchain-based voting system. In International Conference on Information Security(pp. 369-386). Springer, Cham

Sheath Helix in a Metallic Envelope

Ahsan Altaf, Hassan Sajjad, Sana Khan, and Ercumend Arvas
Electrical-Electronics Engineering Department, Istanbul Medipol University, Istanbul, Turkey.
Email: aaltaf@st.medipol.edu.tr

***Abstract*— An exact analytical solution is presented for the problem of electromagnetic transmission by a sheath helix surrounded by a perfectly conducting envelope. The region between the sheath and the envelope is filled with a homogeneous dielectric. Computed results are the axial propagation constant (β) and the field distributions. These exact results are compared with approximate results in the literature which assume identical radial wavenumber (γ) for the region inside and outside the sheath. As expected, the difference between our results and the approximate results in the literature becomes important when the dielectric constant of dielectric is large.**

***Keywords*— Traveling wave tubes, sheath helix, slow wave structure.**

I. INTRODUCTION

Slow wave structures (SWSs) are among the primary components of traveling wave tubes (TWTs). TWTs have been extensively studied [1] – [4]. Practical helix design poses a complex electromagnetic problem. Sheath helices are an approximation of actual helices. It is a circular cylindrical surface of negligible thickness with infinite conductivity in the winding direction and zero conductivity perpendicular to the winding direction.

II. METHODOLOGY

Figure 1 shows geometry of the sheath helix enclosed in a metal envelope. In this study, we are interested in electromagnetic waves propagating in the *z*-direction. That is, the field phasors vary as $e^{-j\beta z}$, where β is the axial propagation constant. The total field can be written as the sum of a TM and a TE field. We therefore let

$$E_z = A_n I_n(\gamma r) e^{-j\beta z} e^{jn\phi} + B_n K_n(\gamma r) e^{-j\beta z} e^{jn\phi} \quad (1)$$

where the I_n and K_n are the modified Bessel functions of the first and second kinds, respectively. The orders *n* of these functions is taken to be an integer because the whole $0 < \phi < 2\pi$ region is included in the field space.

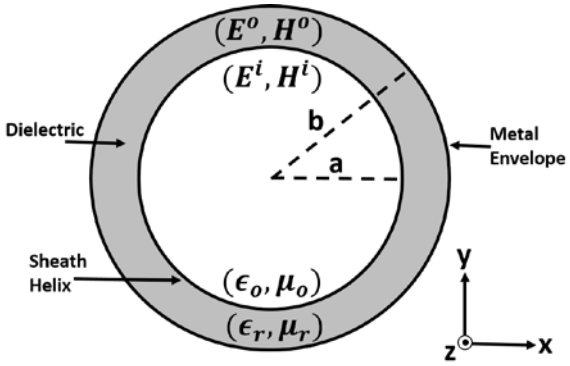

Fig. 1: The original problem.

Inside the sheath helix, the coefficient B_n must be zero because K_n

is unbounded at $r = 0$. The *z*-component of the electric and magnetic fields for the region inside ($0 < r < a$) and outside ($a < r < b$) the helix for $n = 0$ are as follows.

$$E_z^i = A_o I_o(\gamma_i r) e^{-j\beta z} \quad (2)$$

$$E_z^o = [C_o I_o(\gamma_o r) + D_o K_o(\gamma_o r)] e^{-j\beta z} \quad (3)$$

$$H_z^i = B_o I_o(\gamma_i r) e^{-j\beta z} \quad (4)$$

$$H_z^o = [E_o I_o(\gamma_o r) + F_o K_o(\gamma_o r)] e^{-j\beta z} \quad (5)$$

$$\gamma_i^2 = \beta^2 - k_i^2 \quad (6)$$

$$\gamma_o^2 = \beta^2 - k_o^2 \quad (7)$$

where $k_i = \omega\sqrt{\varepsilon_o \mu_o}$, $k_o = k_i\sqrt{\varepsilon_r}$. The superscript *o* refers to region outside the sheath, the superscript *i* refers to region inside the sheath, *a* is the radius of the helix, and *b* is the radius of the metal envelope. The radial propagation constant inside and outside the helix is denoted by γ_i and γ_o, respectively. Other field components can be written in terms of *z*-component of the

fields. In literature [4], γ is assumed to be the same for the interior and exterior regions of the helix ($\gamma_i = \gamma_o = \gamma$) but in general the radial propagation constant should

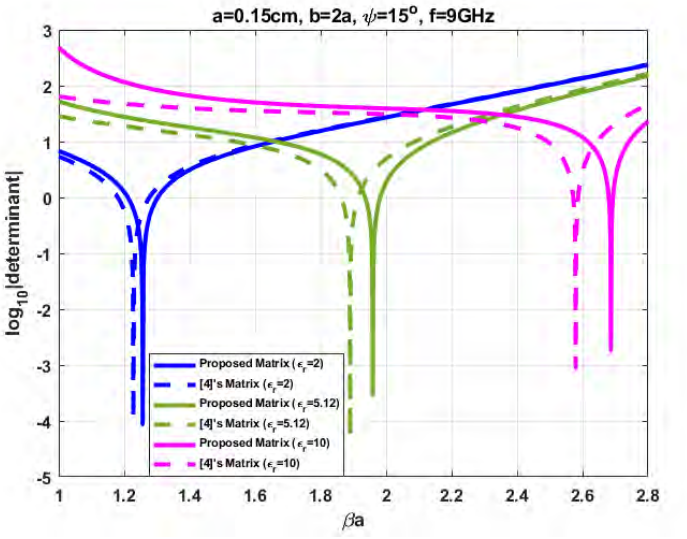

Fig. 3: Propagation constants for different dielectrics.

be different in the two regions. The boundary conditions at the helix and dielectric interface ($r = a$) are given by

$$E_{||}^{i} = 0 \qquad (8)$$

$$E_{||}^{o} = 0 \qquad (9)$$

$$H_{||}^{i} = H_{||}^{o} \qquad (10)$$

$$E_{z}^{i} = E_{z}^{o} \qquad (11)$$

and at the metallic envelope ($r = b$), they are;

$$E_{z}^{o} = 0 \qquad (12)$$

$$E_{\phi}^{o} = 0 \qquad (13)$$

The fields in (8) - (10) are parallel to winding direction. Using the above six boundary conditions, we obtained six homogeneous equations for the six unknowns.

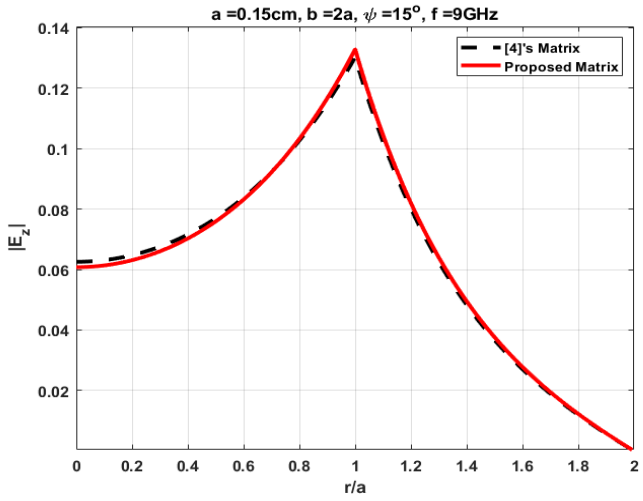

Fig. 4: z-component of electric field.

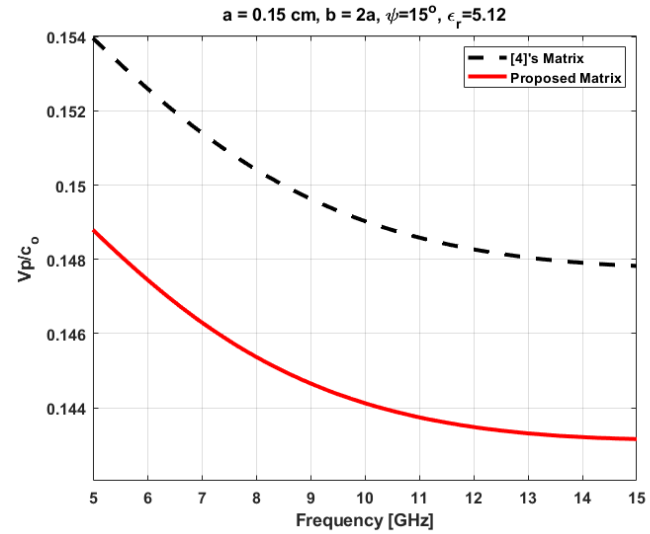

Fig. 2: Comparison of phase velocity for $\epsilon_r = 5.12$.

III. Results and Discussions

By solving the equations, various parameters such as propagation constant, electric field components, and phase velocity are computed. The result for different values of dielectric constant is computed and compared with the literature [4]. From Fig. 2 it is observed that the difference in the value of β is large if the value of the dielectric constant is high. The z-component of the electric field is shown in Fig. 3. The comparison of the phase velocity for $\epsilon_r = 5.12$ with the available literature [4] is shown in Fig. 4. More results will be presented during the conference.

IV. Conclusion

A sheath helix enclosed in a metal envelope is studied. Axial propagation constant, phase velocity, and field distribution are computed and compared with published literature. It is observed that for high dielectric constants the difference in β values is high which results in a considerable change in the phase velocity and hence the performance of the SWS.

References

[1] J. R. Pierce, Traveling Wave Tubes, Van Nostrand, 1950.

[2] A. S. Gilmour, Jr., Klystrons, Traveling Wave Tubes, Magnetrons, Crossed-Field Amplifiers, and Gyrotrons, Artech House, 2011.

[3] Dean A. Watkins, Topics in Electromagnetic Theory, John Wiley, 1958.

[4] B. N. Basu, Electromagnetic Theory and Applications in Beam-Wave Electronics, World Scientific Publishing Co., 1996.

Analysis of Road Accidents using Machine Learning Techniques

Lamija Herceg
Department of Electrical and Electronics Engineering
International University of Sarajevo
Sarajevo, Bosnia and Herzegovina
lamija_1995@live.com

Emine Yaman
Department of Computer Science and Engineering
International University of Sarajevo
Sarajevo, Bosnia and Herzegovina
eyaman@ius.edu.ba

***Abstract*— Road accidents are a major cause of human injuries and fatalities. Their analysis helps to increase the awareness of traffic security importance. In this paper useful information has been extracted from two road accident datasets, sourced from Fatality Analysis Reporting System in the United States of America, using data mining techniques. Naïve Bayes and C4.5 Decision Tree techniques were applied to form several predictions. Studious examination was performed on majority of the factors that affect road accidents, i.e. human factors and environmental factors. The goal of the research is to try to improve safety and reduce hazards on the roads.**

Keywords—road accidents, FARS, injury severity, fatality, data mining, machine learning, classification, Naïve Bayes, C4.5 Decision Tree

I. INTRODUCTION

Accidents are one of the biggest public health threats in the world [1]. It is estimated by World Health Organization that 1.2 million deaths and 50 million injuries worldwide are caused by road traffic accidents each year. The cost of these deaths and injuries has a tremendous impact on the social and economic development of a location or country [2]. Hence, attempts to improve travels' safety and to reduce hazards of road accidents through development and application of traffic safety programs are essential tasks. What is still considered by the traffic experts is to identify the factors affecting the incidence or severity of an occurred crash [3]. Road accidents occur as the result of one, or more than one of the following factors:

- Human factors
- Vehicle factors
- Road and environment factors

Human factors are described as that which the person did, or did not do at the time of the accident. Vehicle factors refer to design or mechanical faults of a vehicle. Road environment factors include all aspects of road design and maintenance, construction work, weather conditions and problems with signage and lighting [4]. Road safety of the 21st century has become a matter of complexity, apart from some residual extreme cases showing atypical accident patterns [5].

Data-led diagnosis plays a pivotal role in achieving a sustainable road safety improvement and addressing several road safety management problems [6]. Most of the road accident data analysis are done by the data mining processes such as feature selection, clustering and classification to identify factors that affect the severity of an accident [7]. Applying data mining techniques to model traffic accident data records can help to understand the characteristics of drivers' behavior, roadway condition and weather condition that are causally connected with different injury severity. These can help decision-makers to formulate better traffic safety control policies [8]. Data mining has been defined as the non-trivial extraction of previously unknown, implicit and potentially useful information from data. Via mining the data of road traffic accident, we can analyze accident distinctiveness in multiangles, multi-level and more comprehensive way, and discover potential for reduction of accidents [9]. There are a number of Data Mining classification algorithms available (like a Random tree, C4.5, Random forest, CART and Naïve Bayes) to predict the target class by analyzing the training dataset to get better boundary conditions which can be used to determine each target class [10].

The classification algorithms require reliable source of dataset in order to make trustworthy predictions. One of such sources is National Highway Traffic Safety Administration (NHTSA). One of the primary objectives of the NHTSA is to reduce the staggering human toll and property damage that motor vehicle traffic crashes impose on our society. Accurate data are required to support the development, implementation, and assessment of highway safety programs aimed at reducing this toll. NHTSA uses data from many sources, including the Fatality Analysis Reporting System (FARS). Providing data about crashes, the FARS is used to identify highway safety problem areas, provide a basis for regulatory and consumer information initiatives, and form the basis for cost and benefit analyses of highway safety initiatives [11].

The endeavor of this study is to investigate the performance of classification methods using machine learning techniques. Besides that, the goal is to make predictions of the future events and to hopefully increase awareness of the importance of traffic participants' behavior.

II. Literature Review

This section discusses various studies which have been conducted to emphasize the use of classification algorithms and feature selection in predicting factors that cause road accidents.

ID3 Decision Tree technique that predicts causes of accidents and accident prone locations on highways has been presented in [12]. Using machine learning algorithms to analyze accident data collected on Lagos-Ibadan road, it was found that Decision Tree can accurately predict the causes of accidents and accident prone locations along the road.

In [13], it has been revealed that the accuracy of Naïve Bayes classifier performed better than various Decision Tree algorithms, and hence, Naïve Bayes algorithm can act as an optimal algorithm for the accident prediction system. It proved to be optimal when lesser attributes are utilized.

The crash data from the records in [14] was used to study hundreds of drivers who were involved in traffic crashes on the main two-lane two-way rural roads of Iran. The results indicated that seat belt is the most important factor associated with injury severity of traffic crashes and not using it significantly increases the probability of being injured or killed.

Some researchers studied the relationship between drivers' age, gender, vehicle mass, impact speed or driving speed measure with fatalities [15, 16].

III. Materials and Methods

According to the National Highway Traffic Safety Administration, 30,000 deaths in the USA are caused by automobile accidents annually. Oftentimes fatalities occur due to a number of factors such as driver carelessness, speed of operation, impairment due to alcohol or drugs, and road environment. Some studies suggest that car crashes are solely due to driver factors, while other studies suggest car crashes are due to a combination of roadway and driver factors [17]. The majority of the possible causes are investigated through datasets.

Two real-world datasets that are related to each other were used in the research for the sake of greater statistical power and comparison. The datasets are retrieved from two public data sources: Knowledge Extraction based on Evolutionary Learning (KEEL) and Open Data Soft. Both of these datasets originate from FARS data system, which is designed and developed by NHTSA's National Center for Statistics and Analysis. The data was collected from the 50 U.S. states for one year period.

The first dataset contains 99,759 instances described by 14 attributes (all of them being nominal. This dataset emphasizes the effect of human factor on road accidents. The class attribute describes the severity of the injury with the degrees of its intensity as:

- no injury
- possible injury
- non-incapacitating injury
- incapacitating injury
- fatal injury.

The attributes of the first dataset are listed in Table I. Majority of them show who the person is or what the person did or did not do at the time of the accident, so they are human related.

TABLE I. Attributes of the first dataset

Dataset 1 (Human factor)
1. State
2. Gender
3. Person Type
4. Seating Position
5. Restraint
6. Air Bag
7. Ejection
8. Extrication
9. Alcohol Involvement
10. Alcohol Test
11. Hispanic Origin
12. Taken to Hospital
13. Race
14. Class

The second dataset contains 32,166 instances described by 10 attributes (9 nominal and 1 numeric). This dataset emphasizes the effect of environmental factors on road accidents. The class attribute provides the information about the number of fatalities by numbers starting from 1 to 10.

The attributes of the second dataset are shown in Table II. Some of them represent the weather conditions and some represent the period at which the accident happened, which is why they are environment related.

TABLE II. Attributes of the second dataset

Dataset 2 (Environmental factor)
1. State
2. No. of Persons in Vehicle
3. Day
4. Month
5. Day in the Week
6. Hour
7. Land
8. Weather
9. Drunk Drivers
10. Class

The first dataset basically deals with all kinds of injuries, from no injuries to fatal ones, while the second dataset deals with the fatal injuries only.

Both datasets are relatively big, thus hard to preprocess. Preprocessing is the most complicated, but the most important step in data mining. It highly affects the performance of the mining techniques. The goal was to achieve the success rate of the classification techniques as high as possible. Different combinations of attributes were tested, and the ineffective attributes were removed. If the data is not perfect, and if it is also abundant, it is hard to detect the instances that provoke the decrease of the success rate. Those may be the outliers, the duplicate values, etc.

IV. Classification Methods

Classification belongs to the category of supervised learning, where machine learns based on provided input and output data and creates a model for the future predictions of output data for which only the input data is provided. The two datasets (tested separately) were split in training and testing set in ratio 66% and 34% respectively, which is usually considered as optimum split. The prediction model was built based on the training set, and the success rate was determined based on the testing set. The flow of the classification technique can be seen in Figure 1.

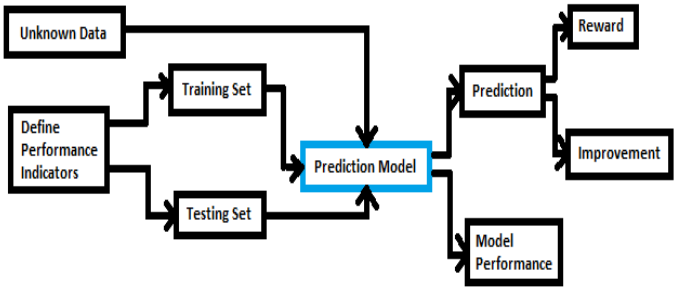

Fig. 1. Classification technique flow

Among many available classification methods, the two classification methods that resulted in highest success rate are Naïve Bayes and C4.5 Decision Tree. The popularity of Naïve Bayes classifier has been increased and it is being adopted by many researches because of its simplicity, computational efficiency, and its good performances for real-world problems [9]. Decision Trees are one of the most powerful directed data mining techniques because they can be used on such a wide range of problems and they produce models that explain how they work [18]. The success rates of the classifiers can be seen in Table III. C4.5 Decision Tree method performed better with both datasets, while Naïve Bayes method has taken less time to build the model.

TABLE III. Success Rates of the Classification Techniques

	Naïve Bayes		C4.5 Decision Tree	
	Correctly classified instances	Time taken to build the model	Correctly classified instances	Time taken to build the model
Dataset 1 Human factor	80.15 %	0.35 sec	80.72 %	4.55 sec
Dataset 2 Environmental factor	92.18 %	0.02 sec	92.53 %	0.23 sec

V. Results

The most interesting relations between data and the class attributes will be mentioned in the following paragraphs. The first dataset, which is mostly related to human factors, has 5 attributes that describe the degree of the injury, which will be presented in blue, red, green, grey and pink from no injury to fatal injury respectively. The other dataset, which is mostly related to environmental factors, states the number of fatalities from 1 to 10, colored in blue, red, green, etc. Since the number of fatalities greater than 3 is very rare, those can be hardly seen in the figures.

The common attribute for the both sets was "State" attribute. Though the data for the sets was not collected in the same year, the dependencies of place (state) of the accident and the class attributes (injury severity and number of fatalities) resulted in the same graph. Namely the three states, Texas, California and Florida, were the most endangered ones when it comes to accidents according to both datasets. The same layout of the results can be seen in Figure 2.

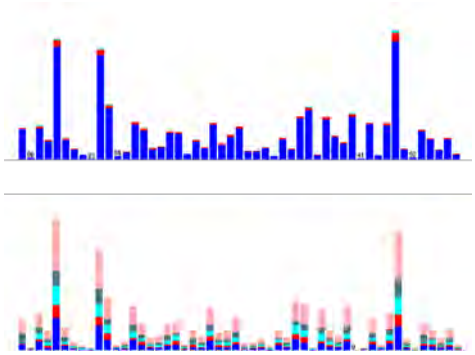

Fig. 2. State attribute dependency for dataset 1 (up) and dataset 2 (down)

Based on the results obtained from the first dataset, it can be concluded that males are the ones that get injured more frequently. However, the degree of injury is distributed the same among both genders. Further on, the person type that gets injured most usually are the drivers. Pedestrians get injured less often, but their injuries are most often fatal. The drivers seating position was proved to be the most dangerous one, followed by the front seat right side, followed by the left and right seat in the back (that are equally dangerous), and followed by the middle seat in the back which is the safest one in the vehicle. The usage of the restraint belt does not affect the occurrence of the road accident, as the number is almost equal, but it highly affects the degree of the injury, as the shoulder belt prevents fatal injuries, which can be seen in Figure 3.

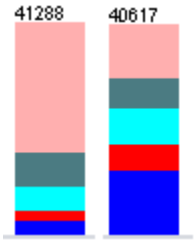

Fig. 3. Restraint influence (1st bar-no belt, 2nd bar-lap and shoulder belt)

The results from the second dataset bring to a conclusion that some environmental factors are more likely to lead to a fatal injury, with one or more death persons. For example, as the number of the people in the vehicle increases, the number of the fatal injuries decreases. The reason may be that more people mean more responsibility and less chance to fall asleep. The smallest number of fatal injuries happens in February, probably because it is shorter than other months and because people are more cautious due to bad weather conditions. According to the results, the periods of the day with the most frequent fatal crashes are 5, 6, and 8 p.m., probably because of the darkness, traffic jam and fatigue. The weather condition that can be highly related to the big number of fatal crashes is the clear weather. 73% of the total number of fatal accidents happens during the clear weather, 23% happen during the cloudy or rainy weather, while snowy, foggy and other weather conditions are related to a small number of fatal crashes, which can be seen in Figure 4. 7% of the total fatal accidents end up with more than 1 fatality.

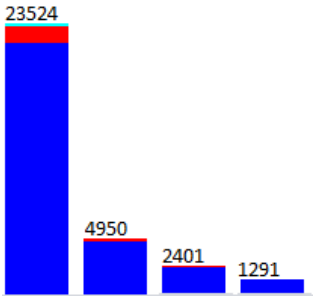

Fig. 4. Weather influence (1st bar-clear, 2nd bar-cloudy, 3rd bar-rainy, 4th bar-other)

VI. Conclusion and Discussion

Attempts were made to discover the role of human factor and environmental factor in severity of road crashes and number of fatalities based on Naïve Bayes and C4.5 Decision Tree. The ability of those two techniques as data mining techniques on predicting severity of road crashes were investigated. While C4.5 Decision Tree has provided better results, Naïve Bayes was faster in building the model. The results revealed that "gender", "person type", "seating position", and "restraint" attributes were related to the degree of injury. Weather conditions, as well as period of day were related to the number of fatalities. Number of persons in the vehicle is negatively correlated to number of fatalities.

In this paper, the research was extended in terms of attributes. Almost all possible factors that affect the road accident were taken into consideration. Further on, the class attributes were including both fatal and non-fatal injuries. The ability of predicting fatal and non-fatal injury is very important since drivers' fatality has the highest cost to society economically and socially. The usage of two dataset helped producing more accurate results, and compare which of the two were more suitable for data mining techniques, that is which performed better.

Though there were no missing values in the datasets, many data were marked as "unknown". If that data was available, it might help improving the models' performance. The attribute selection plays a great role in success rate, and the variations in that area could improve the results.

All in all, the results are satisfying. Information obtained from the research was based on the real-life data and actions of road accident prevention could be constructed from it.

References

[1] L. Evans, "Traffic Safety," Mich Bloomfield, Science Serving Society, 2004.

[2] T. Anuradha, "Data mining approaches to analyze road traffic accident data," International Journal of Emerging Technology in Computer Science & Electronics (IJETCSE), 0976-1353, vol. 4(1), December 2013.

[3] A. Pakgohar, R. S. Tabrizi, M. Khalili and A. Esmaeili, "The role of human factor in incidence and severity of road crashes based on the CART and LR regression: a data mining approach," Elsevier Ltd., 1877-0509, 764–769, 2010.

[4] L. Vogel and C. J. Bester, "A relationship between accident types and causes," Proceedings of the 24th Southern African Transport Conference (SATC 2005), 1-920-01712-7, July 2005.

[5] P. Van Elslande, C. Naing and R. Engel, "Analyzing human factors in road accidents: TRACE WP5 Summary report," Deliverable D5.5, 2008.

[6] U. Lokala, S. Nowduri and P. K. Sharma, "Road accidents bigdata mining and visualization using Support Vector Machines (SVM)," World Academy of Science, Engineering and Technology International Journal of Computer and Systems Engineering, vol. 10(8), 2016.

[7] A. Prasath and M. Punithavalli, "A review on road accident detection using data mining techniques," International Journal of Advanced Research in Computer Science, vol. 9(2), March-April 2018.

[8] M. Chong, A, Abraham and M. Paprzycki, "Traffic accident analysis using machine learning paradigms," Informatica 29, 89–98, December 2004.

[9] J. Kashyap and C. P. Singh, "Mining road traffic accident data to improve safety on road-related factors for classification and prediction of accident severity," International Research Journal of Engineering and Technology (IRJET), 2395-005, 2395-0072, vol. 3(10), October 2016.

[10] B. Atnafu and G. Kaur, "Survey on analysis and prediction of road traffic accident severity levels using data mining techniques in Maharashtra, India," International Journal of Current Engineering and Technology, 2277-4106, 2347-5161, vol. 7(6), November-December 2017.

[11] National Highway Traffic Safety Administration, "National Automotive Sampling System General Estimates System analytical user's manual, 1988-2015, July 2018.

[12] D. T. Akomolafe1 and A. Olutayo," Using Data Mining Technique to Predict Cause of Accident and Accident Prone Locations on Highways," American Journal of Database Theory and Application, 2326-0831, 2326-0858, vol. 2(3), 2012.

[13] V. M. Ramachandiran, P. N. Kailash Babu and R. Manikandan, "Prediction of road accidents severity using various algorithms," International Journal of Pure and Applied Mathematics, 16663-16669, vol. 119 (12), 2018.

[14] A. Kashani, A. Shariat-Mohaymany and A. Ranjbari, "Analysis of factors associated with traffic injury severity on rural roads in Iran," Journal of injury & violence research, April 2011.

[15] M. Bédard, G. H. Guyatt, M. J. Stones and J. P. Hirdes, "The independent contribution of driver, crash, and vehicle characteristics to driver fatalities," Accident Analysis & Prevention, 34(6):717-27, November 2002.

[16] B. C. Tefft, “Rates of motor vehicle crashes, injuries and deaths in relation to driver age,” AAA Foundation for Traffic Safety, June 2017.

[17] Great horned owls (Team09), “Factors of multiple fatalities in car crashes,” SAS Symposium Global Competition project report, January 2016.

[18] F. E. Sapri et al., “Decision Tree model for non-fatal road accident injury,” International Journal on Advanced Science Engineering Information Technology, 2088-5334, vol. 7(1), 2017.

Design and Optimization of Lightweight Broadband Antenna

Fikriye Öz
Süleyman Demirel University
Miltek ARGE Ltd. Co.
Istanbul, Turkey
fikriye.oz@miltek.com.tr

Ahmet Öncü
Boğaziçi University
Miltek ARGE Ltd. Co.
Istanbul, Turkey
ahmet.oncu@boun.edu.tr

***Abstract*—In this paper, the design, and optimization of lightweight, compact-size and broadband double-ridged horn antenna (DRHA) for 2-6 GHz is presented. The desired antenna consists of several parts like feed section design, ridged part design, waveguide section design. Firstly, the antenna is designed according to determined antenna parameter values. Then, these antenna parameters are optimized to obtain the best antenna performance in terms of gain, frequency range and Voltage Standing Wave Ratio (VSWR). The modeled antenna geometry is simulated by using a commercially available 3D EM (electromagnetic) software program. Finally, the antenna is fabricated and measured.**

Keywords—Antenna, double-ridged horn, broadband lightweight,

I. INTRODUCTION

Antennas which have broadband, ultra-wideband, and high gain properties are very important for microwave and millimeter wave applications, electromagnetic compatibility testing, and standard measurements [1]. One of the most common antenna types that provide these properties and studied recently is DRHA. These antennas also offer unique characteristics like directivity, low VSWR, acceptable half-power beam-width over the entire frequency band, easy feeding, relatively simple construction and excellent peak power handling capability [2].

Almost all of DRHA's performance, such as broad bandwidth, directivity, low VSWR etc. depends on its physical geometry. Ridged Structure geometry is the most significant part of the antenna that affects antenna performance [3]. There have been numerous antenna studies on this topic both scientifically and commercially. However, commercially available antennas have bulky geometry and heavyweight. For size and weight reduction of the antenna, several studies have been proposed in recent years [4]. In addition, a lightweight DRHA from 2 GHz to 6 GHz was used in Synthetic Aperture Radar (SAR) systems [5].

The aim of this work is to develop a lightweight DRHA with best antenna characteristics to use in SAR systems. In order to reduce the size and weight of the antenna, we optimized the antenna's important geometrical parameters while considering antenna performance. Initially, we designed a rectangular DRHA according to the theory of waveguide and antenna. Thereafter, the DRHA's geometry is simulated using a commercial 3D EM simulation tool. The parameters of the antenna which substantially affect antenna performance are determined. These parameter values are optimized to obtain better antenna results. Then, DRHA is fabricated and measured.

II. DESIGN AND FABRICATION PROCESS

The antenna design process is composed of three sections. The first section is to obtain the waveguide structure, the second part is to design the feeding structure for coaxial line and the third part is the characteristic impedance calculation of ridged waveguides.

Waveguides work as a bandpass filter in TE or TM waveguide modes. Firstly, DRHA's main dimensions such as width, length, and ridged thickness were calculated according to the theory of ridged waveguides to determine the cut-off wavelength [6]. After then, the antenna feed structure was designed to provide a 50 Ω impedance matching. Finally, tapered ridged structures which are the most significant parts of DRHA were designed. The exponentially tapered ridges change from 50 Ω the waveguide impedance at the feeding point to 377 Ω free space impedance. To improve the impedance matching from a ridged waveguide to the free space, the exponential equation can be used

$$Z(y) = z_0 e^{ky}, \qquad 0 \le y \le L \tag{1}$$

In this equation, y refers to the waveguide aperture-distance and L refers to the axial length of the flare part of the horn opening. The k is a constant calculated as follows

$$k = \frac{1}{L}\ln\left(\frac{Z_L}{Z_0}\right) \tag{2}$$

where Z_0 and Z_L stands for double-ridged waveguide characteristic impedance and free space impedance respectively [7].

After DRHA was designed, the DRHA's determined parameters were optimized without using classical optimization methods. We changed several DRHA's parameters like space between ridged structures, a feeding point for coaxial line and tapered ridged structures manually, until better results were obtained.

Small alterations of DRHA structure affect the precision of antenna characteristics. The effects of only substantial two parameters are given in Figures 2. In Fig. 2(a), *fp* corresponds to the height of the feeding point, whereas, in Fig. 2(b) *s* corresponds to a spacing between ridged structures.

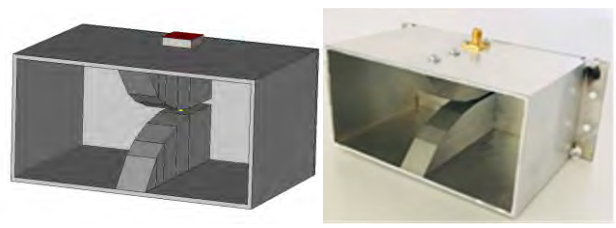

Figure 1. Designed and realized antenna.

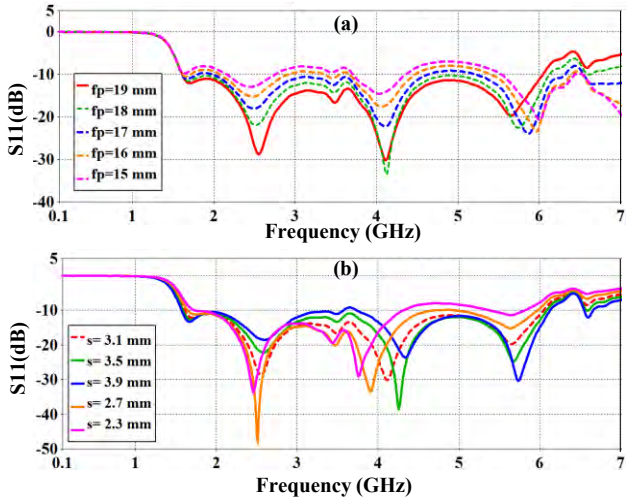

Figure 2. The precision of S11 to the alterations of fp in (a) and s in (b).

III. SIMULATION AND MEASUREMENT

We designed and fabricated a new broadband double-ridged horn antenna to use in SAR systems. VSWR and radiation pattern of the designed antenna were simulated using 3D EM software. The designed antenna is fabricated and its performance is measured by using Rohde Schwarz ZVA 40 vector network analyzer. VSWR and radiation pattern of the designed antenna are shown in Fig. 3 and Fig. 4, respectively.

TABLE I. COMPARISON OF DESIGNED AND COMMERCIAL ANTENNAS PHYSICAL CHARACTERISTICS

Antenna Properties	*Designed Antenna*	*Commercial Antenna*
Width (mm)	120	284
Length (mm)	60	184
Height (mm)	79.65	252
Weight (gr)	343	2039

Physical dimensions of the fabricated antenna are compared with that of a commercial DRHA in Table 1. The proposed prototyped antenna provides many advantages like its quick fabrication, low cost, and low weight. Around two thirds of the designed antennas physical geometry was reduced by using optimization technique and antenna weight is decreased by eighty percent of the commercial antenna weight. The designed antenna is suitable to use in portable SAR systems due to its small geometry and light weight. To obtain desired bandwidth and gain, the proposed designed antenna physical dimensions

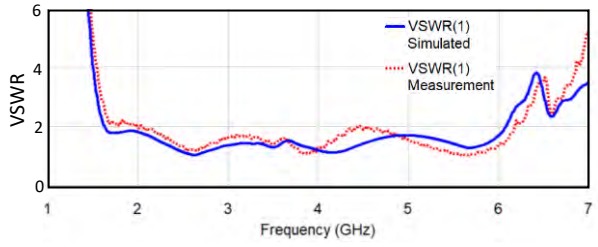

Figure 3 Measured and simulated VSWR results.

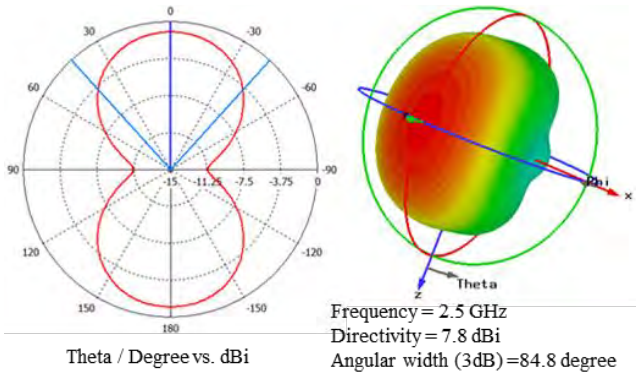

Figure 4: 2D and 3D radiation patterns of the designed antennas.

are optimized. However, designed small antenna, has a disadvantage to achieve high gain properties because of horn antennas gain depends on their horn aperture dimensions.

IV. CONCLUSION

According to the simulation results, the antenna's lower cut-off frequency is 1.64 GHz and the upper cutoff frequency is 6.07 GHz. Hence, antenna bandwidth was determined as 4.43 GHz. According to the measurement results, the lower cut-off frequency of the fabricated antenna is 2.05 GHz and the upper cut-off frequency is 6.18 GHz with a bandwidth of 4.13 GHz. And also, based on the measurement, realized DRHA weight is only 343 grams. As shown in Fig. 4, the measurement and simulation show good agreement. There is a small discrepancy between measured and simulated results that are expected to be originated due to the fabrication inaccuracy while machining the metallic parts of the designed horn antenna. The realized antenna is utilized for a SAR system's measurement to obtain SAR images.

ACKNOWLEDGMENT

This work is supported by MILTEK Milimetrik Teknolojiler R&D Ltd. Co. I would like to thank MILTEK for their financial support.

REFERENCES

[1] Ghorbani, M. and A. Khaleghi. "Double ridged horn antenna designs for wideband applications." Proceedings of 19th Iranian Conference on Electrical Engineering. IEEE, 2011.

[2] Abbas-Azimi, Majid, Farrokh Arazm, and Jalil Rashed-Mohassel. "Design of a new broadband EMC double ridged guide horn antenna." Proceedings of First European Conference on Antennas and Propagation IEEE, 2006.

[3] Genc, Abdullah, et al. "The comparison of the characteristics of the double-ridged horn antennas depending the geometry of ridge profiles for wideband application." Proceedings of Progress in Electromagnetics Research Symposium-Spring (PIERS), 2017.

[4] Huang, Guan-Long, et al. "Lightweight perforated waveguide structure realized by 3-D printing for RF applications." IEEE Transactions on Antennas and Propagation pp. 3897-3904, 2017.

[5] Omuz, B., Öz, F., Özdemir, Ö. and Öncü, A. "Experimental Verification of In-door Ground Based SAR Using Beam Space MUSIC Algorithm." Proceedings of IEEE International Conference on Electromagnetics in Advanced Applications (ICEAA) pp. 213-216, 2018.

[6] S. Hopfer, "The design of ridged waveguide.", IRE Trans. Microwave Theory and Techniques, Vol. 3, No. 5, pp. 20-29, 1955.

[7] Mallahzadeh, A. R., and A. A. Dastranj. "Double-ridged conical horn antenna for wideband applications." International Journal of RF and Microwave Computer-Aided Engineering, pp. 338-345, 2009.

A Doppler Sensor System At 24-GHz ISM Band for Cardiorespiratory Monitoring

Sefa Erdoğan
Boğaziçi University
Institute of Biomedical Engineering
34684, Çengelköy, Istanbul, Turkey
sefa.erdogan@boun.edu.tr

Cengizhan Ozturk
Boğaziçi University
Institute of Biomedical Engineering
34684, Çengelköy, Istanbul, Turkey
cozturk@boun.edu.tr

Ahmet Öncü
Boğaziçi University
Department of Electrical and Electronics Engineering
34342, Bebek, Istanbul, Turkey
ahmet.oncu@boun.edu.tr

***Abstract*— Non-contact vital sign monitoring could be very valuable for in hospital and home care of several health conditions. In this paper, a non-contact 24 GHz Doppler radar system with respiration rate and heart rate monitoring features is presented. The system is also able to detect the cough and apnea.**

Keywords— Doppler radar, 24 GHz, microwave, radar, non-contact monitoring, cough, apnea.

I. INTRODUCTION

Early usage of radar technology in physiological motion detection dates back to 1970s [1]. Since then, continuous wave (CW) Doppler radar has been studied extensively [2]–[6]. The single channel receiver limitations and the requirement of the quadrature receiver system are well explained in [4]. It is also proposed that nonlinear demodulation of in-phase (I) and quadrature (Q) signals yield better results than linear demodulation. In [2], Doppler radar was employed to monitor respiration and cough during respiratory-gated lung cancer radiotherapy. Vital sign detection is realized by time-domain autocorrelation model in [3]. However, both the systems use commercial acquisition systems and software which increase the cost.

In this paper, 24 GHz CW quadrature Doppler radar is presented to monitor respiration rate (RR) and heartbeat rate (HR). The proposed system can also monitor the cough and apnea of the subject. The used K-band RF front-end transmits 24 GHz electromagnetic wave which is then reflected from patients' chest wall. The reflected signal is exposed to phase modulation and it consists of cardiopulmonary information. The received signal also contains noises such as clutter and muscle twitches. To have a near DC signal, received microwave region signal should be down-converted. Prior to the digitization of the analog baseband signal, amplification and antialiasing filters are applied. Filtered analog signals are then digitized by a 12-bit analog to digital converter (ADC). After the data is digitized, ARM-based microcomputer is applied signal processing techniques to extract the vital signs. Extracted vital signs are later sent to an internet server for storage and monitoring.

This work was supported in part by Boğaziçi University Research Fund under grant 6600.

II. DOPPLER RADAR SENSOR SYSTEM

The overall block diagram of the proposed Doppler radar vital sign detection system is shown in Fig. 1. The used RF front-end uses a license free 24 GHz industrial, scientific, medical (ISM) radio band. It is responsible for transmitting the 24 GHz continuous wave (CW) signal and receiving the phase modulated signals that are reflected from the patients' chest wall. Phase modulated signals are then converted to in-phase (I) and quadrature (Q) base-band signals. Before digitizing the data, antialiasing filter and amplification are done with analog components. The lowpass filter cutoff of the system is set to 40 Hz. Since the output of the RF front-end is in millivolts, the gain is set to 20. The filtered quadrature signals are then put over a DC offset to maximize the ADC's dynamic range. The amplification is done with low noise amplifiers and low noise voltage references. Digitization of the quadrature signals is done with 12-bit ADC with 100 kilo-samples per second sampling rate. The digitized data are then sent to an ARM-based microcomputer via a serial peripheral interface (SPI). In the digital domain, the sampling rate is set to be 160 Hz since it is enough to capture the physiological data and minimize the effect of out of band interference.

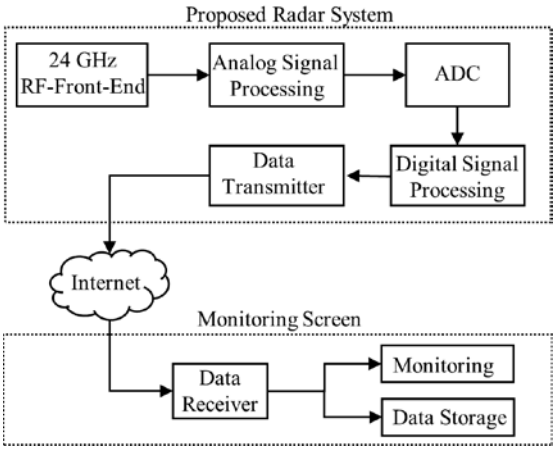

Figure 1 Overall system block diagram

Prior to the arctangent demodulation, DC cancellation is required. It is done by using several digital differentiators and integrators. Arctangent demodulation of the resultant signal provides chest wall motion information. To extract the RR and HR, arctangent demodulated signal is filtered with two different Finite-Impulse Response (FIR) bandpass filters with different cutoff frequencies are set. While the respiration rate is extracted from the signals that are filtered with 0.1 Hz to 0.7 Hz cutoff frequencies, second FIR filter cutoff frequencies are set to 1 Hz to 3 Hz for HR extraction.

Calculated HR, RR, and respiratory displacement data are then sent to an internet server which then can be monitored. Since the signal processing is executed on the proposed Doppler radar system and sent to the internet server, any computer that has an internet connection can be used to monitor the status of the patient. Displayed physiological data are then stored for further usage.

III. Measurements

The subject is asked to sit in front of the proposed radar system while he is wearing a BIOPAC respiratory belt transducer on his chest and finger pulse sensor on his index finger. Measurements are taken during normal breathing while the subject is relaxed. Both the proposed Doppler radar system and the BIOPAC respiratory belt transducer measurement results are plotted in MATLAB and are shown in Fig. 2. To extract the RR and HR, the aforementioned signal processing techniques are applied to the plotted data. The designed Doppler radar system results in 11.25 breaths per minute and 66 heartbeats per minute. BIOPAC respiratory transducer agrees with the designed system with 11 breaths per minute. The finger pulse sensor also agrees with an HR of 66 beats per minute.

As the second task, the subject is asked to breathe normally, cough, breath normally again, and hold his breath to mimic apnea, respectively. The resultant measurement is shown in Fig. 3 with highlighted cough and apnea sections. The BIOPAC respiratory transducer and the proposed Doppler radar system results agree with each other and can be seen in Fig. 3.

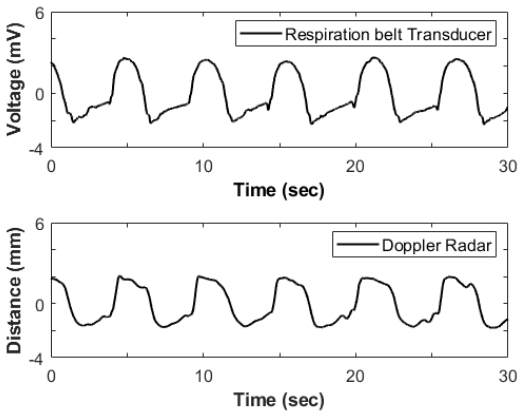

Figure 2 Normal breathing measurements

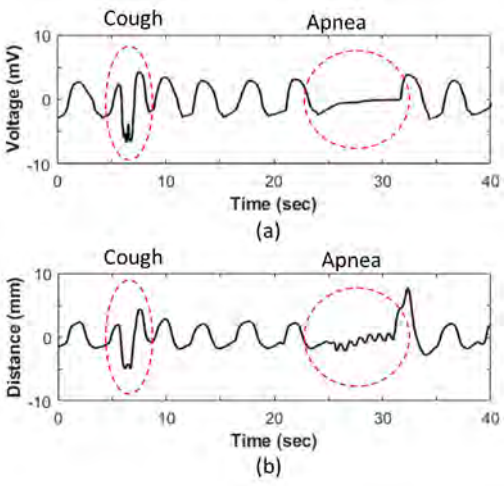

Figure 3 Apnea and forced cough patterns in (a) BIOPAC respiratory transducer and (b) Doppler radar system.

IV. Conclusion

In this work, a 24 GHz Doppler radar system for RR and HR monitoring is successfully developed. Since the BIOPAC respiratory transducer, the finger pulse sensor and the designed Doppler radar unit measurement results agree with each other, it can be concluded that the designed system can be used for non-contact vital sign monitoring. The cough and apnea also can be detected from the chest wall motion graph which makes the designed system a useful device that can be used in sleep centers for detecting breathing abnormalities.

References

[1] C. A. Marsden and B. King, "The use of Doppler shift radar to monitor physiological and drug induced activity patterns in the rat," *Pharmacol. Biochem. Behav.*, vol. 10, no. 5, pp. 631–635, 1979.

[2] C. Gu, R. Li, C. Li, and S. B. Jiang, "Doppler radar respiration measurement for gated lung cancer radiotherapy," in *2011 IEEE Radio and Wireless Week, RWW 2011 - 2011 IEEE Topical Conference on Biomedical Wireless Technologies, Networks, and Sensing Systems, BioWireleSS 2011*, 2011, pp. 91–94.

[3] G. Sun and T. Matsui, "Rapid and stable measurement of respiratory rate from Doppler radar signals using time domain autocorrelation model," *Proc. Annu. Int. Conf. IEEE Eng. Med. Biol. Soc. EMBS*, vol. 2015–Novem, no. 3, pp. 5985–5988, 2015.

[4] Byung-Kwon Park, S. Yamada, O. Boric-Lubecke, and V. Lubecke, "Single-channel receiver limitations in doppler radar measurements of periodic motion," *2006 IEEE Radio Wirel. Symp.*, pp. 99–102, 2006.

[5] B. Lohman, V. M. Lubecke, P. W. Ong, and M. M. Sondhi, "A Digital Signal Processor for Doppler Radar Sensing of Vital Signs," *EMBS Int. Conf.*, no. October, pp. 161–164, 2002.

[6] A. Öncü, "A 24-GHz Doppler sensor system for cardiorespiratory monitoring," *IECON Proc. (Industrial Electron. Conf.*, pp. 5161–5164, 2016.

An Indoor Case Study on Ground Based Synthetic Aperture Radar

Güneycan Kılıç
Electrical-Electronics Engineering
Boğaziçi University
İstanbul, Turkey
guneycan.kilic@boun.edu.tr

Ahmet Öncü
Electrical-Electronics Engineering
Boğaziçi University
İstanbul, Turkey
ahmet.oncu@boun.edu.tr

***Abstract*—In this paper, a ground-based synthetic aperture radar (GB-SAR) system with broadband antennas is designed to collect the experimental data and form in-door radar image. Finally, the 2-D radar image is constructed by employing Tikhonov regularization.**

***Index Terms*—Synthetic Aperture Radar (SAR), Ground Based Synthetic Aperture Radar (GB-SAR), Radar, Vector Network Analyzer (VNA), Antenna**

I. INTRODUCTION

SAR is used to construct 2-D or 3-D radar images, such as landscapes. Since SAR is positioned on a moving platform, it gives a finer spatial resolution than conventional beam-scanning radars over a target region [1].

GB-SAR systems and devices are generally used for radar imaging applications [2]. In this work, we propose a high resolution in-door monitoring and advanced radar signal processing method.

Following the instruction, data acquisition method is expressed and then radar imaging algorithm is identified. Finally, radar image of the measurement is obtained.

II. RADAR SYSTEM

A. Measurements

In this work, two reference reflectors are placed onto tube across the GB-SAR system in a conference room. A GB-SAR system which has a length of 2 meters, computer, broadband antennas and VNA has been developed and the system is shown in Figure 1. VNA and broadband antennas are calibrated from 5 GHz to 6 GHz in 200 steps to increase resolution and data are collected each time after the system moves 20 mm.

The transmitter and the receiver are positioned on a rail. The transmitter sends complex sinusoidal signal and the signal is reflected back to the receiver from scatterers with time delay. In this work, S-parameters of the environment are collected each time after the system moves 20 mm. Finally, a 201×101 matrix is received.

B. Radar Imaging

In our algorithm, the target region is divided into M cells and p_m denotes the position of the scatterer that is at the center of each cell, l_n denotes the position of the transmitting/receiving antennas on the moving rail and $d(l_n, p_m)$ denotes the distance between the scatterer and the transceiver. The structure is visualized in the Figure 2.

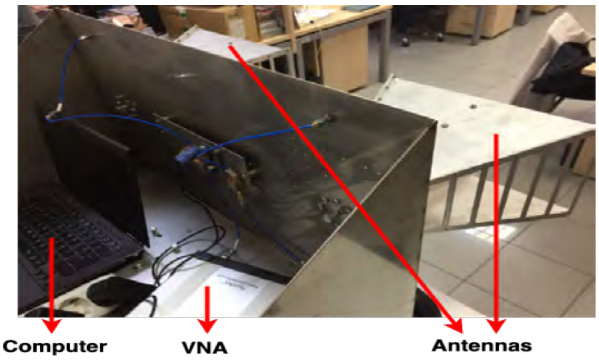

Fig. 1. GB-SAR System Equipments (Computer, VNA and Antennas on the Linear Rail)

The transmitting antenna sends a complex sinusoidal signal $exp(j2\pi ft)$ and the signal is reflected back by the scatterer. The receiving antenna observes this signal as

$$\sigma(p_m)exp(j2\pi f(t-\tau)), \tag{1}$$

where

- τ is time delay and is equal to $2d(l_n, p_m)/c$ and c denotes the speed of light in air.
- $\sigma(p_m)$ is the characteristic of the scatterer at the center of a cell.

It is assumed that the VNA provides the ratio of the transmitted signal and the received signal from 5 GHz to 6 GHz in 200 frequency steps for 101 locations on the rail. A 201×101 matrix is obtained from the VNA and then it is converted into a 20301×1 column matrix.

$$a(f, l_n) = exp(-j2\pi f\frac{2d(l_n, p_m)}{c})\sigma(p_m) \tag{2}$$

In order to image a region, it is assumed that there is a scatterer with characteristic $\sigma(p_m)$ at the center of each $5cm \times 5cm$ cell

$$b(f, l_n, p_m) = exp(-j2\pi f\frac{2d(l_n, p_m)}{c}) \tag{3}$$

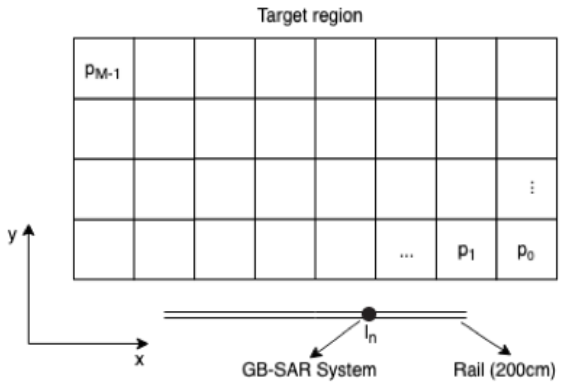

Fig. 2. Target Region as Grid and GB-SAR System on the Rail

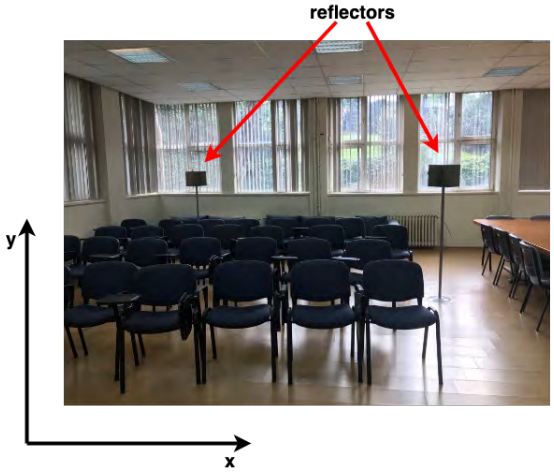

Fig. 3. Measurement Environment (Yorgo Istefanopulos Conference Room)

$$\begin{bmatrix} a_{1,1} \\ \vdots \\ a_{1,101} \\ a_{2,1} \\ \vdots \\ a_{201,101} \end{bmatrix} = \begin{bmatrix} b_{1,1,0} & \cdots & b_{1,1,M-1} \\ \vdots & \ddots & \vdots \\ b_{1,101,0} & \cdots & b_{1,101,M-1} \\ b_{2,1,0} & \cdots & b_{2,1,M-1} \\ \vdots & \ddots & \vdots \\ b_{201,101,0} & \cdots & b_{201,101,M-1} \end{bmatrix} \begin{bmatrix} \sigma(p_0) \\ \sigma(p_1) \\ \vdots \\ \sigma(p_{M-1}) \end{bmatrix}$$

If we summarize our model, $A = B\Sigma$ and A matrix is measured and B matrix is calculated. In particular, the unique solution for Σ matrix is found by employing Tikhonov regularization [3].

$$\Sigma = (\epsilon I + B^H B)^{-1} B^H A \tag{4}$$

Iterative methods might be required for ϵ in larger target regions [4]. After the characteristic of each scatterer is calculated, 2-D radar image is constructed.

III. CONCLUSION

In this work, measurements are made by using an uniquely designed GB-SAR system and S_{11}, S_{12}, S_{21} and S_{22} parameters are collected from the conference room which is shown in the Figure 3. The measurement environment includes chairs, seats, table and two reflectors. One of the reflectors is placed 5.5 meters across the right limit of the linear rail and the other one is placed 6 meter across the left limit of the linear rail. Then proposed algorithm is applied to S_{21} parameters for 2-D radar imaging and the constructed radar image is shown in the Figure 4. Consequently, two reflectors are obtained in the SAR image and the constructed 2-D radar image agrees with the measurement setup.

The conventional delay-and-sum beamforming method is also applied to S_{21} parameters for radar imaging. It is observed that the image results of the delay-and-sum algorithm and Tikhonov regularization are in a good agreement.

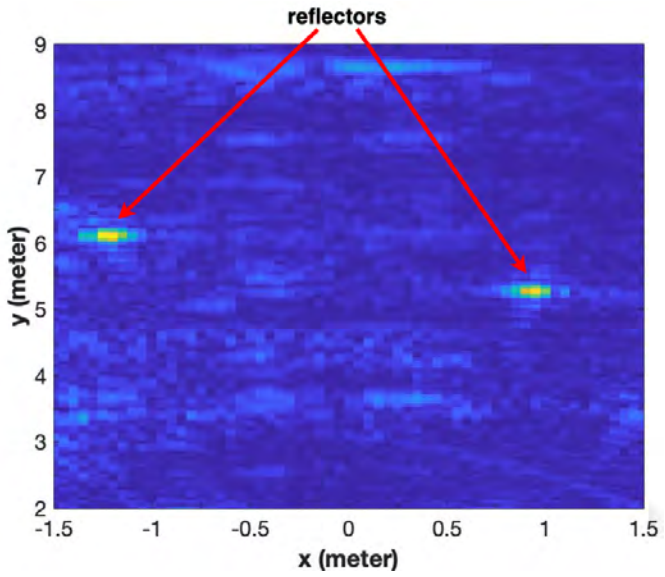

Fig. 4. Constructed 2-D SAR Image of the Conference Room

ACKNOWLEDGEMENT

We would like to thank Assoc. Prof. İlker Bayram for his valuable discussion in radar imaging. We are really appreciated for MİLTEK Group and Boğaziçi University Microwave Radar and Communications Laboratory because of the technical support. This work is supported by Bogazici University Research Fund under grant 14320.

REFERENCES

[1] B. Omuz, F. Öz, Ö. Özdemir and A. Öncü, "Experimental Verification of In-door Ground Based SAR Using Beam Space MUSIC Algorithm," 2018 International Conference on Electromagnetics in Advanced Applications (ICEAA), Cartagena des Indias, 2018, pp. 213-216.

[2] D. Leva, G. Nico, D. Tarchi, J. Fortuny-Guasch and A. J. Sieber, "Temporal analysis of a landslide by means of a ground-based SAR Interferometer," in IEEE Transactions on Geoscience and Remote Sensing, vol. 41, no. 4, pp. 745-752, April 2003.

[3] P. R. Johnston and R. M. Gulrajani, "Selecting the corner in the L-curve approach to Tikhonov regularization," in IEEE Transactions on Biomedical Engineering, vol. 47, no. 9, pp. 1293-1296, Sept. 2000.

[4] L. Ying, D. Xu and Z. -. Liang, "On Tikhonov regularization for image reconstruction in parallel MRI," The 26th Annual International Conference of the IEEE Engineering in Medicine and Biology Society, San Francisco, CA, 2004, pp. 1056-1059.

The Realization of a Linear Rail System to Acquire Ground-Based SAR Data

Eray Can Elumar
Boğaziçi University
Istanbul, Turkey
eray.elumar@boun.edu.tr

Serhat Tadik
Boğaziçi University
Istanbul, Turkey
serhat.tadik@boun.edu.tr

Mahmut Çoban
Boğaziçi University
Istanbul, Turkey
mahmut.coban@boun.edu.tr

Berk Omuz
Boğaziçi University
Istanbul, Turkey
berk.omuz@boun.edu.tr

Ahmet Öncü
Boğaziçi University
Miltek ARGE
Istanbul, Turkey
ahmet.oncu@boun.edu.tr

***Abstract*—In this work, a ground-based synthetic aperture radar (GB-SAR) system is developed for radar imaging. First, we developed a linear rail system by adding a servo motor and two proximity sensors to a linear rail. Then, we placed a metal car on this rail system and mounted broadband rigged horn antennas on the car. We placed a vector network analyzer (VNA) inside the metal car and connected the VNA to the antennas through amplifiers to acquire the S-parameters of the environment. The overall system can be remotely controlled and can acquire stepped frequency continuous wave (SFCW) radar data from the environment. We tested the system in several different environments and successfully acquired SFCW radar data.**

Keywords—Vector Network Analyzer (VNA), Radar Imaging, SAR, GB-SAR, Servo Motor, Linear Rail.

I. INTRODUCTION

Synthetic Aperture Radar (SAR) is a radar system that is capable of producing high-resolution images independent of daylight, cloud coverage and adverse weather conditions. It is emplaced mostly on mobile airborne and spaceborne systems with the purpose of environmental monitoring, various dimensional mappings, and climate change observations. Ground-Based Synthetic Aperture Radar (GB-SAR), in turn, is a SAR system placed on the ground, moving along a linear rail track. Its main objective is to keep track of environmental deformations such as landslides, avalanches and glacial melting [1]. The SAR system emits and receives microwave signals while moving along a path. The combination of the received signals at each location allows the construction of a virtual aperture that is much larger than the physical antenna length, thus increasing azimuth resolution. The amplitude of the received signal gives information about the distance of the target and the phase gives information about the distance of the target to the SAR system and the combination of these data can be used to generate an image of the target scene [2].

II. LINEAR RAIL SYSTEM

The linear rail system is composed of a vector network analyzer (VNA), transmit and receive antennas, a linear rail, Arduino and a computer.

A. Vector Network Analyzer (VNA)

VNA is a radio frequency test instrument that measures the response of a network. It sends a stimulus signal to the device that is tested and measures the amplitude and phase of the received signal [3]. In this work, PicoVNA 106 is used because of its small size, high measurement speed, and high accuracy.

B. Linear Rail

The linear rail has a length of 2 m and is actuated by a servo motor. Servo motor was chosen because servo motors provide their position information through an encoder so it can be precisely controlled. A proximity sensor is placed on both edges of the rail to prevent the SAR system from hitting the edges of the rail system. The servo motor is connected to the motor driver, and the motor driver is controlled using Arduino. There is also an emergency stop button connected directly to the motor driver.

C. Overall Radar System

In the overall system, two 0.8-8 GHz broadband ridged horn antennas are mounted on a metal car placed on the linear rail. The vector network analyzer, Arduino and the computer are placed inside the metal car. A power amplifier is placed on the transmit side of the VNA and an LNA is placed on the receive side. The overall linear rail system is shown in Fig. 1.

Figure 1. Linear Rail System.

The overall system is designed to acquire stepped-frequency continuous wave (SFCW) radar data [4]. To acquire the data, a Python code is run on a Windows-based computer. The Python code controls both the VNA and the servo motor to improve the synchronization between the data acquisition and the rail movement tasks. The Python code first communicates with the VNA to get the S21 parameters at that particular location for a list of specified frequencies. After VNA completes this operation, Python code communicates with the Arduino board to control the servo driver. Arduino communicates with the servo driver to control the servo motor and move the rail to the next position. After the rail is in the next position, VNA acquires new data and this process repeats again until the number of

This work is supported by Bogazici University Research Fund under grant 14320.

specified points is reached. The data acquisition scheme is illustrated in Fig. 2.

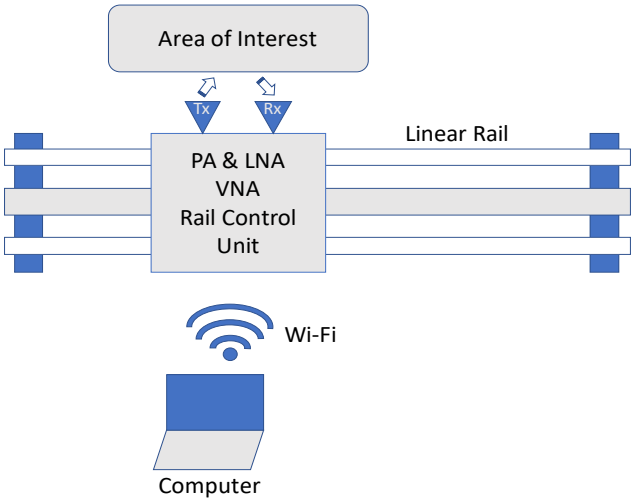

Figure 2. Overall system diagram.

III. DATA ACQUISITION WITH THE LINEAR RAIL

The data acquisition process was done on the stairs located near the Boğaziçi University Electrical & Electronics Engineering Department building. The linear rail was placed on a wheeled table and 2 metal reflectors were placed on the stairs to act as targets, whereas the stairs caused reflections and served as multiple paths. The center of the stairs was aligned with the center of the linear rail. The rail movement was 2 meters long [-1,1] and rail's distance to the stairs and the reflectors was 4.7 meters. The frequency range of 2 GHz to 6 GHz was swept with 201 frequency points and the rail step was 2 cm, which makes a total number of 101 observation points. The GB-SAR system and the targets in the measurement environment are given in Fig. 3. The object to be imaged is on the left, the linear rail on the bottom and the radar system on the right in the image. Radar image can be obtained from this radar data using radar signal processing algorithms such as BS-MUSIC and Tikhonov Regularization. The final radar image obtained from the data of this rail system using BS-MUSIC algorithm can be found in [4].

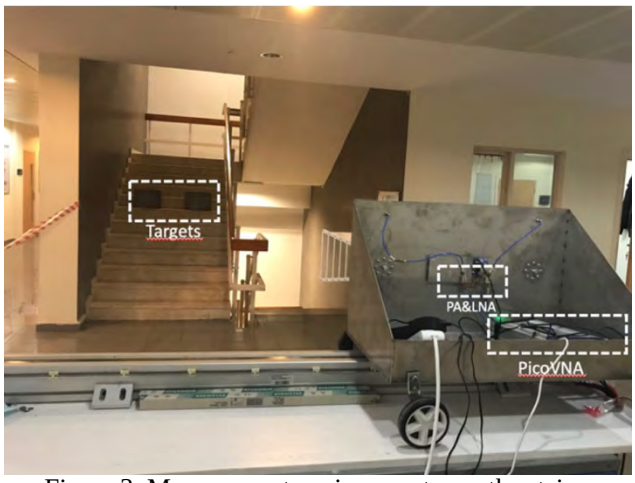

Figure 3. Measurement environment near the stairs.

After acquiring data in the environment in Fig. 3, the data acquisition was repeated in a different environment to show that the system can consistently acquire radar data in different environments. This environment is given in Fig. 4.

Figure 4. Measurement environment at the meeting room.

IV. CONCLUSION

In this paper, a remote-controlled linear rail GB-SAR system is successfully implemented. First, a linear rail system is developed by adding a servo motor and two proximity sensors to a linear rail. Then, broadband ridged horn antennas, VNA and several amplifiers are added to a metal car and the metal car is placed on the linear rail. The overall system can be remotely controlled by a computer. Using the system, S-parameters were successfully acquired in two different environments. The system allows collection of SFCW radar data remotely with ease, which will be a crucial element in further signal processing projects in which measurement times are longer and in remote places.

REFERENCES

[1] A. Moreira, P. Prats-Iraola, M. Younis, G. Krieger, I. Hajnsek and, K. P. Papathanassiou, "A tutorial on synthetic aperture radar," in IEEE Geoscience and Remote Sensing Magazine, vol. 1, no. 1, pp. 6-43, March 2013.

[2] A. Jungner, "Ground-Based Synthetic Aperture Radar Data Processing for Deformation Measurement," M. S. Thesis, KTH Royal Institute of Technology, Stockholm, May 2009.

[3] Pico Technology, "PicoVNA 106: 6 GHz vector network analyzer", PicoVNA 106 datasheet, 2018.

[4] B. Omuz, F. Öz, Ö. Özdemir and A. Öncü, "Experimental Verification of In-door Ground Based SAR Using Beam Space MUSIC Algorithm," 2018 International Conference on Electromagnetics in Advanced Applications (ICEAA), Cartagena des Indias, 2018, pp. 213-216.

Microstrip Low Pass Filter with Wide Stopband

Göksel ÇANKAYA[1], Bilal Furkan GENÇ[1], Anıl ÇAKIR[1], Bera GÜNASLAN[1], Çağatay TURHAN, Taha İMECİ [1]
[1]Department of Electrical and Electronics Engineering
Istanbul Commerce University, Istanbul, Turkey

Zeliha Merve ÇETİNOK[2]
[2]TRT Arabi, Istanbul, Turkey
zeliha.cetinok@trtarabi.com

***Abstract*—In this work, a microstrip filter was designed, simulated, built and tested for different microwave applications. In the micro strip design, a low-pass filter is designed. The purpose of the filter is to create a characteristic with a wide stop band. This model has been given a filter model. Improvements have been made to increase the efficiency of the filter. It has a wide band extending from 1.7 GHz to 3.7 GHz with a cut-off frequency of 1.8 GHz obtained in filter design. The obtained filter can be used for modern microwave applications. Simulation and measurement results are in very good agreement.**

Keywords—micro strip filter, low pass filter.

I. INTRODUCTION

The electromagnetic spectrum has a very wide frequency range and RF and microwave applications operate in specific frequency range (300 kHz - 300 GHz). Within these frequency ranges, there are narrow or wide bands where each specific application can be operated. The filter elements should be used for using the devices that operate in these range for specific applications [1].

Filters which have a significant role in RF and microwave applications are used for many areas such as wireless, mobile and satellite communication. As known, according to design purpose, filters can pass, stop and prevent unwanted signal interferences in the frequency range of interest. These structures have various types such as band pass or band stop, low pass or high pass[2]. In this work, low pass filter has designed by using the microstrip filter [3].

II. DESIGN STEPS

The filter design procedure, consist of three steps, has been realized for a design that provides desired filter specifications. In the first step, a low pass microstrip filter with defective base conductor has been designed by using classic filter design. In second step, we have perfomed to expand the stop band by adding parallel side lines on the microstrip lines in current design since the obtained frequency characteristic does not satisfy the design goals. In third step, in order to improve the characteristic to a significant level, the end portions of added parallel side lines have been expanded. [2] Microstrip patch antennas have been resized to obtain low pass filter values. Achieved an attractive feature for high-frequency wireless applications due to its compact size, low cost, profile and compatibility [4].

High-frequency antennas are very popular for a reliable wireless connectivity as the radiation at high frequencies causes the very serious free space loss. [5] Furthermore, wide band antennas provide significant contribution to current wireless services with exceptionally fast data output and its fine resolution according to researches we have done. Nowadays, these types of antennas are indispensable for wireless applications from point to point such as road traffic control, air traffic control, imaging and satellite communication, and they have become an economical solution at the same time. Usually, gain of these type of microstrip antennas can be improved by some kind of cuts and slightly modification in their shape. In doing so, especially multiple (symmetrical) cuts are applied to increase antenna gain [4]. The dielectric constant is 4.4 in this filter design. Graphic values S21 and S22 of filter we designed are shown. The equation we used for observing the wavelength change is in below.

$$\lambda = \frac{\sigma}{f\sqrt{Eeff}} \quad (1)$$

The mentioned equation λ depicts the wave lenght of the filter, and the square root refers to the dielectric constant. We took dielectric constant as 4.4 but when we take into consideration the dielectric constant of air is 1 in microstrip filter systems, it is necessary to calculate the whole dielectric constant of system.

III. SIMULATION RESULTS

The permeability value (Ɛr) of the material is 4.4, the thickness (h) is 1.6 mm and the tangent value (δ) is 0.0009.

In this study, we made by changing the substrate thickness, thicknesses of 5, 7 and 10 mm were tried at 1.7 GHz frequency and S22 values were -19 dB, -20 dB and -21 dB respectively. It is obvious that the best substrate thickness is 10 mm for filter efficiency.

The number of square is changing the S11 value. We used 8, 12 and 16 squares in the work we did by chancing number of squares in filter and we got 1 GHz, 1.5 GHz and 1.7 GHz S11 value respectively. It is also obvious as the number of squares increases, the cut off frequency also increases.

TABLE I. FILTER SIZE CHANGE

Size (mm x mm)	S21	S22 (dB)
25 x 12	1.8 GHz	-21
25 x 13.5	1.6 GHz	-18
24 x 14.4	1.5 GHz	-17

Figure 1 shows the S21 test result of manufactured filter.

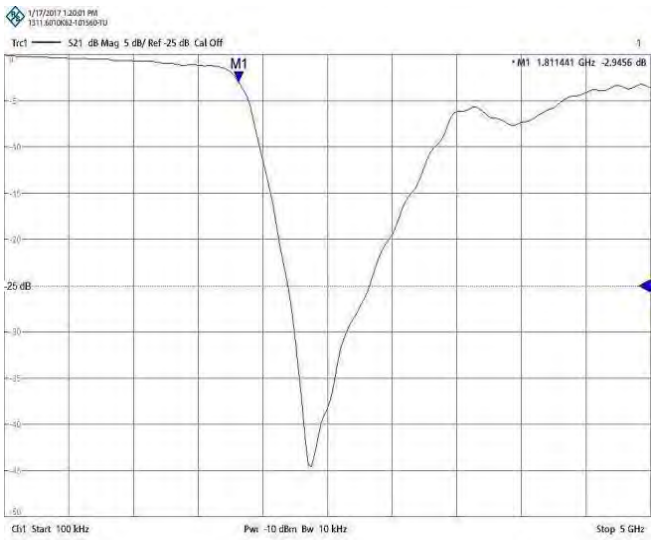

Fig. 1. S21 test result of filter

Figure 2 shows the S22 test result of manufactured filter.

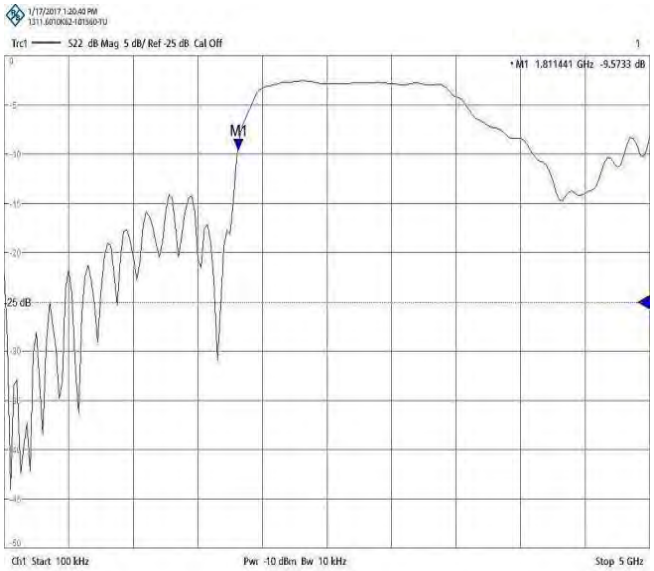

Fig. 2. S22 test result of filter

The picture we have manufactured filter which is connected with its connectors has given in figure 3.

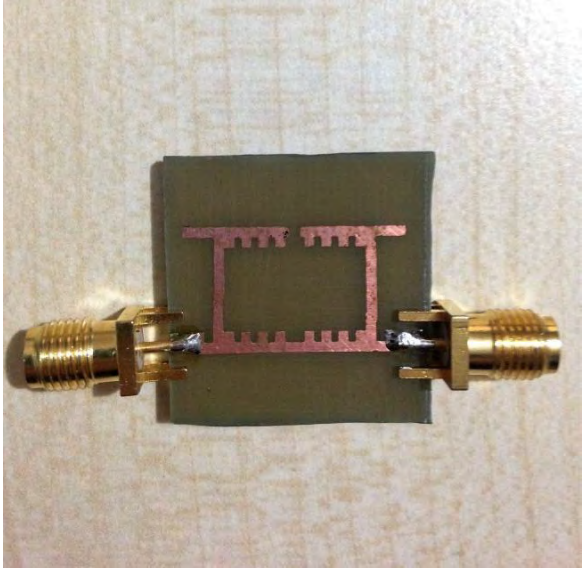

Fig. 3. Manufactured filter.

IV. CONCLUSION

In this article, a low pass microstrip filter is designed in three steps. The filter has been reached to wide stop band after all analisys on this paper. The resonator impedances have been chosen with a right way for ideal result. As a result of analyzes and simulations, the band stop filter its bandwidth extended from 1.7 GHz to 3.7 GHz with a cut-off frequency of 1.8 GHz has been produced. In produced device, measurements we have done and simulation are in very good agreement.

REFERENCES

[1] Packiarj D. and Vinoy K. J. and Ramesh M. and Kalghatgi A. T.,: "Design of Compact Low Pass Filter with Wide Stop Band Using Tri-section Stepped Impedance Resonator", International Journal of Electronics and Communications. NNGT Int. J. on Networking and Communication, Vol. 1, July 2014.

[2] Ertay A.O., Abbak M., Suer C.,"İyileştirilmiş Geniş Durdurma Bandlı Taban İletkeni Kusurlu Alçak Geçirgen Bir Mikroşerit Süzgeç Tasarımı",EMO Bilimsel Dergi,Cilt 4, Sayı 8, Syf 35-40, Aralık 2014.

[3] Jung E.Y., Lee J.W., Lee T.K., "SIW-based array antennas with sequential feeding for X-band satellite communication", IEEE Trans. Antennas Propagation, 2012, 60, (8), pp. 3632–3639.

[4] Murugan D., Madhan M.G., Piramasubramanian S.,: "Design and performance prediction of 10 GHz micro strip array antenna structures" ,IEEE Computing Communication & Networking Technologies (ICCCNT), 2012 Third International Conference on. 26-28 July 2012.

[5] Sonnet Suites, Version 13.52 www.sonnetsoftware.com.

Microstrip Band-Stop Filter with Open Stubs and Fractal Structure for UWB Applications

Lamija Herceg
Department of Electrical and Electronics Engineering
International University of Sarajevo
Sarajevo, Bosnia and Herzegovina
lamija_1995@live.com

***Abstract* - This paper introduces a new configuration of the ultra-wideband band-stop filter. After the optimization of the conventional open stub BSF in terms of performance, space and price, the final design is proposed as composition of four parallel open-circuited stubs connected by fractal-structured microstrip line. The filter operates in high frequencies with wide bands. It is a combination of two passbands, namely low pass from 0.1 GHz to 2.5 GHz and band-pass from 4.5 GHz to 9 GHz, separated by the rejection region from 2.5 GHz to 4.5 GHz. Compact size and low price enable the wide application of this filter configuration, while passing frequencies allow the operation in unlicensed frequency spectrum popular for high speed communications.**

Keywords—ultra-wideband; band-stop filter; microstrip; open stubs; fractal structure; Sonnet software

I. INTRODUCTION

The demand in high speed communication has led to the design and development of the wideband filters to support applications such as UWB technology that promises communication speed of up to 1000 Mbps. Because of its attractive feature in high speed wireless applications, the ultra-wideband communication has been authorized by Federal Communication Commission (FCC) with unlicensed frequency spectrum of 7.5 GHz from 3.1 GHz to 10.6 GHz in February 14, 2002 [1]. Therefore, the UWB band-pass filter (BPF) with a passband from 3.1–10.6 GHz, sharp out-of-band rejection especially at a lower stop band due to its extensive use in other technologies, low insertion loss, small and flat group delay is highly required [2]. Band-stop filter characterized by the mentioned features as well as the advantages like compact size, low cost and high performance was the design goal. Microstrip band-stop filters (BSFs) are being widely used in telecommunication systems [3]. Various techniques have been developed to synthesize and design microstrip BSFs.

In this paper, a band-stop filter (BSF) consisting of four parallel open-circuited stubs connected by fractal-structured microstrip line was adopted for the UWB filter design. Microstrip technology is used for simplicity and ease of fabrication. The design and simulation are performed using method of moments based electromagnetic simulator Sonnet Software. The filter is made to operate partially in the unlicensed high frequency region and partially in the low frequency region, avoiding the frequency spectrum of the growing 5G technology. In this way the current requirements of passband and sharp out-of-band rejection were satisfied.

II. DESIGN METHODOLOGY

The UWB filter design in this study starts with a conventional model composed of two quarter-wavelength open stubs separated by quarter-wavelength inverters. The conventional open-stub BSF was modified so that the satisfying response would be obtained for the demand of the popular UWB technology. Many trials led to the final design of the UWB filter that consists of four open stubs mounted on a microstrip line with a number of slits, that is, in the shape of a fractal curve. The configuration can be seen in Figure 1.

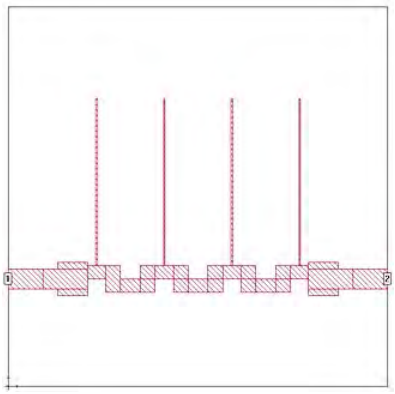

Fig. 1. Configuration of the proposed band-stop filter

Conventionally, by cascading more open stubs onto a microstrip, one can obtain wider rejection bandwidth and a deeper rejection. The side effects are the high insertion loss in the passband and increased circuit size [4]. However, it was possible to regulate the response and still keep the desired characteristics. A band-stop filter is used to suppress a signal from 2.5 to 4.5 GHz and allow all other signals at simulated frequencies to pass. Therefore, two passbands were created in the range from 0.1 GHz to 10 GHz. The simulated filter response can be seen in Figure 2. The passband covers bands from 0.1 to 2.5 GHz and from 4.5 to 9 GHz with an insertion loss between 0.3–1.5 dB, including connector losses. The simulated return losses are 15 dB and 10 dB, respectively, in most of the passband. The rejection region is very sharp, reaching 45 dB.

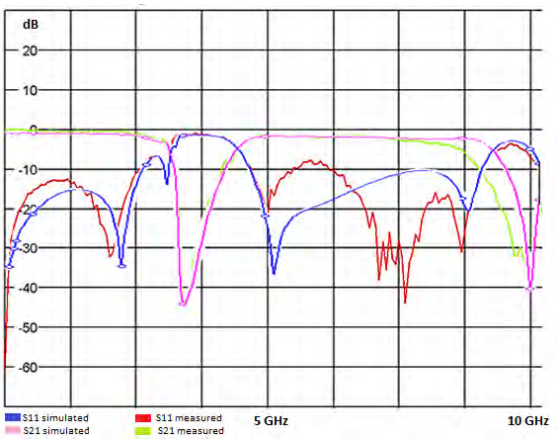

Fig. 2. Band-stop filter response (simulated and measured)

Passing regions depend on the different parts of the schematic. The middle microstrip line (without stubs) is the one that generates low-pass filter with very high cut-off frequency around 10 GHz. When stubs are added, they provoke the rejection band to appear in the low pass region, which, in total, ends up being band-stop filter response.

The height of the open stubs is based on the wavelength at the mid-band frequency. With the application of fractal shape on the middle line the distance between the four open stubs shortens, so the initial filter size is reduced.

The substrate material used is FR4 with a relative dielectric constant of 4.4. The thickness of the substrate is 1 mm. The whole backside of the substrate is the ground plane. The width of the feed line is approximately 8.03 mm and the open stubs are 0.13 mm wide. The four open stubs are 12.83 mm long and the separation between the centers of the four open stubs is 5.08 mm. The filter box is very small with the total size of 29.41 mm x 29.41 mm. The fabricated filter can be seen in Figure 3.

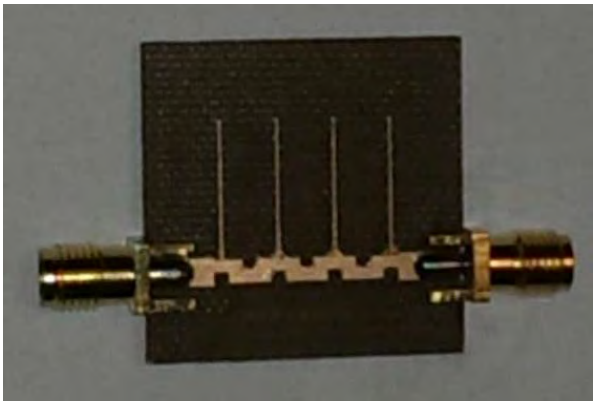

Fig. 3. Fabricated band-stop filter

The measured results agree very well with the simulated results and that can be seen in Figure 2. The difference can be noticed in the insertion losses, especially in the second passing region after 5 GHz. In spite of the non-expected performance, it still satisfies the set requirements. For the different performance, the change in the configuration can be made. The next paragraph offers the possible modifications.

III. Configuration Variations

Variations in size of the open stubs, as well as in the line connecting them, result in interesting responses. Some of the changes in filter schematics may involve:

- the height of the open stubs, which affects the frequency of the band-pass region. If they are shorter, band-pass region moves to the right, that is, it occupies higher frequencies;
- the width of the open stubs, which affects the width of the band-stop region. Wider open stubs result in wider rejection bandwidth;
- the number of the open stubs, which affects the width of the band-stop region. By cascading more open stubs onto the microstrip line wider rejection bandwidth and the deeper rejection may be obtained.

The filter response may be improved in terms of insertion losses that should be decreased. That can be achieved by increasing the width of the open stubs or increasing the width of the line entering the ports, as they affect the S_{21} magnitude.

IV. Conclusion

The UWB band-stop filter met the requirements of good performance, low losses, compact size of approximately 3 cm x 3 cm, and affordable price. Its region of operation allows the high speed communications. To remove the unwanted frequency bands from the microwave and radio frequency signals a band-stop filter (BSF) plays a very important role in wireless communication systems [5]. The open stub method ensured the two passband regions, while fractal structure ensured the smooth response and small box size. The agreement between simulated and measured results has been achieved.

Acknowledgement

We would like to thank Tamara Elektronik for fabrication and Assoc. Prof. Dr. Hamid Torpi from Yildiz Technical University for measurement.

References

[1] Transition.fcc.gov/Bureaus/Engineering_Technology/Orders/2002/fcc02048

[2] P. K. Singhal, S. Mathur and R. N. Baral, “Ultra-wide microstrip band pass filter using short circuited stubs,”, Journal of Electrical and Electronics Engineering Research, vol. 3(6), pp. 101-107, August 2011

[3] S. Yang, “Simulation of a bandstop filter with two open stubs and asymmetrical double spurlines,” International Journal of Advanced Research in Electrical, Electronics and Instrumentation Engineering, vol. 3(9), ISSN (Print) : 2320-3765, ISSN (Online): 2278-8875, September 2014

[4] S. Yang, “Simulation of a bandstop filter having two open stubs and an embedded open stub,” International Journal of Advanced Research in Electrical, Electronics and Instrumentation Engineering, vol. 3(11), ISSN (Print) : 2320-3765, ISSN (Online): 2278-8875, November 2014

[5] D. Kumar and A. De, “Effective size reduction technique for microstrip filters,” Journal of Electromagnetic Analysis and Applications, vol. 5(4), pp. 166-174, April 2014

Dual-band filter utilizing SIR and modified H-shaped structure

Faruk Bešlija
Department of Electrical and Electronics Engineering
International University of Sarajevo
Sarajevo, Bosnia and Herzegovina
fbeslija@ius.edu.ba

***Abstract* — A design of a dual-band filter implementing a stepped-impedance resonator (SIR) and a modified H-shaped structure is presented. This filter is designed to operate on a wide frequency range from 0 to 25 GHz, in a lowpass region up to 3.38 GHz and a bandpass region from 14.38 to 21.65 GHz, with a wide stopband region between 4.46 and 14.09 GHz. The filter exhibits a very good performance in terms of the passband losses and the desired stopband rejection values. It is also possible to manipulate the cutoff frequencies by adjusting the indicated dimensions. Simulation and measurement results are matching, except for certain high frequencies, due to FR-4 lossy structure. A usage of low-cost materials and a compact design make this filter favorable in terms of dimensions and manufacturing costs.**

Keywords — dual-band; stepped-impedance resonator; lowpass; bandpass; microstrip filter; H-shape; return loss

I. INTRODUCTION

The progress in the field of wireless communications has created a need for the radio frequency (RF) systems that can offer a multiband performance at a competitive manufacturing price [1]. In order to achieve a multiband response, there are a few strategies that can be implemented. Firstly, it is possible to combine multiple single-band filters into a multiband filter [2-4]. These single-band filters can either be cascaded [3-5], embedded into each other [3, 6], or implemented by combining two sets of resonators with common input and output [3, 4]. However, these methods appear consuming in terms of size and complexity of the filter [1], as it is obvious that a single circuit operating in two designated bands is to be preferred over multiple circuits doing the same job, due to its reduced dimensions and costs [4]. In this paper, a dual-band filter design with a lowpass and a bandpass region will be proposed, utilizing the stepped-impedance resonator (SIR) and a modified H-shaped structure. This design is preferred over the utilization of the multiple single-band filters, due to its reduced size [1-4] and a good stopband performance [1]. The filter to be presented relies on the SIR topology combined with the modified H-shape to achieve the desired LP and the BP response, exhibiting an LP response up to 3.58 GHz and a BP response from 14.38 to 21.65 GHz. It also provides the stopband region of at least 10 dB on a range from approximately 4 to 10.7 GHz. The filter itself is very compact and realized on a low-cost substrate, satisfying both size and production cost preferences.

II. FILTER STRUCTURE

A. Electromagnetic Performance

The relative permeability and the thickness of the layers in the simulation are set according to the manufacturing capabilities of the lab where the filter is produced. For the ground layer, an FR-4 substrate layer is observed, with thickness of 1 mm and dielectric constant of 4.4. For the upper layer, 5 mm thick layer of air is observed. For metal settings, a lossless metal with an infinite bulk conductivity is set. Other settings were left at their default values at Sonnet software.

B. Physical Structure and Dimensions

Firstly, the box dimensions for the filter design are selected. One of the parameters that can easily alter the filter response on a wide frequency spectrum is the box resonance, which can be estimated through Sonnet software. In order to prevent the box resonance, one may design the box in such way that the box resonance frequencies are eliminated. Experimentally, it has been found that the golden ratio causes the least number of box resonance frequencies. The dimensions of the box were minimized with respect to this ratio, until there were no estimated box resonance frequencies, which happened for 10.2 mm width by 6.3 mm height. The additional 3 mm were added to each side to ease the soldering process, resulting in a final dimension of the box of 16.2 mm width by 6.3 mm height.

Secondly, the design which would ensure the desired dual-band response is considered. Starting with the SIR as an initial element (Fig 1. H1, H2, W1, W2), a rectangular metallization centered on both sides would result in a multiband response, where one of the bands would be a lowpass. However, it does not look possible to control the cut-off frequency of the lowpass region from here, nor the number of bands and the corner frequencies for the other regions. By removing the central horizontal region of this rectangle, the response of the filter starts to show the outlines of the desired response in both lowpass and bandpass region. The H-shaped structure (Fig 1. H5, H7, W4) serves here both as a single-band bandpass filter and a tool to improve the rejection in the frequency range

between the operating regions of the LPF and the BPF. Although this design ensures the desired cut-off frequencies for both regions, the resulting return loss at the BP region is very poor. This issue requires design modifications which would both improve the downfall in the return loss in the BP region and preserve the current response at the other regions.

Thirdly, the H-shaped structure is adjusted, so that the rejection in the region between the LPF and the BPF is preserved as much as possible, while the return loss at the BP region is improved, that is, s_{11} parameter value is at least -10 dB. This is done by introducing four equal slits on the inner sides of the horizontal metallization (Fig 1. H4 - H5). These adjustments result in both preserved response of the other regions and the return loss correction of the BP region. They also introduce the shift of the BP region to the left, meaning, the BP region cut-off frequencies and bandwidth may be adjusted by changing the height of this slit.

Finally, two additional elements are added to correct the response of a very small simulation step: 4 small boxes (Fig 1. H3, W5) to correct the randomly picked frequencies of the higher spectrum, 4 vertical lines ("fangs", Fig 1. H6, W7) to improve the transition of the response at the lower corner frequency of the BP region.

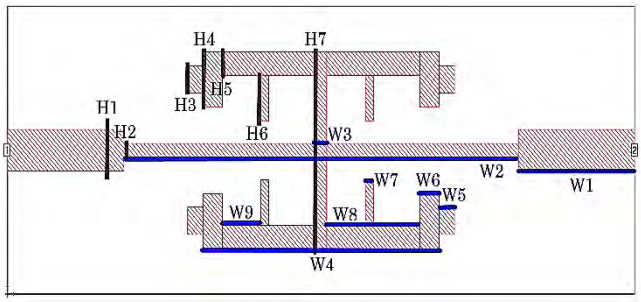

Fig. 1 Microstrip implementation of the filter

The dimensions of the filter are given as: w1 = 3, w2 = 10.3, w3 and h2 = 0.3, w4 = 6.1, w5 = 0.4, w6 and h5 = 0.5, w7 = 0.2, w8 = 2.4, w9 and h6 = 1, h1 = 0.9, h3 = 0.6, h4 = 1.2, h7 = 4.3 (all in mm).

Fig. 2 Filter (manufactured)

III. Simulation and Experimental Results

The simulation results suggest that the filter exhibits nearly prescribed behavior in terms of the corner frequencies, an LP response up to 3.58 GHz and a BP response from 14.38 to 21.65 GHz, the bandwidths and the rejections. The experimental results comply with the simulation results for the frequencies below 10 GHz. Although the simulated results indicate no losses for the BP response, the experimental results suggest the presence of up to 1.5 dB loss, which may be attributed to the fact that the FR-4 is prone to losses at the higher frequencies.

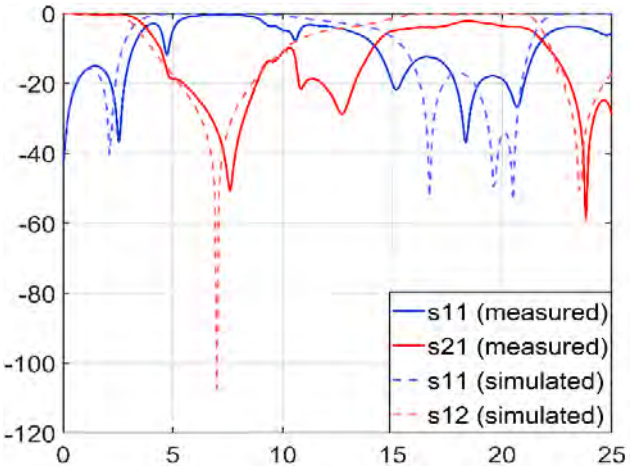

Fig. 2 Frequency response (magnitude vs frequency)

IV. Conclusion

A filter design implementing SIR and modified H-shaped structure was presented. The filter design was conducted observing a wide frequency range from 0 to 25 GHz. The filter exhibits a solid performance with virtually no passband loss, and a passband return-loss constantly over 20 dB, while maintaining the rejection of at least 10 dB at the frequency range from about 4 to 10.7 GHz in the stopband region. The proposed filter is very compact and utilizes a low-cost fabrication material, which highly reduces its production costs. Furthermore, it has been shown that the cutoff frequencies of this filter can be modified by adjusting certain dimensions in the filter design.

V. Acknowledgement

Author would like to thank Tamara Elektronik, Istanbul, for the fabrication and Associate Professor Dr. Hamid Torpi from the Yildiz Technical University for the measurement.

VI. References

[1] C. Y. Chen and C. Y. Hsu, "A simple and effective method for microstrip dual-band filters design," in IEEE Microwave and Wireless Components Letters, vol. 16, no. 5, pp. 246-248, May 2006.

[2] Y. P. Zhang and M. Sun, "Dual-Band Microstrip Bandpass Filter Using Stepped-Impedance Resonators with New Coupling Schemes," in IEEE Transactions on Microwave Theory and Techniques, vol. 54, no. 10, pp. 3779-3785, Oct. 2006.

[3] X. Y. Zhang, J. Chen, Q. Xue and S. Li, "Dual-Band Bandpass Filters Using Stub-Loaded Resonators," in IEEE Microwave and Wireless Components Letters, vol. 17, no. 8, pp. 583-585, Aug. 2007.

[4] J. T. Kuo, T. H. Yeh and C. C. Yeh, "Design of microstrip bandpass filters with a dual-passband response," in IEEE Transactions on

Microwave Theory and Techniques, vol. 53, no. 4, pp. 1331-1337, April 2005.
[5] L.-C. Tsai and C.-W. Huse "Dual-band bandpass filters using equal-length coupled-serial-shunted lines and Z-transform techniques" IEEE Trans. Microw. Theory Tech. vol. 52 no. 4 pp. 1111-1117 Apr. 2004.
[6] C. Y. Chen, C. Y. Hsu and H. R. Chuang "Design of miniature planar dual-band filter using dual-feeding structures and embedded resonators" IEEE Microw. Wireless Compon. Lett. vol. 16 no. 12 pp. 669-671 Dec. 2006.

Design and Fabrication of Microstrip Filter

Nermin Sejdić
Department of Electrical Engineering
International University of Sarajevo
Sarajevo, Bosnia and Herzegovina
nermin.sejdic@hotmail.com

***Abstract* – In this project I proposed Microstrip Filter with its projection, design, simulations and final analysis. The aim of the research is to introduce a new configuration of microstrip filter design. As the result, microstrip filter was composed of rectangular box in center, containing two parallel coupled lines on both sides with spacing between them. Feed lines are connected to the two ports, each on one side. The microstrip filter is simulated having a bandwidth from 2.4 to 5.5 GHz, where S11 = -31.489932 dB and S12 = -0.8056058 dB. Simulated data were in satisfactory agreement with measured results.**

***Keywords* - Coupled-line Bandpass Microstrip Filter (CBMF), Federal Communication Commission (FCC)**

I. INTRODUCTION

Filter design is one of the most interesting fields in microwave engineering. A wide number of different topologies allows to obtain specific responses for a wide range of applications. Inductive filters constitute a strategy of special interest due to their simplicity and easy manufacturing processes associated with these configurations [1]. There are many filters available in market but due to some reasons it has certain disadvantages. The lumped- element filter will not be good choice if a sharp rejection is needed because of its limited „Q" value. Helical filters are the best, as they provide excellent rejection profile but suffer from big size, assembly and tuning problems. Surface acoustic wave filters provides excellent performance but their shortcoming is lousy. The demand in high speed communication has led to the design and development of wide band filters to support the applications such as UWB technology that promises communication speed of up to 1000 Mbps. Because of its attractive feature in high speed wireless applications, the ultra-wide band communication has been authorized by FCC with unlicensed frequency spectrum of 7.5GHz from 3.1 GHz to 10.6 GHz in February 14,2002 [2]. Main challenge of using this type of technology is that we need to control undesired interferences. In order to have filter that successfully operates, large bandwidth is required. For CBMF, the fractional bandwidth of BPFs usually exceeds 100%. Based on the traditional parallel-coupled line structure, very strong coupling structure will be a must for such a wide bandwidth.

II. CBMF (COUPLED-LINE BANDPASS MICROSTRIP FILTER)

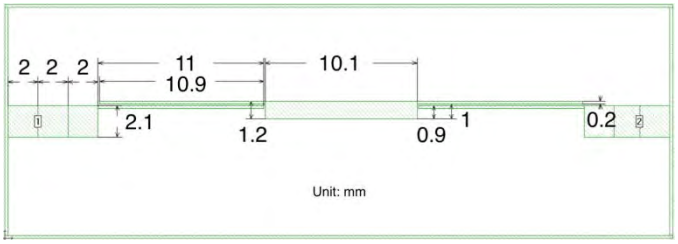

Figure 1. – Top view of CBMF

TABLE I. FILTER MEASUREMENTS

Name	Length	Width
Central Box	10.1 mm	1.20 mm
Coupled lines	11.00 mm	0.20 mm
Feedline Box	2.00 mm	2.10 mm
Spacing		0.10 mm

TABLE II. FILTER PARAMETERS

Parameters	Values
Dielectric thickness (Ɛr)	1.00
Cell size	0.10 mm
Box size	45.5 x 15.5 mm
Frequency	4.1 – 9.5 GHz

Figure 2. – Manufactured Microstrip Filter

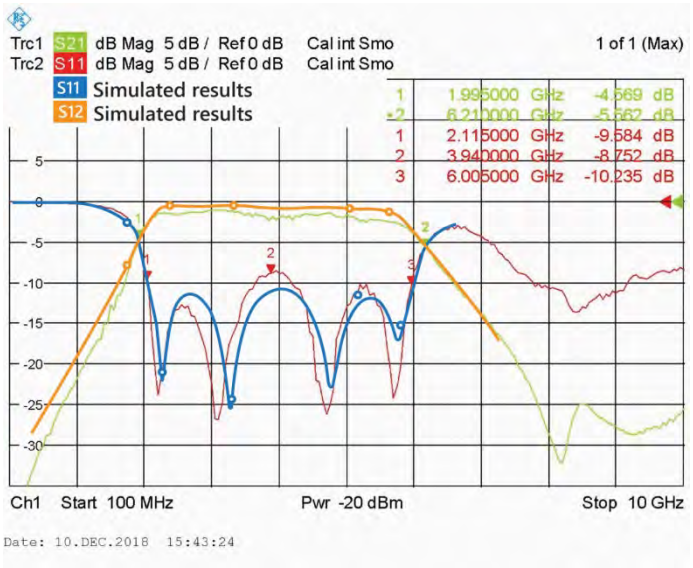

Figure 3. – Simulated and Measured Frequency vs magnitude output graph

III. PARAMETRIC STUDIES

In this table below, we observed how the frequencies are changing while changing different dielectric and air thicknesses. We observe S11 and S12 to make it ideal as possible.

TABLE III. CHANGING OF DIELECTRIC THICKNESSES AND AIR SPACE

Dielectric Thickness / Air (mm)	S11 (dB)	S12(dB)
1.2 / 6.0	3.28 GHz / -33.136385	3.28 GHz / -0.7505
1.4 / 7.0	3.16 GHz / -31.230012	3.16 GHz / -0.7122415
0.8 / 8.0	3.56 GHz / -29.222411	3.56 GHz / -0.8935692
0.6 / 8.0	4.62 GHz / -23.724173	3.76 GHz / -1.0708300
0.4 / 7.0	3.82 GHz / -21.385199	4.60 GHz / -1.7455671

Table IV is representing S11 and S12 while changing Dielectric and Air thickness together with Spacing between coupled lines.

TABLE IV. CHANGING COUPLED LINE SPACING AND DIELECTRIC THICNKESSES AND AIR SPACE

Dielectric Thickness / Air (mm)	Coupled line Spacing	S11(dB)	S12(dB)
1.0 / 10	0.2	3.92 GHz / -23.675388	2.72 GHz / -1.0870346
1.0 / 10	0.3	2.82 GHz / -19.709529	2.88 GHz / -1.4339948
1.6 / 7.0	0.3	2.64 GHz / -26.133362	2.64 GHz / -0.9873447
0.4 / 7.0	0.2	4.24 GHz / -21.415083	4.20 GHz / -1.8072443

Data set below in Table V is showing how the variables are depending on each other. Variables that we changed are: Coupled line Spacing, Central Box Width, Dielectric Thickness and air space. With small changes, measurements and outputs of filter are varying. Last bolded column is representing ideal and our final Microstrip filter. After many simulations and tries, we had found most suitable Microstrip filter.

TABLE V. CHANGING: DIELECTRIC THICKNESS AND AIR SPACE TOGETHER WITH COUPLED LINE SPACING AND CENTRAL BOX WIDTH

Dielectric Thickness / Air	Box Width / Coupled line Spacing	S11(dB)	S12(dB)
1.0 / 10	1.7/0.2	3.58 GHz / -34.571456	4.38 GHz / -1.1862205
1.2 / 6.0	1.0/0.2	2.66 GHz / -20.592003	4.00 GHz / -1.1212135
1.4 / 7.0	2.5/0.1	2.72 GHz / -20.142215	2.74 GHz / -0.8133966
0.4 / 7.0	2.2/0.1	4.80 GHz / -20.692008	2.98 GHz / -1.9248371
1.0 / 10.0	**1.2/0.1**	**3.42 GHz / -31.489932**	**3.42 GHz / -0.8056058**

IV. CONCLUSION

The main characteristic of this design is to find as good as possible filter in order to obtain ideal response and to meet nowadays requirements with wireless communication technologies [3], [4]. Simulation was conducted in a 3D planar high-frequency electromagnetic software called Sonnet. The research methods included some filter dimensioning, operational requirements analysis, fine tuning and parametric sensitivity analysis, optimization analysis, software simulation, filter manufacturing using PCB techniques, and filter testing procedures. The simulation results have shown that the proposed filter can provide impedance bandwidth from of 1.99 – 6.2 GHz. From the Figure 3., we can clearly see that simulated results of S11 (blue colored line) and S12 (orange colored line) have smoother output than measured S21 (green line) and S11(red line). After the testing procedures, the measured results were compared with the simulated results, it was concluded that the two designs in regards of filter performance and operation characteristics are identical with acceptable difference.

V. REFERENCES

[1] Francisco Javier Pérez Soler, Mónica Martínez Mendoza Fernando Daniel Quesada Pereira, David Cañete Rebenaque Alejandro Alvarez Melcon, and Richard J. Cameron., "Design of Bandpass Elliptic Filters Employing Inductive Windows and Dielectric Objects", IEEE Trans. Microw. Theory Tech., vol. 54, no. 11, Nov. 2006, pg.1-2

[2] Transition.fcc.gov/Bureaus/Engineering_Technology/Orders/2002/fcc02048

[3] H. Wang, L. Zhu and W. Menzel, "Ultra-Wideband Bandpass Filter with Hybrid Micro strip/CPW Structure," IEEE Microwave and Wireless Components Letters, vol. 15, pp. 844-846, December 2005

[4] L. Zhu, H. Bu, and K. Wu, “Aperture compensation technique for innovative design of ultra-broadband micro strip bandpass filter,” in *IEEE MTT-S Int. Dig.*, vol. 1, 2000, pp. 315–318.

Design and Simulation of a Quad Band Combiner for LTE Base Stations

Sabri YILMAZ
Dept of ECE, Yildiz Technical University, Istanbul, Turkey
f0516009@std.yildiz.edu.tr

Hakan P. Partal
Dept of ECE, Yildiz Technical University, Istanbul, Turkey
Dept of EECS, Syracuse University, Syracuse, NY
hpartal@ieee.org

***Abstract*— This paper presents a hybrid microwave quadruplexer architecture with a cavity structure and a shielded microstrip substrate which are combined inside one single housing. The purpose of the quadruplexer design is basically for cellular communications with operation frequencies of 825MHz (channel 1), 2060 MHz (channel 2), 2600 MHz (channel 3), and 3600 MHz (channel 4) and, the bandwidths of about 270, 280, 220, and 500 MHz, respectively. The proposed quadruplexer consists of two cavity type band pass filters (BPF) (channels 2 and 3) by using 3D coaxial microwave resonators and two PCB based low pass and high pass filters (channels 1 and 4) by using shielded microstrip line substrates. The quadruplexer design is modelled, simulated, and optimized using Keysight's Advanced Designed System (ADS) software and, simulated frequency response is published.**

Keywords—*cavity filters, coupling, multiplexers, microstriplines.*

I. INTRODUCTION

The basis of the cutting-edge products rely on the telecommunication technologies. In the past 50 years, telecommunication technologies have taken a crucial role for the most developed countries for their technological experience. One of the most important components in telecommunication, microwave filters has been getting important day by day. With the increasing number of cellular bands for 4G/LTE and 5G, the cellular station's and mobile RF front-end's critical components have shifted from the power amplifier to the filter. [3] In the next decades, Internet of Things (IoT) technologies and 5G cellular technologies will be able to be configured between each other. By this coexistence of the multiple standards will be essential the RF filters if the seamless combining to provide for high channel capacity is to success.

II. THE QUADRUPLEXER DESIGN

The designed four-channel quadruplexer here is a multiband combiner which consists of hybrid cavity resonators and commonly used microstriplines and design details are given below.

A. Shielded Microstripline Low Pass and High Pass Filter Design

The both proposed LPF and BPF were designed as 5th order generalized Chebyshev response with cut-off frequencies of 960MHz and 3350MHz, respectively, and teflon (PTFE based material) of dielectric constant ε_r is 2.1 was used as the dielectric substrate. A metal enclosure covers the all filter structure and make them grounded hence the electromagnetic interferances from the other channels are reduced. The shielded microstripline filter design parameters are as follows: For the low pass filter (LPF), H=20.4mm, h=2.54mm, t=0.42mm, and for the high pass (HPF), H=19.63mm, h=1.9mm, t=0.127mm, where H is the height of the metal housing, h is substrate height and t is conductor thickness. The ADS model of the HPF is depicted in Fig.1.

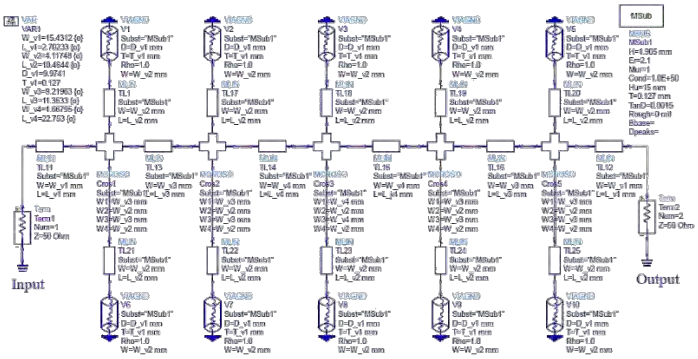

Fig. 1. ADS circuit model of the proposed HPF

B. Design of Microwave Cavity Band Pass Filters

a) Cavity Band Pass Filter Design for Channel-2 & 3:

The filter of the channel-2 is a 7th degree network and the folded configuration of resonators were realized as three conjoined trisection.[2]

The coupling values between the resonators can be calculated by using the low pass prototype "*g*" values. The coupling coefficients can be calculated by using equation [1]. The required input and output external quality factors are obtained as $Q_e = 5{,}903$, [2]. The 2-D circuit model in ADS software is given in Fig.2. The 3-D model of the band pass filters (channels 3 and 4) and the frequency responses are shown in Fig.3

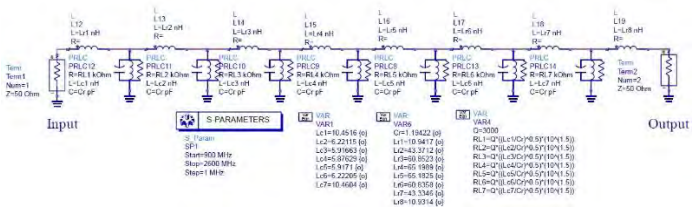

Fig. 2. ADS schematic design of the BPF of channel 2 with the lumped elements

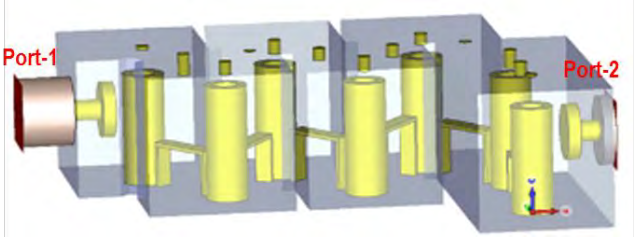

(a)

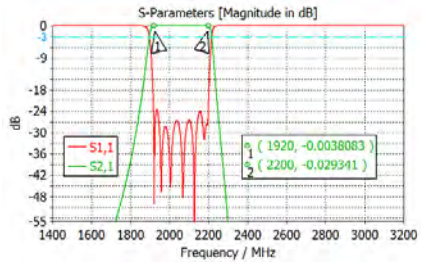

(b)

Fig. 3. 3D EM simulation model and results of the channel 2 BPF, (a) 3-D view of the filter, (b) Insertion loss (S21) and return loss (S11) responses.

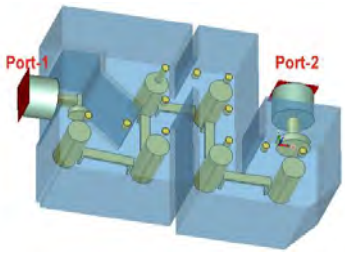

(a)

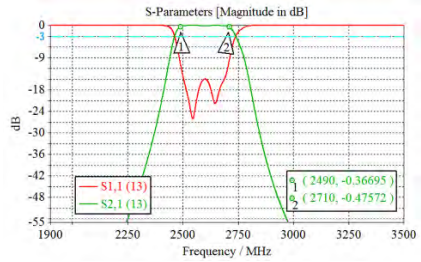

(b)

Fig. 4. The EM simulation results of proposed BPF for channel-3, (a) 3-D view of the filter, (b) Insertion loss(S21) and return loss results(S11).

III. QUADRUPLEXER DESIGN AND SIMULATION RESULTS

The simulation results of the output frequency response with 2-D circuit model are depicted in Fig.5. In the graph, S (5,1), S (5,2), S (5,3) and S(5,4) represent the pass band response (insertion loss) of each individual filter. The simulated quadruplexer filter responses in Figs. 3b and 4b show that the four frequency bands used in LTE cellular base stations are combined with low insertion loss in bands and good attenuation levels out of bands.

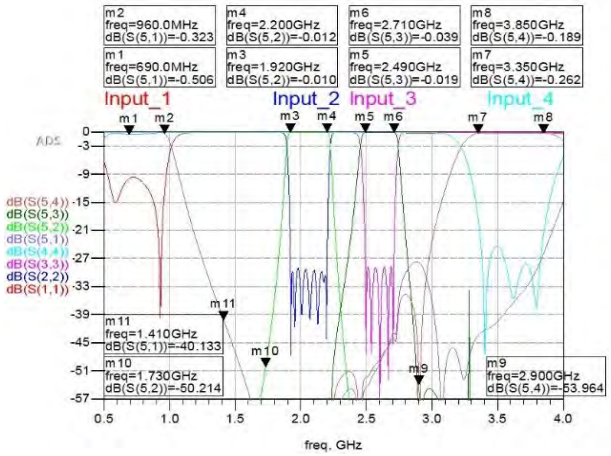

Fig. 5. The final simulation results of the combiner, Insertion loss and return loss results. (The Output Response of the Combiner)

The final quadruplexer should be modelled in an EM simulation tool such as Ansys HFSS or CST as depicted in Fig.6. If a final model is to be manufactured, the EM simulations and optimizations must be performed. It is outside of the scope of this paper but this process, which usually takes substantial amount of time, is needed before building an industrial prototype.

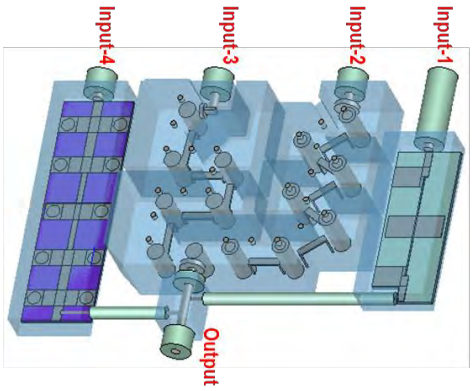

Fig. 6. 3D model of the Quadruplexer (a transparent view is shown)

IV. CONCLUSION

A four channel quadruplexer filter is presented in this paper. The final band pass filters, low pass and high pass filters were integrated inside a one case and simulated. Design steps were summarized and the frequency responses of all channels were validated through closed form microwave circuit simulator. Cavity based BPFs are used when neighboring band separations are narrow due to their extremely high Q factors. Microstrip based LPF and HPF are used for the outer channels as they do not interfere with mid-band channels which are further away.This paper is aimed to be a helpful reference for filter designers. Once 3D EM simulations and optimizations are performed, it will be possible to realize a commercial quadruplexer for use in conventional cellular bands including the early development of 5G network.

V. ACKNOWLEDGEMENT

This work has been partly supported by TÜBİTAK (The Scientific and Technological Research Council of Turkey) and Radarcomm, Ltd, under TEYDEB program.

VI. REFERENCES

[1] J. B. Ness, "A Unified Approach to the Design, Measurement, and Tuning of Coupled-Resonator Filters," *IEEE Trans. Microwave Theory Tech.*, vol. 46, no. 4, pp. 343-351, April 1998.

[2] R. J. Cameron, C. M. Kudsia and R. R. Mansour, "Microwave Resonators," in *Microwave Filters for Communication Systems: Fundamentals, Design, and Applications*, New Jersey, Wiley-Interscience A john Wiley & Sons, Inc.,Publication, 2007, pp. 407-408.

[3] "Key Elements for the 5G Network," SDxCentral, LLC, [Online]. Available: https://www.sdxcentral.com/5g/definitions/key-elements-5g-network/. [Accessed 7 12 2018].

Coupled-line Bandpass Filter

Ahmed Babić
Department of Electrical and Electronics Engineering
International University of Sarajevo
Sarajevo, Bosnia and Herzegovina
babicahmed@outlook.com

***Abstract* - In this paper, design, simulations and analysis of coupled-line bandpass filter is shown. The filter is completely unique due to its geometry, bandwidth and obtained results. It contains design, electromagnetic performance assessment, optimization, parameter variations, software simulation, operational analysis and brief author's comments. The proposed frequency was 5 GHz - 8 GHz. Through the design and simulations, around 5.4 GHz - 8.7 GHz is achieved. This filter is cheap to produce, since materials which are used are FR-4 for dielectric material and Copper as a metal type.**

Keywords – filter, coupled line, bandpass filter, frequency, design, simulation, dielectric, metal

I. INTRODUCTION

FIlter design is one of the most interesting fields in microwave engineering. A wide number of different topologies allows to obtain specific responses for a wide range of applications. Inductive filters constitute a strategy of special interest due to their simplicity and easy manufacturing processes associated with these configurations.[1] The basic structure of Microstrip line consists of a conductive strip separated from ground plane by dielectric. [2] A bandpass filter only passes the frequencies within a certain desired band and attenuates others signals whose frequencies are either below a lower cutoff frequency or above an upper cut-off frequency. [3] The broadband wireless access (BWA) is an important issue in current developments of the modern wireless communication system. To meet this trend, the bandpass filters with relatively wide bandwidth are frequently required in the RF front ends. In microwave communication systems, the bandpass filter is an essential component, which is usually used in both receivers and transmitters. [4] Figures 1 and 2 shows the simulation and design in Sonnet Suites [5].

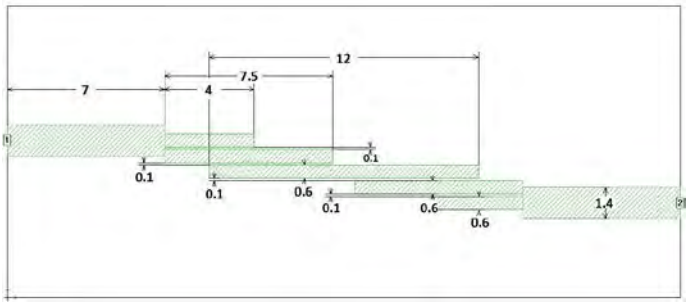

Fig. 1. Top view of bandpass filter

It can be observed on the Figure 1., that filter's left and right side are mirror symmetrical, all dimensions and spacing from both sides are equal. Port's thickness is 1.4 mm, while all other segments are 0.6 mm thick. Spacing between all segments is 0.1mm. Length of segments varies from 4 mm to 12 mm.

Brief specifications of the designed filter are:

* Dielectric constant Ɛr = 4.4 (FR-4)
* Substrate thickness = 10 mm (air), 1 mm (dielectric),
* Frequency range of simulations 3GHz - 10 GHz
* Bandwidth 3.3 GHz
* The filter box space is 30 mm x 13 mm
* Cell size is 0.1x0.1mm
* Number of cells : 300 (X direction), 130 (Y direction)
* Spacing between segments is 0.1 mm.

II. SIMULATION AND OUTPUT DATA

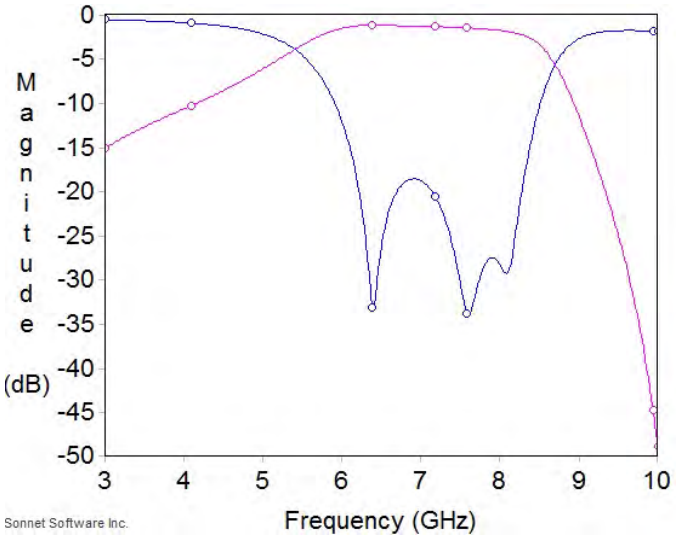

Fig. 2. Frequency vs magnitude output graph of the bandpass filter

As it is shown on the graph, this filter passes frequencies between 5.4GHz and 8.7 GHz. These values are more than satisfying, since expectations had a bandwidth range around 3GHz.

III. PARAMETRIC STUDIES AND VARIATIONS

On the coupled line bandpass filter, physical properties and parameters were changed, and simulation output is analyzed. Parameters that were changed in this case were metal type, dielectric material, thickness of dielectric and input/output segments thickness.

A. Thickness of input/output segments

TABLE I. S-PARAMETERS WHEN THICKNESS OF INPUT/OUTPUT PORTS IS CHANGED

Thickness of input/output	S11(dB)	S12(dB)
1.4 mm	-34 dB	-1.12 dB
1.7 mm	-42.21 dB	-1.18 dB
1.0 mm	-9.66 dB	-4.06 dB
2.0 mm	-33.58 dB	-1.31 dB

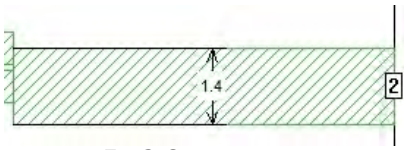

Fig. 3. Output segment

In the figure 3, Output segment is shown which is the same as Input segment. Variation of its thickness is done. It can be concluded from the table that this segment gives the best result with the thickness of 1.4 mm. Due to S12 it is taken thickness of 1.4 mm, because it gives magnitude of -1.12 dB.

B. Metal type

TABLE II. S-PARAMETERS WHEN METAL IS CHANGED

Metal type	S11(dB)	S12(dB)
Copper	-34 dB	-1.12 dB
Gold	-33.5 dB	-1.15 dB
Aluminum	-33.36 dB	-1.16 dB
Brass	-32.69	-1.24 dB
Silver	-34.08	-1.125 dB

In the table, parameters are shown when metal type is changed. Copper is the most commonly used and it is very affordable. This metal type gives the best output result, even though other metals are giving similar ones.

C. Dielectric thickness

TABLE III. S-PARAMETERS WHEN THICKNESS OF DIELECTRIC IS CHANGED

Thickness of dielectric	S11(dB)	S12(dB)
1	-34 dB	-1.12 dB
1.6	-25.92 dB	-1.02 dB
0.4	-17.87 dB	-2.4 dB

Thickness of dielectric plays a huge role in designing filter. Optimum result is while 1 mm thickness is used. 1.6 mm thickness gives result with a smaller bandwidth, not a clean signal and it is decided to reject that output. Thickness of 0.4 is not satisfying the desired output at all, since it is required to be above -2dB at least.

D. Dielectric material

TABLE IV S-PARAMETERS WHEN DIELECTRIC MATERIAL IS CHANGED

Dielectric material	S11(dB)	S12(dB)
FR-4	-34 dB	-1.12 dB
Alumina 96%	-53.99 dB	-0.2 dB
Quartz (fused)	-44 dB	-0.13 dB
Silicon dioxide	-46.99 dB	-0.126 dB
Ferro A6M	-55.191 dB	-0.249 dB
Polyimide	-39.61 dB	-0.272 dB

In this case, type of dielectric material is changed. Thickness of dielectric (1 mm) and metal type (Copper) remained the same by default. From the table it is seen that FR-4 is not giving the best results, but this filter will be fabricated and FR-4 is taken due various reasons. This type of material is very common, accessible and affordable. Alumina 96% is giving very strange output with small bandwidth, not satisfying the expectations and it is not taken into consideration.

IV. CONCLUSION

Design of the filter, thickness of segments, gap width, play the most important role in fabricating microstrip filter. This paper has shown how different parameter variations are affecting the bandwidth of the coupled line bandpass filter. Even though some dielectric materials are giving better results, due to practical reasons, availability, affordability, FR-4 is chosen as a dielectric material. Parameters which are changed during design of the filter are shown in the third part of the paper. Analyzing the output, it is observed that this filter has a wide range of more than 3.3 GHz.

V. REFERENCES

[1] Francisco Javier Pérez Soler, Mónica Martínez Mendoza Fernando Daniel Quesada Pereira, David Cañete Rebenaque Alejandro Alvarez Melcon, and Richard J. Cameron, ”Design of Bandpass Elliptic Filters Employing Inductive Windows and Dielectric Objects”, IEEE Trans. Microw. Theory Tech., vol. 54, no. 11, 2006, pg.1-2

[2] Jia-Sheng Hong, “Microstrip Filter For RF/Microwave Application”, John Willey and Sons, Inc, Second edition, pp. 129– 133, 2001

[3] S. Srinath “Design of 3rd Order Coupled Line Bandpass Filter for Wireless Application using Agilent ADS” IJIRSET Vol.5, Issue 7, July 2016

[4] D.M. Pozar, “Microwave engineering”, 2nd edition, 1998 John-Wiley & Sons.

[5] Sonnet Suites, ver. 16, Sonnet Software Inc., North Syracuse

Design and Analysis of S-Shaped Slitted Microstrip Patch Antenna

Lamija Herceg
Department of Electrical and Electronics Engineering
International University of Sarajevo
Sarajevo, Bosnia and Herzegovina
lamija_1995@live.com

***Abstract* - This paper introduces a new configuration of the microstrip patch antenna. After the optimization of the rectangular antenna in terms of performance, space and price, the final design is proposed as the S-shaped patch with two additional slits. The resonance frequency of the antenna is 8.63 GHz, with the reflection coefficient of -37.76 dB, making the antenna suitable for the X band applications. The maximum achieved gain is 5.4 dBi. Compact size of 24 mm x 16 mm, as well as the affordable materials used, enable the wide application of this configuration.**

Keywords—patch antenna; microstrip; S shape; FR4; Sonnet software

I. INTRODUCTION

With the strong advancements in wireless communications, there is a growing demand for miniature, low-cost, easy-to-fabricate, multiband, dualband and wideband antennas for use in commercial communications systems [1]. A communication system is usually required when the information is to be conveyed over a distance. In today's modern communication industry, antennas are the most important components required to create a communication link. A development in large scale integration which is the result of electronic circuit miniaturization is the apex factor contributed for the recent advances of microstrip antennas [2]. A microstrip patch antenna offers a low profile, light weight, low fabrication cost, which provides great advantages over traditional antennas. However, narrow bandwidth came as the major disadvantage for this type of antenna [3]. The shape and design of the patch become very versatile in terms of operating frequency, polarization, pattern and impedance [2]. Different designs were investigated in order to obtain the optimized results.

In this paper, a compact design of an S-shaped slitted patch antenna (MPA) with the resonance frequency of 8.63 GHz is introduced. Microstrip technology is used for simplicity and ease of fabrication. The design and simulation are performed using method of moments based electromagnetic simulator Sonnet Software. The simulation resulted in the return loss plot and gain plot that satisfy the set requirements. Even though the antenna has generated four bands below the -10 dB threshold for the reflection coefficient, the band with the lowest coefficient (-37.76 dB) was chosen for the analysis. The S-shaped-configuration results were improved by adding the two additional slits, which resulted in higher gain and better current distribution. The compact size and affordable materials make the antenna suitable for wide applications.

II. DESIGN METHODOLOGY

The design of the proposed S-shaped slitted MSA starts with the rectangular shaped patch. S shape is easily formed by cutting two slits from the mentioned patch. In addition to that, the two additional smaller slits are cut from the two opposite sides to obtain better radiation. The designed antenna structure along with its dimensions is shown in Figure 1. and Table 1.

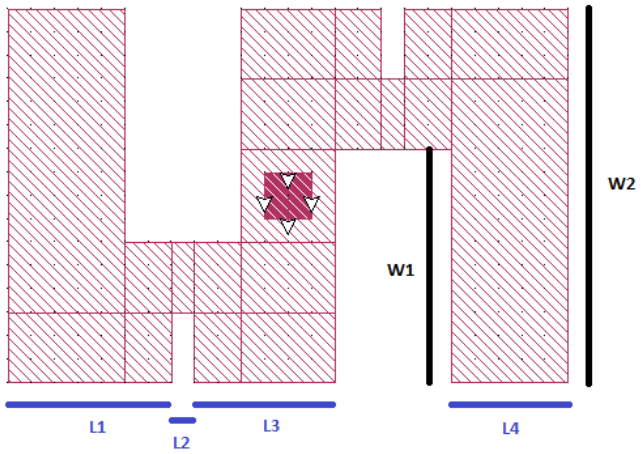

Fig. 1. Configuration of the proposed antenna

TABLE I. Dimensions of the antenna

L1	L2	L3	L4	W1	W2
7 mm	1 mm	6 mm	5 mm	10 mm	16 mm

The total size of the antenna is 24 mm x 16 mm. It has a symmetrical structure, which means that the denoted lengths and widths are repeatable through the design. The antenna was placed in a box whose size is approximately ten times larger than the antenna's size itself, and the top cover was chosen to be free space.

The electromagnetic performance of the designed antenna depends highly on the dielectric layers composition and width, the metal type, and the port properties. The dielectric layer in the study consists of a 1.6 mm-thick FR-4 substrate with the relative permittivity of 4.4 and the dissipation factor of 0.02, and a layer of air whose thickness is 100 mm. Along with the

dielectric constant and loss tangent, the metal type plays a crucial role in antenna performance. The patch is generally made of conducting material such as copper or gold and can take any possible shape [3]. In this study, the lossless copper is used in the S shape. The fourth main factor that affects electromagnetic performance of the antenna is the feed line, which is attached to the middle point of the antenna and a port with the resistance of 50 Ω. Location of the feed, as well as the additional slits, highly affect the surface current distribution. The feed attached to the middle point of the antenna resulted in the currents distributed over greater part of the surface, as it can be seen in Figure 2.

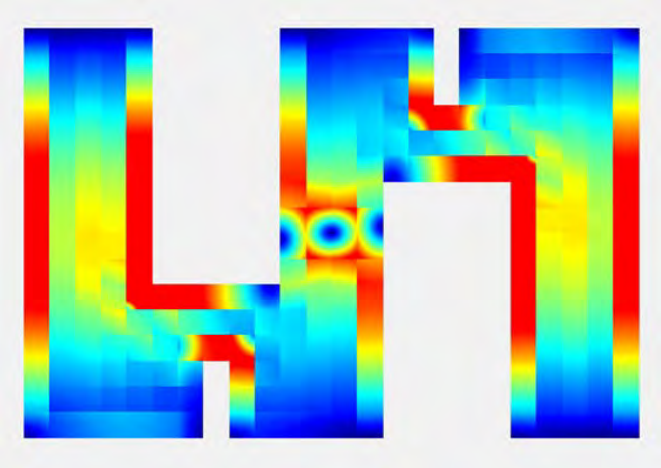

Fig. 2. Surface current distribution

Bandwidth and gain are the most desirable parameters in microstrip patch antenna designs. Enhancing both bandwidth and gain is a challenging task [4]. First graph that is consider is the return loss graph that is used to determine the reflection coefficient and the bandwidth.

From the return loss (S_{11}) plot shown in Figure 3. Of the proposed microstrip patch antenna it is observed that the reflection coefficient at the input of the proposed S-shaped microstrip patch antenna is −37.76 dB of analysis at the resonance frequency. According to the simulated results, the bandwidth from 8.604 GHz to 8.656 GHz is achieved, and the antenna's center frequency equals 8.63 GHz.

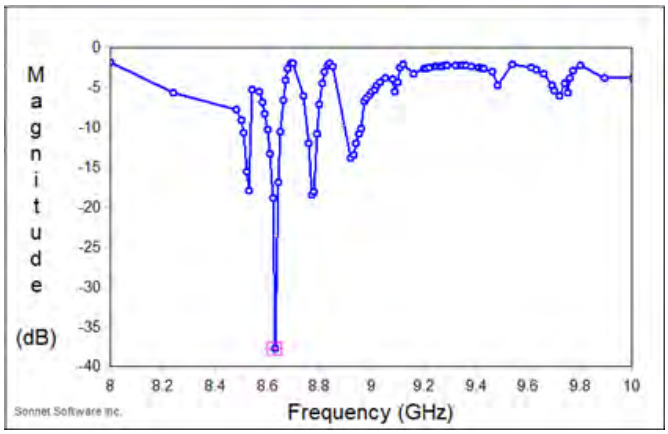

Fig. 3. S_{11} plot of the proposed patch antenna

The gain of the antenna reaches 5.4 dBi in its highest point. The polarization graph can be seen in the Figure 4. E Theta is achieved to be greater than 5 dBi, while E Phi is achieved to be much less than the set threshold of -5 dBi, having the maximum of -21.75 dBi.

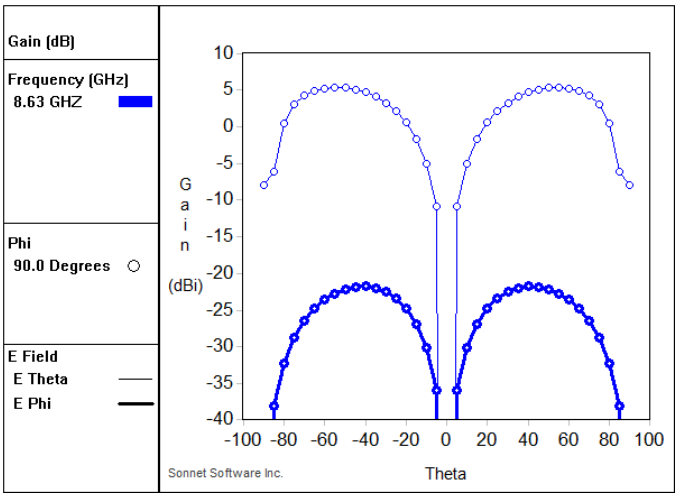

Fig. 4. Gain plot of the proposed patch antenna

III. Conclusion

Microstrip antennas have become a rapidly growing area of research. Their potential applications are limitless, because of their light weight, compact size, and ease of manufacturing [5]. The designed and simulated microstrip patch antenna has shown good performance and size characteristics. It satisfied the set requirements of return losses and gain. However, the bandwidth should be increased.

A few approaches can be applied to improve the microstrip antenna bandwidth such as increasing the substrate thickness, introducing parasitic element either in coplanar or stack configuration, and modifying the shape of a common radiator patch by incorporating slots.

References

[1] R. Kumar and E. K. Saurabh, "Wireless applications of multiband micro-strip S-shaped patch antenna," International Journal of Technical Research (IJTR), vol. 5(1), 2278-5787, March 2016.

[2] B. Abirami and M. Shalini, "Designing of S shaped microstrip patch antenna for broadband application using slotting technique," International Journal for Research in Applied Science & Engineering Technology (IJRASET), vol. 4(11), 2321-9653, November 2016.

[3] B. S. Niboriya, C. Choudhary and G. Prabhakar, "S-shape wideband microstrip patch antenna with enhanced gain and bandwidth for wireless communication," International Journal of Computer Applications, vol. 73(7), 0975 – 8887, July 2013.

[4] D. Singh, A. K. Gupta and R.K.Prasad, "Analysis and design of S-shaped microstrip patch antenna," IOSR Journal of Electronics and Communication Engineering (IOSR-JECE), vol. 7(4), 2278-8735, September 2013.

[5] J. M. Patel, S. K. Patel and F. N. Thakkar, "Comparative analysis of S-shaped multiband microstrip patch antenna," International Journal of Advanced Research in Electrical, Electronics and Instrumentation Engineering, vol. 2(7), 2320 – 3765, July 2013

1×9 Substrate Integrated Waveguide (SIW) Power Divider

Orcun Kiris
Microwave and Antenna Systems Group
TUBITAK Space Technologies Research Institute
Ankara, Turkey
orcun.kiris@tubitak.gov.tr

Mesut Gokten
Microwave and Antenna Systems Group
TUBITAK Space Technologies Research Institute
Ankara, Turkey
mesut.gokten@tubitak.gov.tr

Lokman Kuzu
Microwave and Antenna Systems Group
TUBITAK Space Technologies Research Institute
Ankara, Turkey
lokman.kuzu@tubitak.gov.tr

***Abstract*—This paper presents a 1×9 SIW power divider design based upon the referenced 1×3 SIW power design by concatenating them successively. The designed nine-way power divider has nearly equal amplitude and uniform phase distribution between *9.34-10.38* GHz. The maximum magnitude and phase differences between each output ports are about *0.5* dB and *2.5* degrees, respectively, at the operating frequency band. The performance of the designed power divider is quite close to ideal power equality factor (9.54 dB) for nine-way power division.**

Keywords— Substrate Integrated Waveguide, power divider.

I. INTRODUCTION

Conventional waveguide power dividers are widely utilized in microwave and the millimeter wave communication subsystems to achieve high-Q and high power handling capability with low insertion losses. However, waveguide power dividers suffer from the drawbacks of the waveguides such as relatively high cost, large size, inflexibility and difficulty of mass production. Also, waveguide technology requires bulky and lossy transitions to be integrated with the planar structures because of their size and nonplanar physical characteristics. On the other hand, microstrip power dividers have been commonly utilized due to their low cost, low size, flexibility and ease of integration with planar circuits. However, they have high ohmic and insertion losses especially at the millimeter wave frequencies. Substrate Integrated Waveguide (SIW) is a new wave guiding structure that is proposed in [1], [2] to overcome these difficulties. SIW structures have been constructed by two parallel rows of electroplated via holes in a planar dielectric substrate that has conductive top and bottom layers. SIW shows similar propagation characteristics with rectangular waveguides known as low-loss structures due to this structural property. Also, SIW structures can be fabricated as a printed circuit board (PCB) assembly, and hence, they have similar advantages with microstrip structures such as low profile, low weight and low loss. Furthermore, SIW based components have low transition loss since they can be monolithically integrated with planar feed networks. To benefit from the advantages of SIW technology in power division operations, SIW power dividers have been developed.

The conventional waveguide power divider approaches can be used in the design of the SIW power divider due to similarity in the propagation characteristics with rectangular waveguides. In the literature, two main waveguide power divider types which are T-Junction and Y-Junction power dividers are applied with using SIW technology [3]. Thanks to these fundamental two-way power divider types, various multi-way power dividers that have even numbered output ports can be obtained with the help of the successive addition technique. A 1×16 SIW multi-way power divider utilizing the successive addition technique is proposed in [4]. Moreover, many power divider studies using same technique with different even numbered output ports are available in the literature [5]-[10]. However, successive addition of these fundamental power divider types cannot meet the needs of the odd numbered power division operation because these basic two-way SIW divider types only allows "1×2^n" (n=1, 2, 3…) power dividers. To meet the odd numbered output ports requirement with this method, the input power has to be divided into minimum "2^n" numbered ports but this is greater than required output port number and unnecessary ports should be terminated. The input power is divided more than required due to unused ports and this leads additional insertion and reflection losses. For instance, when needed nine-way division operation, the seven of the sixteen output ports should be terminated in conventional successive addition method. Furthermore, unused ports bring along the suitable RF terminator cost and usable space consumption problems. In order to effectively meet the needs of power dividers that have odd numbered output ports, a novel basic 1×3 SIW power design is presented in [11]. The measurement results of the proposed power divider indicate that the structure provides equal amplitude and uniform phase distribution at the operating frequency band [12].

II. DESIGN OF THE POWER DIVIDER

The proposed 1×9 SIW power divider is based on the referenced 1×3 SIW power design that can be called milestone of the power dividers with odd numbered output ports. The nine-way divider is designed by adding a same three-way divider to each output port of the referenced three-way power divider. The input power divided into three at the first three-way power divider and the divided powers at each output ports are divided into three again at the secondary three-way power dividers.

The schematic view of the designed 1×9 SIW power divider is shown in Fig. 1. It is designed on 1.575 mm thick Rogers 5880 ($\varepsilon_r = 2.2, \tan\delta = 0.0009$ *at 10 GHz*) that is the same substrate used for design of the power divider in [11]. The red dashed-lines presents the connection points between first and secondary 1×3 SIW power dividers. All vias in the design are identically the same and equally spaced. Furthermore, the structure seen in Fig. 1 has a mirror-image

This work is partially supported by TUBITAK Space Technologies Research Institute (TUBITAK UZAY).

symmetry with respect to the blue dashed-line and the S-parameter results of symmetrical ports are equal to each other (namely, $S_{21}=S_{10\,1}$, $S_{31}=S_{91}$, $S_{41}=S_{81}$, $S_{51}=S_{71}$).

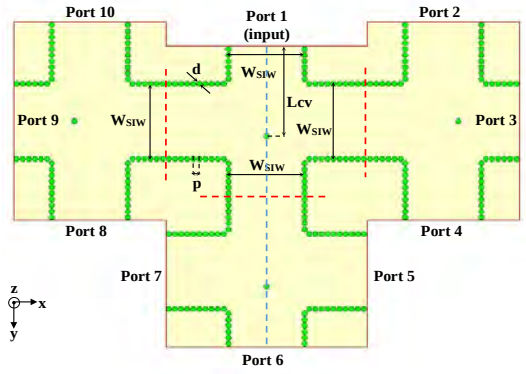

Fig. 1. Designed 1×9 Power Divider

The input power is divided into nine output ports when the structure is excited from Port 1. E-field distribution of this divider at the operation frequency is shown in Fig. 2.

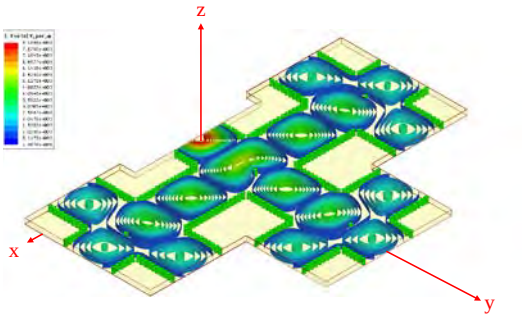

Fig. 2. Designed 1×9 Power Divider

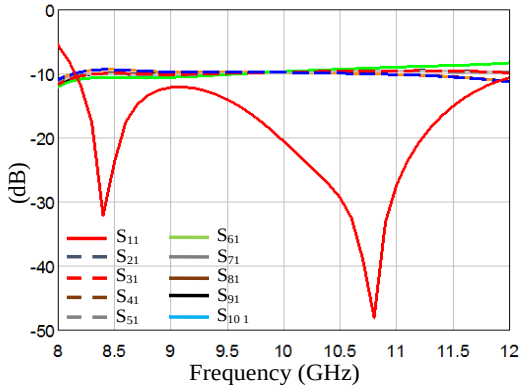

(a)

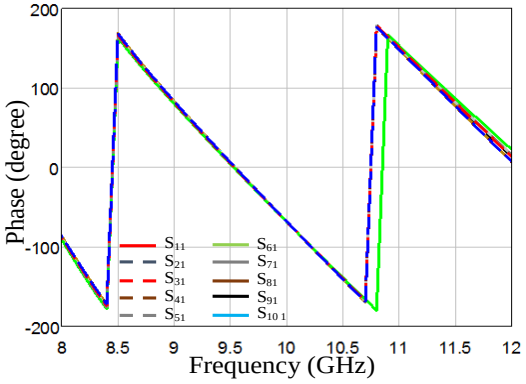

(b)

Fig. 3. (a) Magnitude and **(b)** Phase Results of the designed 1×9 SIW power divider EM simulation.

The designed 1×9 SIW power divider can be utilized in several microwave and millimeter-wave structures that requires uniform feeding such as the same phase and power level at all of the output ports. The simulation results of the divider are given in Fig. 3.

As seen in Fig 3, the designed power divider provides nearly equal amplitude and uniform phase distribution at the output ports between *9.34 - 10.38* GHz frequencies. The magnitudes of insertion losses (S_{21}, S_{31}, S_{41}, S_{51}, S_{61}, S_{71}, S_{81}, S_{91} and $S_{10\,1}$) are very close to the ideal value *(-9.54 dB)* and the maximum phase differences between the output ports are within the range of *2.5* degrees in the operating frequency band. Also, the return loss (S_{11}) values are considerably low particularly during the frequency band and it is less than *-13 dB*. This power divider has demonstrated the advantages of a low-profile, design simplicity and low insertion losses at each output ports. The fabrication process of the designed power divider continues.

REFERENCES

[1] J. Hirokawa, and M. Ando, "Single-Layer Feed Waveguide Consisting of Posts for Plane TEM Wave Excitation in Parallel Plates," IEEE Transactions on Antennas and Propagation, vol.46, no.5, pp.625-630, May 1998.

[2] [2] D. Deslandes and K. Wu, "Integrated Microstrip and Rectangular Waveguide in Planar Form," IEEE Microwave and Wireless Components Letters, vol. 11, no. 2, pp. 68-70, Feb. 2001.

[3] [3] S. Germain, D. Deslandes, and K. Wu, "Development of substrate integrated waveguide power dividers", IEEE CCECE Canadian Conference on Electrical and Computer Engineering, vol.3, pp. 1921-1924, 2003.

[4] [4] Z. C. Hao, W. Hong, H. Li, H. Zhang, and K. Wu, "Multiway broad-band substrate integrated waveguide (SIW) power divider", IEEE AP-S Int. Symp., pp. 639 –642, Paper 3-8 1A, Jul. 2005.

[5] [5] Jin Li and Tianlin Dong "Design of a Substrate Integrated Waveguide power divider that uses a neural network,"2010 2nd International Conference on , Computer Engineering and Technology (ICCET), vol.7, no., pp.V7-448-V7-452, 16-18 April 2010

[6] [6] Chen, K., Yan, B.,and Xu, R., "A novel W-band ultra-wideband substrate integrated waveguide (SIW) T-junction power divider,"2010 International Symposium on Signals Systems and Electronics (ISSSE), vol.1, no., pp.1-3, 17-20 Sept. 2010

[7] [7] X. Xu, R. G. Bosisio, and K. Wu, "A new six-port junction based on substrate integrated waveguide technology" IEEE Trans. Microw.Theory Tech., vol. 53, no. 7, pp. 267 –273, Jul. 2005.

[8] [8] Meiying Zou, Zhenfeng Yin, Zhenhai Shao, Lianfu Liu, and Xueyong Zhu, 2011 International Conference on"Design of Ka-band substrate integrated waveguide power dividers/combiners," Computational Problem-Solving (ICCP), 2011 International Conference on , vol., no., pp.361-363, 21-23 Oct. 2011

[9] [9] Zou, X., Tong, C.-M., Yu, and D.-W., "Y-junction power divider based on substrate integrated waveguide," Electronics Letters, vol.47, no.25, pp.1375-1376, December 8 2011.

[10] [10] Kaijun Song, Yong Fan, and Yonghong Zhang, "Eight-Way Substrate Integrated Waveguide Power Divider With Low Insertion Loss," IEEE Transactions on Microwave Theory and Techniques, vol.56, no.6, pp.1473-1477, June 2008

[11] [11] O. Kiris, V. Akan, M. Gokten and L. Kuzu, "Three-way substrate integrated waveguide (SIW) power divider design," 2016 IEEE/ACES International Conference on Wireless Information Technology and Systems (ICWITS) and Applied Computational Electromagnetics (ACES), Honolulu, HI, 2016, pp. 1-2.

[12] [12] O. Kiris, V. Akan, M. Gokten and L. Kuzu, "Implementation of three-way power divider based on substrate integrated waveguide,"

2017 USNC-URSI Radio Science Meeting (Joint with AP-S Symposium), San Diego, CA, 2017, pp. 111-112.

Bosnian Currency Recognition Using Region Convolutional Neural Networks

Ali Abd Almisreb, Sherzod Turaev

Faculty of Engineering and Natural Sciences
International University of Sarajevo
Sarajevo, Bosnia and Herzegovina
aalmisreb@ius.edu.ba,
sturaev@ius.edu.ba

***Abstract*— In this paper, a region convolutional neural network (R-CNN) is implemented in order to recognize Bosnian paper and coin currencies. Convolutional neural network (CNN) is implemented to train R-CNN. The training is conducted based on a collected dataset of 153 images. The dataset is split into 136 and 17 images for training and testing respectively. The training is conducted using GPU GTX 1050. The proposed model has achieved 99.22% accuracy of the recognition.**

Keywords*— Deep Learning, R-CNN, CNN, GPU, currency recognition

I. INTRODUCTION

At present, there are many techniques utilized to image classification, fingerprint based recognition, iris and ear recognition, etc. As well known, currency papers are one of the most used medium for circulation, whereas, the currency characteristics vary from country to another. Relying on image recognition approaches, specialists investigate and make comparisons of different algorithms on their specific identification methods by studying several characteristics of the currency paper such as the currency color and specific data representation of currency, eventually, they will find out their specific identification techniques.

Convolutional Neural Networks (CNN), or as well known as deep learning, requires a huge amount of data. The accuracy of the currency recognition algorithm will be dramatically increased by utilizing a big set of data for training. Therefore, the recognition will continuously enhance with more data allocated for training [1]. Another approach suggested by [2] for currency recognition. This approach is based on Ensemble Neural Network (ENN). It anticipated for solving the problem of currency recognition by applying image compression on grayscales of distinct types of images. The compression process is done by utilizing every pixel as an output, and then feed it into the neural network in order to perform image preprocessing, and finally increasing the data. Having more sets helps to produce lower error rate of a single network by means of identifying the individual neurons. In 2008, another Currency detection algorithm is proposed based on compressed gradation. The Artificial Neural Network (ANN) assists in eliminating the noise from the background by implementing a special linear transformation function and ensuring that the image features will not be affected. The threshold value of the grayscale images was set to be in range between 0 and 125. In order to enhance the robustness for currency detection, an edge detection method was considered. Therefore, to achieve that, a set of three-layer backpropagation neural network was presented, which is effectively detected by different classifications [3]. Hidden Markov Model (HMM) is used for currency recognition too. In this method, recognizing the currency paper is no longer limit to the color and the size of the paper but it is based on the texture of currency. Therefore, the any damage of currency surface can be overcome. On the other hand, unclean paper currency could not be recognized [4]. In general, R-CNN composed of several stages. Mainly, create the regions of interest which are bounding boxes that have a high similarity of containing an interesting object. Next, feature extraction from each region proposal by using a CNN. Another image which contains a bounding-box is warped in order to match the size of the input layer in the CNN and then provide it to the next layer. After feature extraction, the features vector is fed to support vector machine (SVM) which in turns will provide the final classification decision. RCNN is trained in multiple stages. [5]. The rest of the paper is organized as follows: the proposed methodology and the achieved results and finally the conclusion.

II. METHODOLOGY AND RESULTS

In this paper, we used a dataset consists of 153 images. The dataset covers the front and back sides of the following Bosnian currency notes: 5, 10, 20 and 50 cents and 1, 2, 5, 10, 20, 50 and 100 Bosnian Mark (KM). Then, image labeling is conducted to assign a specific label for each image as illustrated in Figure 1. Image labeling is an essential step to train the deep learning model. The next step is to split the dataset into training and testing images. In our case, we allocated 136 images for training and 17 images for testing. A CNN comprises of 11 layers which is created to

train the main object detector which is R-CNN [6]. Table 1 shows the proposed CNN. It consists of 2 convolutional layers followed by ReLU layers. Softmax is used to conduct the classification instead of SVM.

The CNN is considered as a model for extracting the currency note characteristics. The R-CNN model is trained over a single GPU GTX 1050. The overall achieved accuracy is 99.22% as illustrated in Figure 2. It shows also R-CNN is training over 10 epochs. Figure 3 depicts the model's loss curve.

The final result is presented in Figure 4, it shows that the trained model is succeed in recognizing the coins with high confidence. This figure shows also that the model is able to detect the object.

Table 1: The proposed CNN architecture

1	image input	1000x600x3 images with 'zero-center' normalization
2	Convolution	32 3x3 convolutions with stride [1 1] and padding [1 1 1 1]
3	ReLU	ReLU
4	Convolution	32 3x3 convolutions with stride [1 1] and padding [1 1 1 1]
5	ReLU	ReLU
6	Mas Pooling	3x3 max pooling with stride [2 2] and padding [0 0 0 0]
7	Fully Connected	64 fully connected layer
8	ReLU	ReLU
9	Fully Connected	12 fully connected layer
10	Softmax	Softmax
11	Classification output	crossentropyex

Figure 1: Image labeling

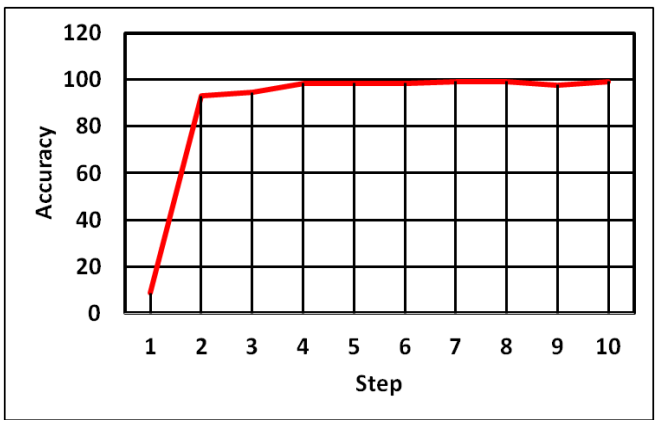

Figure 2: R-CNN training curve

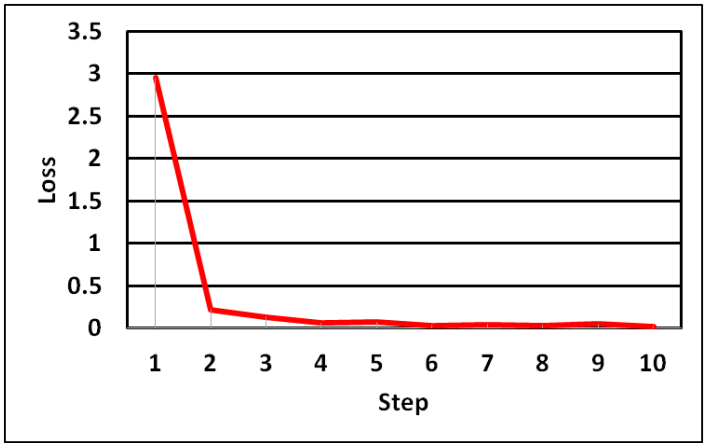

Figure 3: Loss curve

Figure 4: Experimental results

III. Conclusion

Currency recognition is an important factor nowadays due to its significant role in implementing smart shops which are entirely depend on deep learning algorithms. In this research, we have introduced a R-CNN model for recognition of Bosnian currency elements. The model has achieved a good accuracy in recognition of currencies. This idea can be generalized for recognition of the currencies of different Balkan countries.

References

[1] Wu R., Yan S., Shan Y., Dang Q., and Sun G. "Deep image: Scaling up image recognition". *arXiv preprint arXiv*: 2015 Jan 13, pp. 1501.02876.

[2] Debnath, K.K., Ahdikary, J.K. and Shahjahan, M., "A currency recognition system using negatively correlated neural network ensemble," *2009 12th International Conference on Computers and Information Technology*, Dhaka, 2009, pp. 367-372.

[3] Gunaratna, D.A.K.S., Kodikara, N.D. and Premaratne, H.L., "ANN based currency recognition system using compressed gray scale and application for Sri Lankan currency notes-SLCRec", *Proceedings of World academy of sciecne, engineering and technology*, 2008, 35, pp.235-240.

[4] Hassanpour, H. and Farahabadi, P.M., "Using Hidden Markov Models for paper currency recognition", *Expert Systems with Applications*, 2009, 36(6), pp.10105-10111.

[5] Girshick, R., "Fast R-CNN", *In Proceedings of the IEEE international conference on computer vision*, 2015, pp. 1440-1448.

[6] Girshick, R., Donahue, J., Darrell, T., and Malik, J., "Rich Feature Hierarchies for Accurate Object Detection and Semantic Segmentation", *Proceedings of the IEEE Conference on Computer Vision and Pattern Recognition*. 2014, pp. 580-587.

Three Element Hairpin Bandpass Filter

Elmedin Skopljak
Department of Electrical and Electronics Engineering
International University of Sarajevo
Sarajevo, Bosnia and Herzegovina
elmedinskopljak@hotmail.com

***Abstract* – This paper represents the three element hairpin bandpass filter with its design, analysis and simulation. This paper contains introduction about filters, then design and output graph of three element hairpin bandpass filter, after that there are parametric studies and variations and in the end there is author's comment and conclusion. The achieved frequency of the designed hairpin bandpass filter is around 2.54 - 3.01 GHz. Materials which we need for fabrication of this filter is copper as a metal, and FR-4 for dielectric. They are most commonly used for fabrication filters, and also the cheapest.**

Keywords – filter, hairpin, bandpass filter, frequency, design, simulation, dielectric, metal

I. INTRODUCTION

Filters play important roles in many RF/microwave applications. [1] A bandpass filter is one that passes frequencies within a certain range and attenuates frequencies outside that range. For most of the wireless applications high quality and compact sized RF/microwave filters at low cost are required. [2] Out of various bandpass microstrip filters, hairpin filter is one of the most commonly used. The concept of hairpin filter is same as parallel coupled half wavelength resonator filters. [3] There are many benefits of this type of filter. Some of them are: small size and simple structure, best possible space utilization as compared to coupled and parallel coupled microstrip realizations, its band in which passes frequencies, which is below 3 GHz, and many wireless applications take place at the frequency below 3 GHz. [4] Figures 1 and 2 shows the simulation and design in Sonnet Suites [5].

In Figure 1 we can see that filter's left and right side are mirror symmetrical and all dimensions and spacings from both sides are equal. The thickness of input/output segments are 2.5 mm, the gaps between elements are both 0.2 mm, and all three elements are almost the same. The difference is just that the element in the middle is higher for 1 mm than the other two elements.

Brief specifications of the designed filter are:

* Dielectric constant Ɛr = 4.4 (FR-4)
* Substrate thickness = 10 mm (air), 1 mm (dielectric),
* Frequency range of simulations 2 GHz - 4 GHz
* Bandwidth 2.54 GHz – 3.01 GHz
* The filter box space is 24.9 mm x 20 mm
* Cell size is 0.1x0.1mm
* Thickness of metal 0.1 mm
* Type of metal - Copper

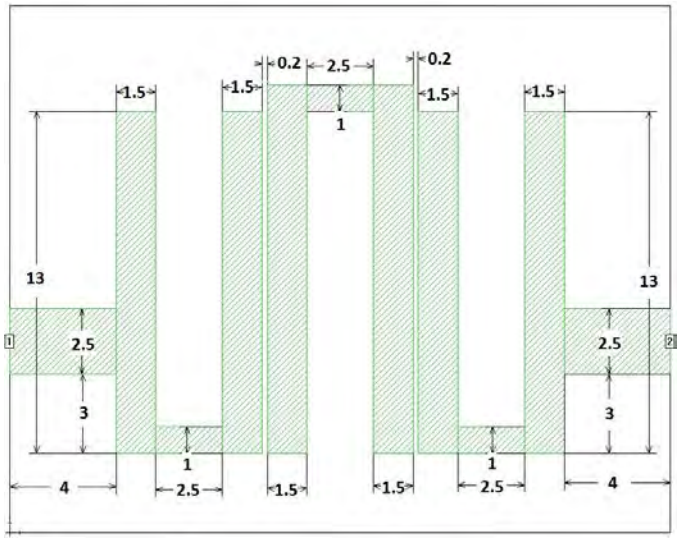

Fig. 1. Top view of three element hairpin bandpass filter with all dimensions in milimeters

II. SIMULATION AND OUTPUT DATA

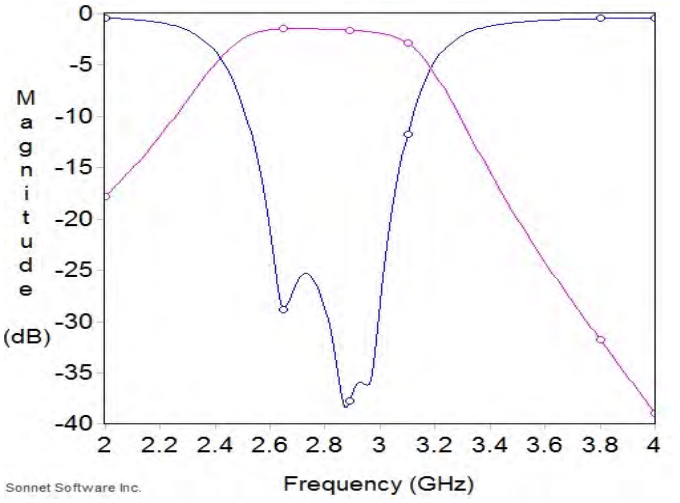

Fig. 2. Frequency vs magnitude output graph of the bandpass filter

III. Parametric Studies and Variations

On the three element hairpin bandpass filter, physical properties and parameters were changed, and simulation output is analyzed. Parameters that were changed in this case were thickness of input/output segments, gaps between elements, metal type, dielectric thickness, and dielectric material. Parameters which are chosen for the filter are: thickness of input/output segments is 2.5 mm, gap is 0.2 mm, metal type is copper, dielectric material is FR-4, and dielectric thickness is 1 mm. In all these cases of changing parameters just one specified parameter is changed, other parameters stay the same as mentioned above.

A. *Thickness of input/output segments*

TABLE I. S-PARAMETERS WHEN THICKNESS OF INPUT/OUTPUT SEGMENTS ARE CHANGED

Thickness of input/output	S11(dB)	S12(dB)
1.0 mm	-23.13 dB	-1.77 dB
2.0 mm	-26.90 dB	-1.52 dB
2.5 mm	-38.25 dB	-1.45 dB
3.0 mm	-39.39 dB	-1.45 dB

From the Table I, it can be concluded that after increasing of the thickness of input/output segments, results are better.

B. *Gaps between elements*

TABLE II. S-PARAMETERS WHEN GAPS BETWEEN ELEMENTS ARE CHANGED

Gaps (mm)	S11(dB)	S12(dB)
0.1 mm	-31.42 dB	-1.26 dB
0.2 mm	-38.25 dB	-1.45 dB
0.3 mm	-28.09 dB	-1.69 dB
0.4 mm	-25.17 dB	-1.94 dB
0.5 mm	-22.18 dB	-2.24 dB

In the Table II, it can be seen how S-parameters are changing when increasing gaps between elements is performed. It can be concluded that increasing of gaps will cause worse results.

C. *Metal type*

TABLE III. S-PARAMETERS WHEN METAL TYPE IS CHANGED

Metal type	S11(dB)	S12(dB)
Copper	-38.25 dB	-1.45 dB
Gold	-38.33 dB	-1.51 dB
Brass	-38.71 dB	-1.63 dB
Aluminum	-38.42 dB	-1.52 dB
Silver	-38.29 dB	-1.46 dB

As it can be seen from the Table III, metal type from which filter is made does not play an important role, because the results are very similar, and they are all good.

D. *Dielectric thickness*

TABLE IV. S-PARAMETERS WHEN THICKNESS OF DIELECTRIC IS CHANGED

Thickness of dielectric (mm)	S11(dB)	S12(dB)
1 mm	-38.25 dB	-1.45 dB
1.6 mm	-29.87 dB	-1.12 dB
0.4 mm	-17.57 dB	-3.64 dB

In the Table IV, it can be noticed that dielectric thickness plays important role in the designing of the filter, and changes in the thickness of the dielectric will cause changes on output graph.

E. *Dielectric material*

TABLE V S-PARAMETERS WHEN DIELECTRIC MATERIAL IS CHANGED

Dielectric material	S11(dB)	S12(dB)
FR-4	-38.25 dB	-1.45 dB
Alumina 96%	-0.03 dB	-56.94 dB
Silicon dioxide	-48.84 dB	-0.18 dB
Polyimide	-48.28 dB	-0.35 dB
Quartz (fused)	-51.03 dB	-0.18 dB

In this case, type of dielectric material is changed. From the Table V, it can be seen that FR-4 does not give the best result, but still it is good for fabrication. FR-4 is chosen because it is the most commonly used and the easiest for fabrication. Alumina is the worst dielectric material for this type of filter.

IV. Conclusion

This paper shown design, analysis and simulation of three element hairpin bandpass filter. It is very simple type of filter which is very useful in wireless applications. The bandwidth of the filter is 0.47 GHz. This filter is not expensive for fabrication, because the metal from which it is made, and the dielectric material on which it will be printed are not expensive. Next step is fabrication of the filter.

V. References

[1] L. Singh, P.K. Singhal "Design and Analysis of Hairpin Line Bandpass Filter" IJARECE Volume 2, Issue 2, February 2013

[2] N. Parikh, P. Katare, K. Kathal, N. Patel, G. Chaitanya "Design and Analysis of Hairpin Micro-Strip Line Bandpass Filter" IJIREEICE, Volume 3, Issue 5, May 2015

[3] G. Sharma, S. K. Sharma, S. Bhullar, N. Kumar, S. Chauhan "Design and Simulation of Compact Hairpin Bandpass Filter" IJMCTR, Volume 2, Issue 4, April 2014

[4] V. S. Kushwah, A. S. Tomar "ANN Modeling of Microstrip Hairpin-Line Bandpass Filter" IJCSNT, Volume 3, No. 1, 2014

[5] Sonnet Suites, ver. 16, Sonnet Software Inc., North Syracuse

Inset fed T-shaped patch antenna for 2.4GHz

Haris Ačkar, Sehabeddin Taha Imeci
Department of Electrical and Electronics Engineering
International University of Sarajevo
Sarajevo, Bosnia and Herzegovina
haris_ackar@hotmail.com,
simeci@isu.edu.ba

***Abstract*— The paper presents a new configuration of compact T-shaped microstrip path antenna on 1.6mm FR-4 substrate. The microstrip patch antenna is simulated using the Sonnet Software. This design can be used as transmitting antenna operating at 2.4 GHz radio signals with bandwidth ranging from 2.44 GHz to 2.495GHz, and with input match S11 less than -30dB on 2.465GHz frequency. The Gain of the proposed antenna is 4dB. The proposed antenna design can be widely utilized for radio communication between smart Internet of Things (IoT) devices, and this antenna can be easily implemented on any kind of printed circuit board, because it is designed on FR-4 substrate.**

Keywords—microstrip antenna; T-shaped; FR-4; gain

I. INTRODUCTION

In the modern IoT world, when we have a lot of smart devices for remote sensing and home automation, in some cases we need to have small suitable antenna for transmitting data to those smart home devices. Most of those devices are used to make our life easier.

A lot of papers are introduced and the authors are talking about Wireless Sensor Network (WSNs) operating at 2.4GHz have turned out to be the one of the most exciting areas of research in the past few years [1, 2]. Besides that, there are many interesting Microstrip antennas and array designs at 2.4Ghz, for Low Energy Bluetooth or RFID [3, 4], but in this paper the focus will be on simple design of transmitting antenna for 2.4GHz radio, which is widely used for remote sensing and remote control.

In the literature can be found a lot of different antenna designs for 2.4GHz [5, 6].

II. ANTENNA DESIGN

The antenna design is based on FR-4 substrate material of 1.6mm thickness. The proposed design is shown on Fig. 1. The Antenna has an inset fed, and small metal areas around T shape. Those areas are used to ensure that the antenna has enough radiation power on resonant frequency, and better current distribution, that can be seen in Fig. 4, in the third section of the paper. Also, these small metal areas are added in order to increase the bandwidth of the antenna.

With this type of the antenna, it is possible to easily change channels on 2.4GHz radio signal. For example, if the data rate is 1Mbps, channel spacing will we 1MHz. With bandwidth of 55MHz, it is possible to control a large number of remote devices. Dimensions of the antenna are presented in Table 1. This antenna design is very simple and can be easily reproduced in any CAD software.

TABLE I. ANTENNA DIMENSIONS

W1	56 mm	H1	26 mm
W2	52 mm	H2	23 mm
W3	20 mm	H3	27 mm
W4	12 mm	H4	23 mm
W5	20 mm		
W6	14 mm		

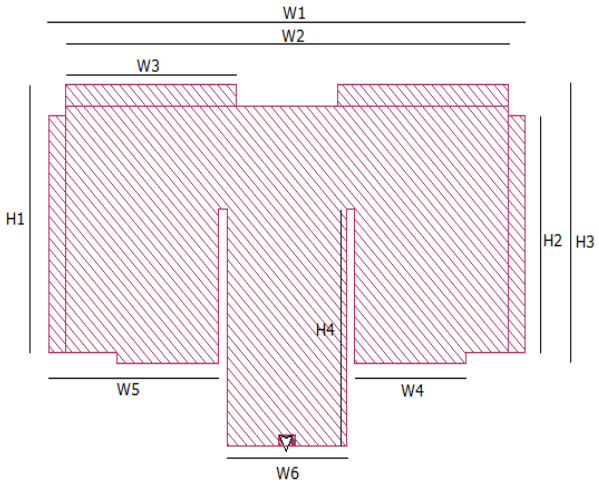

Fig. 1: Antenna design with marked dimensions

III. RESULTS

This antenna is designed and analyzed using the Sonnet Software. The input match S11 of the antenna is shown between 2 and 3 GHz in figure 2. In Fig. 2. is shown input match of -31dB on resonant frequency of the antenna. The input match is less than a -10 dB in the frequency range between 2.44GHz and 2.495GHz.

In Fig. 3. it is shown the gain pattern of the antenna. Horizontal polarization of the antenna has 4dB Gain at the resonant frequency, and vertical polarization has the gain of -40dB. Fig. 4. illustrates current distribution in the antenna on resonant frequency. From figure 3., it is possible to see that the radiation of the antenna comes mostly from the center of the T shape, and also from the additional metal regions on the left and right side of T shape. The Cross polarization level is well below -40dB as seen in figure 3.

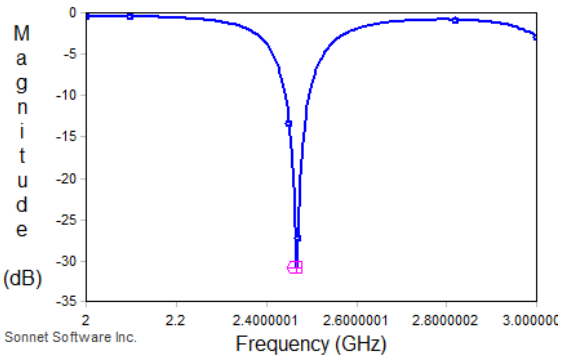

Fig. 2: Input match of the proposed antenna design.

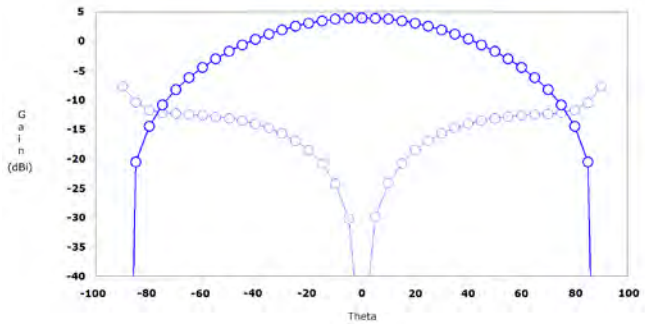

Fig. 3: Gain pattern of the proposed antenna design at 2.465GHz

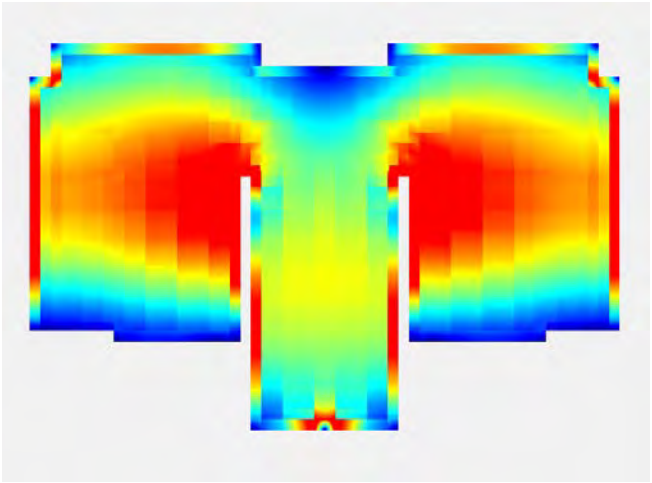

Fig. 4: Current distribution of proposed antenna design at 2.465GHz

IV. Conclusion

A T-shaped microstrip patch antenna for 2.4GHz radio communication is presented.. The antenna has simple design, and it can be easily drawn in any CAD Software. The antenna is designed on a FR-4 substrate, which has 1.6mm thickness. Because of the fact that FR-4 is a standard substrate for most of the printed circuit boards, this antenna design can be easily implemented on any printed circuit board on FR-4 substrate. The Sonnet simulations reveals that the designed patch antenna is capable of operating between 2.44GHz and 2.495GHz. For various data rates, we can easily have more channels for radio communication, for example on 1Mbps data rate, we can have 50 communication channels, for lower data rates we can have even more communication channels.

References

[1] Ransing, R. S., & Rajput, M. (2015, January). Smart home for elderly care, based on Wireless Sensor Network. In *2015 International Conference on Nascent Technologies in the Engineering Field (ICNTE)* (pp. 1-5). IEEE.

[2] Stojkoska, B. L. R., & Trivodaliev, K. V. (2017). A review of Internet of Things for smart home: Challenges and solutions. *Journal of Cleaner Production*, *140*, 1454-1464.

[3] Buffi, A., Serra, A. A., Nepa, P., & Manara, G. (2010). A focused planar microstrip array for 2.4 GHz RFID readers. *IEEE Transactions on Antennas and Propagation*, *58*(5), 1536-1544.

[4] Sarma, A., Sarmah, K., & Sarma, K. K. (2015, February). Low return loss slotted rectangular microstrip patch antenna at 2.4 GHz. In *2015 2nd International Conference on Signal Processing and Integrated Networks (SPIN)* (pp. 35-39). IEEE.

[5] Khraisat, Y. S. (2012). Design of 4 elements rectangular microstrip patch antenna with high gain for 2.4 GHz applications. *Modern applied science*,*6*(1), 68.

[6] Yang, F., Zhang, X. X., Ye, X., & Rahmat-Samii, Y. (2001). Wide-band E-shaped patch antennas for wireless communications. *IEEE transactions on antennas and propagation*, *49*(7), 1094-1100.

Microstrip Bandstop Filter With Perturbed L-shaped Elements at 10GHz

Adna Beganović and Amina Obradović Piro
Department of Electrical Engineering
International University of Sarajevo
Sarajevo, Bosnia and Herzegovina
adna_beganovic.98@hotmail.com , aminao_95@hotmail.com

***Abstract* –Project of designing Microstrip Bandstop Filter included projection, design, simulations and final analysis. In the forefront this research is an introduction of new configuration of Microstrip Bandstop Filter, designed in L-shape. It is composed of six parts, and are included five L-shaped elements and one rectangular box. This box has two ports, each on one side. The microstrip filter is simulated having a bandwidth 10.4 GHz, where S11 = -0.17 dB and S12 = -23 dB.**

***Keywords* –Microstrip Bandstop Filter (MBSF), L-shape,**

I. INTRODUCTION

Bandstop filter also known as rejected band filter, where the filter has a function to hold the frequency in the range f1to f2 and f1 skip frequencies below and above f2. The bandstop filter is the opposite of bandpass filter [1]. Nowdays, there is a huge market where are available many filters, but there are new applications that request better accuracy. Conventionally the microwave bandstop filter (BSF) is implemented either by all shunt stubs or by series connected high-low stepped-impedance microstrip line sections. However, generally these are not easily available in microwave band due to the high impedance microstrip line and the spurious pass-bands. To remove these disadvantages, defected ground structures (DGSs) for microstrip lines have been presented in recent years. Bandstop filter for X-Ban application have been presented in [2] a DGS with folded L-shaped arms. The resonant behaviors of the DGS used in to introduces transmission zeroes to the filter response and consequently improves its stopband performance.[3] This paper work deals with design and development of a microstrip filter at frequency at 10 GHz. In this structure are used L-shape resonators coupled both electrically and magnetically to the main line. The distance between the resonators is 0.25mm. Also changing the angle on the L-shaped the frequency in the bandstop filter is changed, the ideality of the frequency is with angle 41º. Changing the angle below and above the frequency limit are changed. The difference between the angle can be small, but the difference in the frequency are huge, with big peak and that make the signal unstable. In some applications BSF are used as reducers of noise especially in case of signal transmission. The L-shaped can be used in many aspects improving the required frequency, but it is most used for radars,wireless computer networks and satellite communication.

II. Designing Band stop Filter

In this section design steps and simulation results are given. Figure 1 has shown the top view of Microstrip Bandstop Filter including the dimension of the each part of shape.

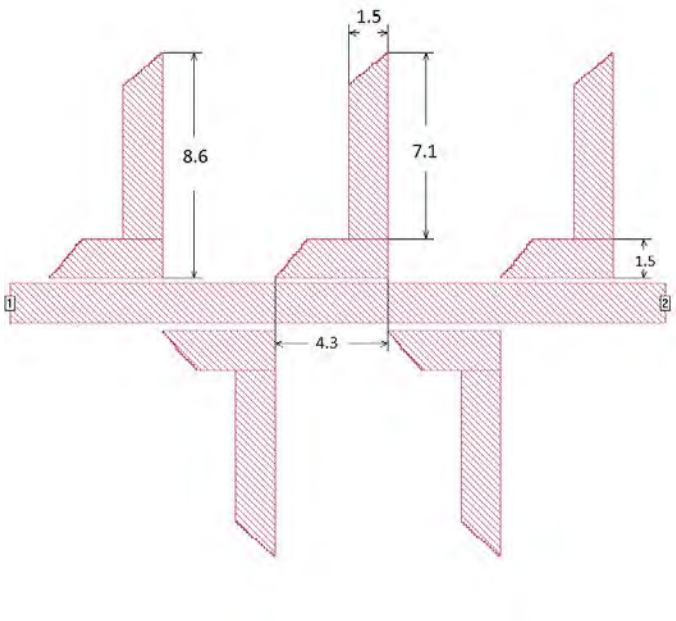

Figure 1. – Top view of MBSF

In this table is shown the dielectric thickness of the air, the size of the box, cell size and frequency that are used in the designing this filter.

TABLE I. FILTER MEASUREMENTS

Parameters	Values
Dielectric thickness (Ɛr)	1.00
Cell size	0.1 mm
Box size	25.0 x 30.0 mm
Frequency	10 GHz

Figure 2. has shown Simulated Frequency and magnitude output graph.

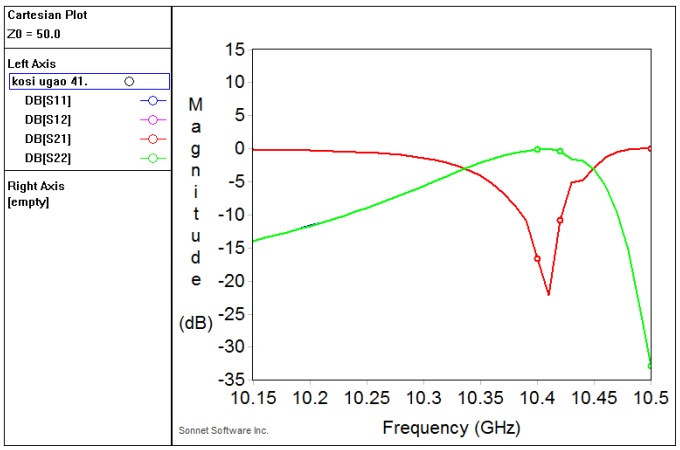

Figure 1. – Simulated Frequency vs magnitude output graph

III. Parametric Studies

In the table below observed is how the frequencies are changing while changing the angle in the L-shaped.Also, observed S11 and S12 to make it ideal as possible.

TABLE II. CHANGING ANGLE

Angle (°)	S11 (dB)	S12 (dB)
41	-0.38dB/ 10.42 GHz	-10.67dB/ 10.4 GHz
47	-7.56dB/ 10.27GHz	-17.22 Db/ 10.5 GHz
34	-2.7 dB/ 8,45 GHz	-36.2 dB / 7.71 GHz
42.4	-4.7 dB/ 9 GHz	-14.5 dB/ 9.23 GHz
39.9	-10dB / 10.42GHz	-16.2 dB/ 10.3 GHz

Data set below in Table III is showing the dimensions of the L-shape and the central box of the filter. Before getting this dimension, we used a lot of simulation where we changed the dimension of L-shape or central box. Small changes, measurements and outputs of filter are varying. After many simulations and tries, we had found most suitable Microstrip filter.

TABLE III. DIMENSIONS OF THE FILTER

Shape	Dimensions
L-shape (hole)	8.6 x4.3 mm
Vertical part of L-shape	7.1 mm
Horisontal part of L-shape	4.3 mm
Width L-shape	1.5 mm
Central box	25x1.5 mm

IV Conclusion

This design of bandstop filter has aim to find the best possible response and to implement nowdays this type of filters in radars, wireless computer networks and satellite communication. All simulation has been done in Sonnet software wich is well known as one of the best software for designing 3D planar high-frequency filters. Type of filter that we designed is most used for radars, wireless computer networks and satellite communication. What we have done in software is dimensioning, analysis, sensitivity analysis, simulations and testing procedure. After conductiong parameter study, 10.4 GHz of the design specification were met with -23 dB of S12 and -0.17 dB of S11. Next step is the fabrication of the filter.

.

V. References

[1] Dain W. Astuti, Ferdi Y, Mudrik A.”Bandstop Filter for Radar Aplication with L Resonantor”

[2] R. Habibi Ch Ghodadi, M. Ojarvordi and N. Ojavordi, “Very Compact broad bandstop filter using periodic L-shaped stubs based on self-complementary structure for X-band application” Electronic Letters Vol. 48. No 23.2012.

[3] Mohammad Pourbagher, Nasser Ojaroudi, Changiz Ghobadi, and Javad Nourinia,"*Compact Band-Stop Filter for X-Band Transceiver in Radar Applications*," ACES Journal, Vol. 30, No. 4, pp. 423-426, April 2015.

[4] Sonnet Suites, ver. 16.54, [http://www.sonnetsoftware.com%60] www.sonnetsoftware.com`

Z-Shaped Microstrip Patch Antenna with square endings

Amel Bajrić, Harun Šenderović
Dep. of Electrical and Electronics Engineering, International University of Sarajevo

***Abstract*— In our work, design and simulation of a compact microstrip patch antenna is studied. The research methods include antenna design architecture consideration and optimization through an analysis of different input parameters and simulations. The antenna operates at 8.8 and 11.85 GHz. Radiation pattern of electric field phi-polarized gains are 5.01 and 5.7 dBi respectively. Radiation pattern of electric field phi polarized gain is 5.07 dB and theta-polarized gain is 6.27 dB respectively. The goal of the study was dual band patch antenna in X and Ku Bands.**

Index Terms — microstrip antenna, patch, compact

I. INTRODUCTION

The use of high permittivity microwave substrate in designing the antenna is an effective way to reduce the size of microstrip antenna at fixed operating frequency [1]. This paper presents a compact microstrip antenna design supported by simulation. Simulations are obtained from the software called Sonnet Suites which uses Method of Moments as an electromagnetic solution technique [2]. In another work available online they have three L-type slots in a Z-shape microstrip patch antenna and they have maintained two resonances at 1.12 GHz, and 1.68GHz [3]. Also, in the other work, the team of students of „Institute of Management and Technology" in Odisha, India, made the simulation of microstrip patch antenna with I- slot Using Discrete Particle Swarm Optimization (DPSO), with frequencies of 3.4 GHz and 4.1 GHz. [4]. Additionally, in a different work, design and analysis of patch antenna using metamaterial (MTM) structure is presented. The proposed reception apparatus is structured at a height 3.2 mm from the ground plane. This structure is worked at 1.89 GHz and 2.553 GHz. At 1.89GHz, the transmission capacities are expanded up to 29.2 MHz and 19.8 MHz in contrast with 10.1MHz of RMPA alone[5].

II DESIGN AND SIMULATION RESULTS

In this work, a Z-shape microstrip patch antenna was designed by feeding it from bottom-center. One square symmetricly added to both ends of the antenna in order to get appropriate frequencies. This resulted with having best gain that is much better than without these squares. Highest gain was obtained at 11.86 GHz and lowest gain was obtained at 8.8 GHz. Our Z-shape antenna as you can see in picture below have these sizes. The length is 38.02 mm. the square we added is by default size 1.0 x 0.95 mm and we were changing its size to get different frequencies and gains that is shown in tables below. Thickness of middle part is 3.0 mm that is actually almost double the other two parts that are by 2.1 mm thick. Figure 1 has the top view of the antenna.

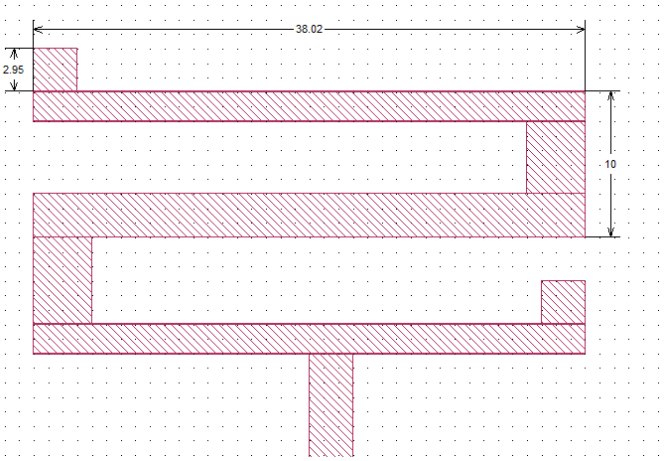

Fig. 1. Z-shape antenna

In Table I it is shown change in gain in different frequencies when size of squares is changed.

TABLE I Changed size of squares at the end

Size (mm)	Frequencies (Gain **dBi** if Theta = 25.0, −25.0)	
1.0 x 0.95	8.8 GHz(5.07, -17.8)	11.85 GHz (-5.5, 6.2)
2.0 x 1.95	8.75 GHz(5.05, -15.50)	11.86 GHz(5.7, -5.06)
3.0 x 2.95	8.7 GHz(4.35, -10.06)	11.8 GHz(-4.5, 4.32)

In Table II there is a change in gain in different frequencies when width is changed.

TABLE II Changed width in upper and lower horizontal part

Width (mm)	Frequencies (GHz) (Gain **dBi** if Theta = 25.0, −25.0)	
2.1	8.86 GHz(5.07, -17.8)	11.85 GHz(-5.5, 6.2)
3.05	8.6 GHz(4.75, -11.4)	11.85 GHz (4.75, -11.5)
1.05	9.025 GHz(5.11)	11.95 GHz(5.59, -6.04)

S11 is seen in figure 2

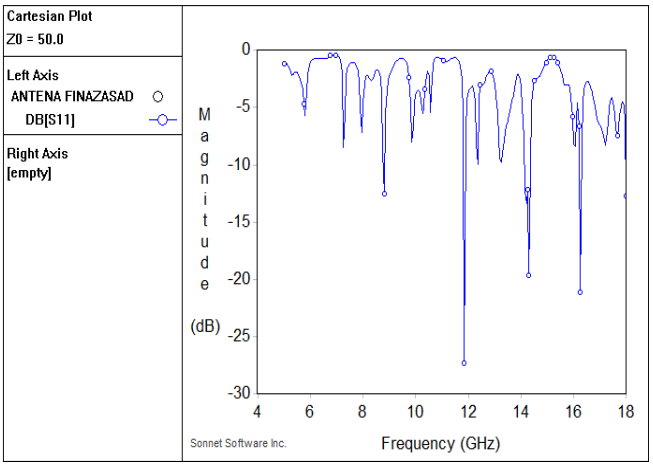

Fig. 2. Response viewer of Z-shape antenna

Phi polarized Far field radiation pattern for 8.8 Ghz is seen in figure 3

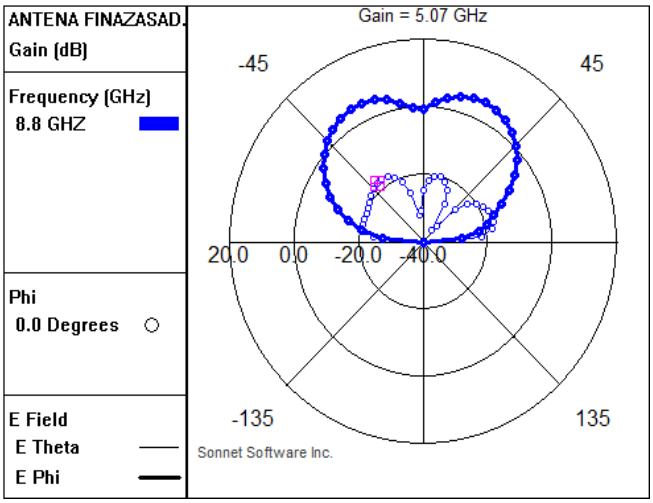

Fig. 3. Far field at 8.8 GHz

Theta polarized Far field radiation pattern for 11.85 GHz Â is seen in figure 4

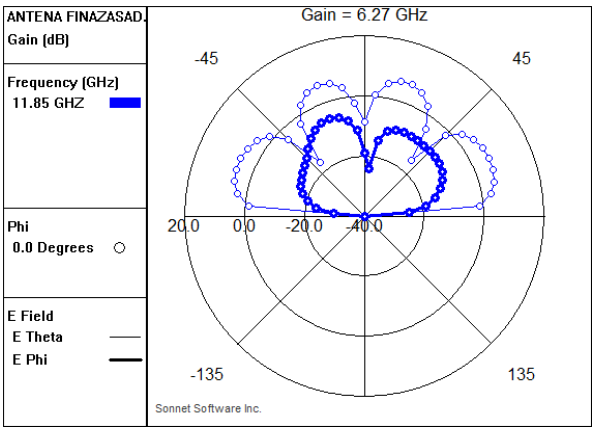

Fig. 4. Far field at 11.85 GHz

Current distribution for the frequency of 8.8 GHz is in Figure 5

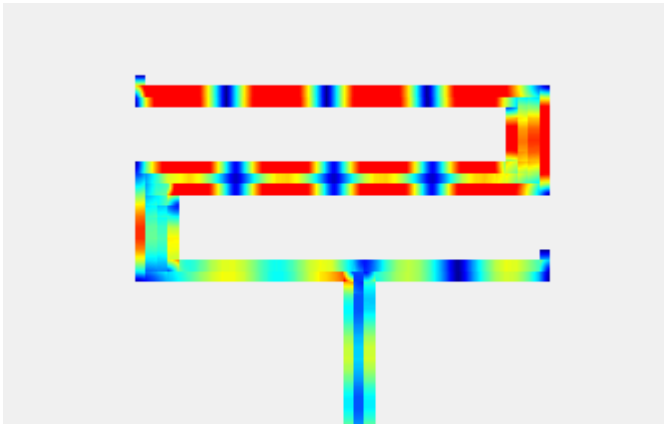

Fig. 5. Current distribution, 8.8 GHz frequency

II. CONCLUSION

In this work, a Z-shaped microstrip patch antenna is designed and simulated. The microstrip patch antenna configuration containing square endings attached to the both sides of the body and the feed line following the center of the rectangular body. The tests which were conducted for achieving better results involved altering of location of port on feeding line and dielectric material thickness, and concluded our test by combining the best results.

REFERENCES

[1] N. Gunavathi and D. S. Kumar. “A compact coplanar waveguide-fed slot antenna for uwb applications,” In Electronics and Communication Systems (ICECS), 2014 International Conference on, pages 1-4. IEEE, 2014.

[2] Sonnet Suites, www.sonnetsoftware.com, ver.16.54

[3] A Novel Multiband Directional Antenna for Wireless Communications Chun-Xu Mao, Steven Gao, Senior Member, IEEE, Yi Wang, Senior Member, IEEE, Benito SanzIzquierdo. (2016.)

[4] Gourav Singh Rajpu. (2012). Design and analysis of rectangularr microstrip patch antenna using metamaterial for better efficiency. 51-58.

[5] .Keshav and Laxmikant M.V.P. Chakravarty, Department of Electronics and Computer Science. Antenna Design, Simulation and Fabrification. (2015).

Design of Coupled-line Bandpass Microstrip Filter

Mustafa Indžić
Eldar Tihak
Department of Electrical Engineering
International University of Sarajevo
Sarajevo, Bosnia and Herzegovina

***Abstract* – In this work, design, simulation and test of a three element compact microstrip bandpass filter is studied. Two symmetric lines were attached to the ports and a rectangle line was in between those lines. The aim of the research is to introduce a new configuration of microstrip filter design.Simulation results that were found are: S11 at 1.41 GHz gets -22.75 dB while S21 gets -0.4001 dB.**

***Keywords* - Coupled-line Bandpass Microstrip Filter (CBMF)**

I. INTRODUCTION

Filter design is one of the most important areas in microwave technology. The key component of the microwave communication system is filter and there are various types of filters that are used in microwave communication systems. In the past decades, the traditional parallel coupled-line bandpass filter has been extensively studied and widely used in RF front-ends design. The performance of traditional parallel coupled-line bandpass filters suffers from the existence of spurious passbands generated at the multiples of the operating frequency. This intrinsic limitation degrades the stopband rejection behavior and limits its field reliability [1]. This paper will concentrate on the design of a compact size microstrip bandpass filter. Bandpass filter is a passive component which is able to select signals inside a specific bandwidth at a certain center frequency and reject signals in another frequency region, especially in frequency regions, which have the potential to interfere the information signals [2]. Band pass filter could either be realized using lumped components or distributed components. Lumped components consist of discrete elements like inductors, capacitors etc. Distributed elements consist of transmission line segments that simulate different values of inductance and capacitance. The demand in high speed communication has led to the design and development of wide band filters to support the applications such as UWB technology that promises communication speed of up to 1000 Mbps [3].Microstrip bandpass filter is a key component in a radio frequency receiver for the growing wireless communication applications operating in multi-band, especially in the new developed wireless local area networks [4]. This paper presents a coupled line microstrip bandpass filter design supported by simulation. Simulations are obtained from the software called Sonnet Suites [5].The analysis of the designed filter will be presented briefly in further sections.

II. DESIGN STEPS OF CBMF (COUPLED-LINE BANDPASS MICROSTRIP FILTER)

Figure 1 presents the top view of the filter:

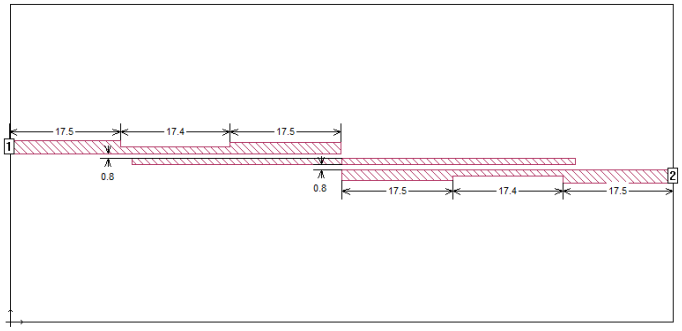

Figure 1. – Top view of CBMF

Figure 2 has the S parameters of the filter. As you can see S11 is -22.27 dB in resonance frequency of 1.41 GHz and S21 is -0.4.

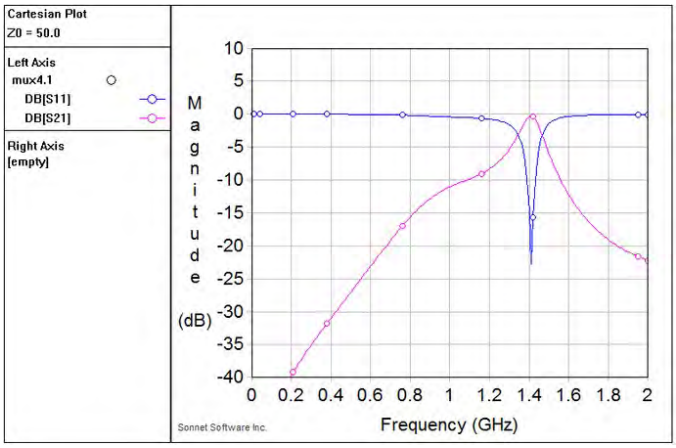

Figure 2. - Simulated Frequency (GHz) vs. magnitude (dB) output graph

In table 1, as it can be seen in Figure 1, width and length of central box, coupled lines and spacing are showed. So, these are the parameters of the filter:

TABLE 1:DIMENSIONS OF THE FILTER

Name	Width (mm)	Length (mm)
Central Box	1	70,2
Coupled Lines	2	52,4
Spacing	0,8	-

III. PARAMETRIC STUDIES

In table 2, we observed how the frequencies are changing while changing different dielectric and air thicknesses. We observe S11 and S21 to make it good as possible.

TABLE 2: SIMULATED RESPONSE FOR DIFFERENT DIMENSIONS

Dielectric/Air thickness (mm)	S11(dB)	S21(dB)
1.524/5.0	1.38GHz/-21.9125	1.38GHz/-0.5335
1.8/5.4	1.39GHz/-18.3415	1.39GHz/-0.4803
1.2/4.8	1.36GHz/-13.4287	1.36GHz/-0.8929
1.3/5.0	1.37GHz/-23.2394	1.37GHz/-0.6382
2.0/6.0	1.4GHz/-24.3	1.4GHz/-0.3916

The table 3 is representing S11 and S21 while changing Dielectric and Air thickness together with gap between coupled lines.

TABLE 3: SIMULATED RESPONSE FOR DIFFERENT GAPS

Dielectric/Air thickness (mm)	Gap (mm)	S11(dB)	S21(dB)
1.524/5.0	1	1.38GHz/-21.9125	1.38GHz/-0.5335
1.3/5.0	1	1.37GHz/-23.2394	1.37GHz/-0.6382
2.0/6.0	1	1.4GHz/-24.3	1.4GHz/-0.3916
1.524/5.0	0,8	1.39GHz/-19.705	1.39GHz/-0.3959
1.3/5.0	0,8	1.37GHz/-17.049	1.39GHz/-0.4915
2.0/6.0	0,8	1.41GHz/-22.75	1.42GHz/-0.4001

Variables that we changed are: Coupled line Spacing, Central Box Width, Dielectric Thickness and air space. With small changes, the measurement and output of the filters vary. After many simulations and tries, we had found most suitable Microstrip filter.

IV. CONCLUSION

In this work, a Microstrip Coupled - Line Bandpass Filter is designed, simulated and tested. Simulation was performed in a 3D planar high-frequency electromagnetic software called Sonnet. The performance of the filter is observed based on its S-parameters which are return loss (S11) and the insertion loss (S21). The research methods included operational requirement analysis, parameter sensitivity analysis, optimization analysis, software simulation and filter testing procedures.

V. REFERENCES

[1] Si-Weng Fok, Pedro Cheong, Kam-Weng Tam, Rui Martins, A Novel Microstrip Bandpass Filter Design using Asymmetric Parallel Coupled-Line, IEEE Circuits and Systems Conference, June, 2005

[2] G. Matthaei, L. Young, and E.M.T. Jones, Microwave Filters, Impedance-matching Networks, and Coupling Structures, Artech House, Norwood, MA.-February,1980

[3] Nermin Sejdić, Design and Fabrication of Microstip Filter, conference paper-CMTEEF Computational Method in Electrical engineering and finance, IUS, Bosnia and Herzegovina6-9 May,2018

[4] Hong, J. S. and M. J. Lancaster, Microstrip Filters for RF/Microwave Applications, John Wiley & Sons, Inc., New York, 2001.

[5] Sonnet Suites, www.sonnetsoftware.com, ver.16.54

A Short Survey on Mobile Operating Systems

Bakir Brkic, Himzo Hasak, Omar Hassan,
Lejla Hodzic, Ali Abd Almisreb

Department of Computer Science and Engineering
International University of Sarajevo
Sarajevo, BiH
aalmisreb@ius.edu.ba

***Abstract*— This paper is intended to provide a review of papers written about mobile operating systems as well as some of the mobile application development platforms. The paper goes through chronological advancement of the mobile operating systems and explains the leading operating systems present today. Furthermore, it goes on to describe the importance of cross-compilation on today's process of mobile applications implementation.**

Keywords—review, mobile, operating systems, platforms.

I. INTRODUCTION

Operating system is responsible for executing applications and programs. Mobile environment includes mobile applications to run on the mobile devices. These applications are built specifically for mobile operating systems and, evolving very fast in the past decade. These devices, called smartphones, can be found relatively cheap and are present in every technological environment practically. Since high-speed networks are available, many application stores are introduced to the virtual market. As a result, the influence, advancement and the importance of mobile industry, including smartphone devices, mobile operating systems, application development platforms and mobile applications, are increasing and it may continue to have even greater impact on people's life [1]. The deployment of mobile wireless network is increased the global usage of mobile phones. Furthermore, development of 3G network made all the commodities we enjoy today on our mobile phones possible. [2]. Therefore, it has been a rise in interest in the mobile industry. This advancement in smartphone technology brought some challenges, including the development of the applications for such devices. Furthermore, many universities decided to deploy some kind of a new system of teaching how to code in order to build mobile applications [3].

II. MOBILE OPERATING SYSTEMS

The literature used in this scientific review of mobile operating systems and development platforms were published in the time frame of the last 15 years, in which the advancement and the difference in trends regarding this topic can be seen. The oldest scientific paper we used is written in 2004, while the most recent one is from 2018. Majority of the papers are written as part of academic research and there are a few really useful papers written by experts in practice. The academics, scientist and engineers who wrote these papers span between many different countries around the world. Operating system can be defined as an intermediary program between hardware and software. It has a task to execute programs and efficiently use the hardware, while being easy to use for the end user [4]. The creation of one mobile operating system is not an easy task. It is required for the technological part of the development to be planned strategically. It has great importance to bear in mind the third-party applications and devices and making sure the operating system is able to adjust with them. The operating systems should also be made to adapt and be compatible to different processors and hardware [5]. Before 2010, it was a great challenge to get all the technology work seamlessly with all the new requirements made. Not only the mobile phones supported calls and SMS messaging, but also more and more features have been added, such as multimedia gadgets and wireless internet. Mobile phone manufacturers had the obligation to come up with the new ideas for more efficient and reliable software platforms that would be able to catch up with the new trends entering this industry. Today, with the iOS and Android being the most popular mobile operating systems, it is hard to remember the operating systems that used to be before them, such as Symbian OS, Windows Mobile, Linux, REX and Nucleus [6]. Back in the 2009, statistics on global mobile phones sales states that the Symbian OS and RIM Blackberry were the leading operating systems [7]. In 2008, 10 years after Symbian OS is founded, all of the shares are transferred to Nokia. However, Nokia was only one of the companies that created this operating system. Others are Ericsson, Motorola and Psion. Nokia can attribute much of its success to the Symbian OS and because of this success, other manufacturers used to pick Symbian as an operating system of choice [8]. The mobile phone environments are one of the closest environments at the beginning of the new millennium, before Symbian and Java brought the change which led to the open platform technologies revolution. With such competitive market, time is really important factor and even a couple of days of earlier release may be considered as a market win. However, the problem used to be in developing mobile apps, since it is very challenging because of the need for special techniques and knowledge [9]. In the time before the huge popularity of smartphones, the major players in mobile platform development are telecom providers who has a huge impact on how the industry will be shaped and what services are going to be offered. Now with the emergence of smartphones and their wide acceptance new way of software development is also emerging. Developers are now separate entities not tied to the telecom providers or device manufacturers. They are innovating and sharing new ideas through Open Source community and this is what makes the mobile platform development much more interesting, more innovative [10]. The entire mobile industry has been changed the moment Android entered the market in 2010. Today, Android is a popular mobile operating system, developed and maintained by Google. The introduction to the new mobile operating system promoted the competition in this industry, since they

have entered the same market as the iPhone, and the comparison between the popularity between Android, iOS and Windows Phone OS through time can be seen on the Figure 1, which was extracted through Google Trends website. It can be said that the success of the Android lies in the fact that it is open-source, so many technological and electronic corporations used it while creating their mobile phones, while the same cannot be said for iPhone [11]. The architecture of Android is consisted of Linux kernel, applications, application framework and libraries [7]. Android operating system is based on Linux and is developed by Google mostly in programming language Java. It is not only made for smartphones, but also for the watches, televisions and cars. Today, there is around 2 million applications made for Android, which proves the great popularity this operating system has. The first version of Android, Alpha 1.0, was launched in 2007, after which there has been 15 more versions: Beta 1.1, Cupcake 1.5, Donut 1.6, Éclair 2.0-2.1, Froyo 2.2-2.2.3, Gingerbread 2.3-2.3.7, Honeycomb 3.0-3.2.6, Ice Cream Sandwich 4.0-4.0.4, Jelly Bean 4.1-4.3.1, KitKat 4.4-4.4.4, Lollipop 5.0-5.1.1, Marshmallow 6.0-6.0.1, Nougat 7.0-7.1.2, Oreo 8.0-8.1 and Pie 9.0 [4]. Some studies suggest that developers and students who are learning to develop mobile applications will most likely use Android as a platform of choice for developing their own applications, even among the groups who are personally mostly using iOS [12]. The iOS operating system is developed by Apple Inc. in 2007 and it is based on Unix operating system, mainly written in programming languages Objective-C and Swift. App store, which is the official application store for the iOS, has almost as many applications as Android, being the second largest application store. iOS version history is consisted of the following versions chronologically: iPhone OS 1, iPhone OS 2, iPhone OS 3, iOS 4, iOS 5, iOS 6, iOS 7, iOS 8, iOS 9, iOS 10, iOS 11 and iOS 12. The main difference between iOS and its competitors, is that one cannot legally run iOS on a different machine that was not manufacture by Apple Inc [4]. The Windows Phone Operating System is developed by Microsoft in programming language C#. All the versions of the Windows Phone are: 7, 7.5, 7.8, 8 and 10. The number of applications on Windows Phone store is smaller compared to the Google Play store and the App store [4]. Software engineering can be defined as a process in which software is created by a team or an individual. Software engineering in terms of mobile application development has some additional requirements and challenges when compared to the traditional software engineering, for example, interaction with other applications, handling the sensors, security, specific user interface, testing complexity and power consumption [6]. While the mobile platforms are rapidly advancing and the need for software developers for such systems rises, it also brings a few significant problems with it. One problem is the fact that software has to be constantly changed and updated and it leads to poorly maintained and structured code. Customer related risks (wrongly written software requirements or software that does not meet customer needs), communication related risks, market risks resource risks, financial risks and maintenance risks are only some of the current challenges existing in modern development process [7]. The number of all possible actions one is able to do with their smartphone rises with each year. This is not only a challenge for the operating system and application developers regarding implementation, but also regarding the security. Having gadgets safe and secure is number one priority, along with the reliability and efficiency [8]. Different software design patterns can affect the development, efficiency and maintainability of applications. Some of the mostly used software patterns are: singleton, memento, state, iterator, factory, builder and flyweight [9].

III. Conclusion

This paper reviewed some of the past and present trends regarding mobile operating systems and application development platforms. It is important to study and research this topic, since it is said that mobile platform development has a very dynamic and fluid movement, particularly in the smartphone market

References

[1] K. W. Tracy, “Mobile application development experiences on Apples iOS and Android OS,” IEEE Potentials, vol. 31, no. 4, pp. 30–34, 2012.

[2] Y. Wu, J. Luo, and L. Luo, “Porting mobile web application engine to the Android platform,” in Proceedings - 10th IEEE International Conference on Computer and Information Technology, CIT-2010, 7th IEEE International Conference on Embedded Software and Systems, ICESS-2010, ScalCom-2010, 2010, no. Cit, pp. 2157–2161.

[3] W. Hu and H. Guo, “Curriculum architecture construction of mobile application development,” in Proceedings of 2012 International Symposium on Information Technologies in Medicine and Education, ITME 2012, 2012, vol. 1, pp. 43–47.

[4] O. C. Novac, M. Novac, C. Gordan, T. Berczes, and G. Bujdoso, “Comparative study of Google Android, Apple iOS and Microsoft Windows Phone mobile operating systems,” in 2017 14th International Conference on Engineering of Modern Electric Systems, EMES 2017, 2017, pp. 154–159.

[5] M. A. Nazarenko, “Mobile Operating Systems and Integrated Apps Quality Management System,” in 2018 IEEE International Conference “Quality Management, Transport and Information Security, Information Technologies” (IT&QM&IS), 2018, pp. 63–65.

[6] Y. C. Cho and J. W. Jeon, “Current software platforms on mobile phone,” in ICCAS 2007 - International Conference on Control, Automation and Systems, 2007, pp. 1862–1867.

[7] N. Gandhewar and R. Sheikh, “Google Android : An Emerging Software Platform For Mobile Devices,” Int. J. Comput. Sci. Eng., vol. Supplement, no. 12, pp. 12–18, 2011.

[8] F. Lin and W. Ye, “Operating system battle in the ecosystem of smartphone industry,” in Proceedings - 2009 International Symposium on Information Engineering and Electronic Commerce, IEEC 2009, 2009, no. 2004, pp. 617–621.

[9] P. Abrahamsson et al., “Mobile-D : An Agile Approach for Mobile Application Development,” Int. J. Serv. Ind. Manag., pp. 174–175, 2017.

[10] A. Holzer and J. Ondrus, “Mobile application market: A developer’s perspective,” Telemat. Informatics, vol. 28, no. 1, pp. 22–31, 2011.

[11] [11] M. Butler, “Android: Changing the mobile landscape,” IEEE Pervasive Comput., vol. 10, no. 1, pp. 4–7, 2011.

[12] C. C. Teng and R. Helps, “Mobile application development: Essential new directions for IT,” in ITNG2010 - 7th International Conference on Information Technology: New Generations, 2010, pp. 471–475.

Microstrip Low Pass Filter with floating center rectangular patch design

Halid JUSIC, Enes ATICI and Faruk MATORUGA
Department of Electrical and Electronics Engineering
International University of Sarajevo, Bosnia and Herzegovina

***Abstract*—In this paper, a microstrip lowpass filter was designed and simulated for different microwave applications. Improvements have been made to increase the efficiency of the filter. It has a wide simulation band extending from 0.1 GHz to 6 GHz with a cut-off frequency of 3.4 GHz obtained in filter design. The obtained filter can be used for modern microwave applications.**

Keywords—microstrip, low pass filter, band extending, cut-off frequency

I. INTRODUCTION

While a radio frequency module working, it receives or transmits signal with distortion or with parasite. That makes signal complicated. Filters are used for eliminating these signals. Filters can be classified in 4 categories based on frequency characteristic: low-pass filters, high-pass filters, band-pass filters and band-stop filters[1]. A low pass filter, which made up of a microstrip structure, is a filter which passes low-frequency signals and blocks high-frequency signals. There are several configurations of microstrip components, which are often utilized for lowpass filter implementations. Among these, planar resonators are more important due to their compact size, ease of fabrication and integration with other microwave circuits.[2]. Another interesting approach is to use spiral structures in designing lowpass filters, so based on this resonators, two different configurations are presented in [3]and [4] that have achieved relatively low passband ripple but their stopband width is not very high.

In this paper a new resonator is proposed that is a modified version of the spiral resonator. From spiral version of resonator we get new rectangular shape of resonator. This new resonator will be introduced in next section.

II. DESIGN AND SIMULATION RESULTS

A new thing related to low pass filters that was inroduced by Sohrab Majidifar, Seyed Vahab AL-Din Makki ,Arash Ahmadi, and Shahpour Alirezaee in their paper "Compact Microstrip Lowpass Filter using Stepped Impedance Spiral Resonator ", is exactly the usage of that spiral resonator [5].

We have set some default values for our filter: a substrate with 2.2 dielectric constant and 0.0009 loss tangent. The substrate thickness is selected 15 mil. Transmission zero was at 2.78 GHz with -32.56 dB attenuation in Sohrab's paper, while transmission zero in our case was 4.4GHz with attenuation -43 dB. The proposed filter of this paper is shown in Fig. 1

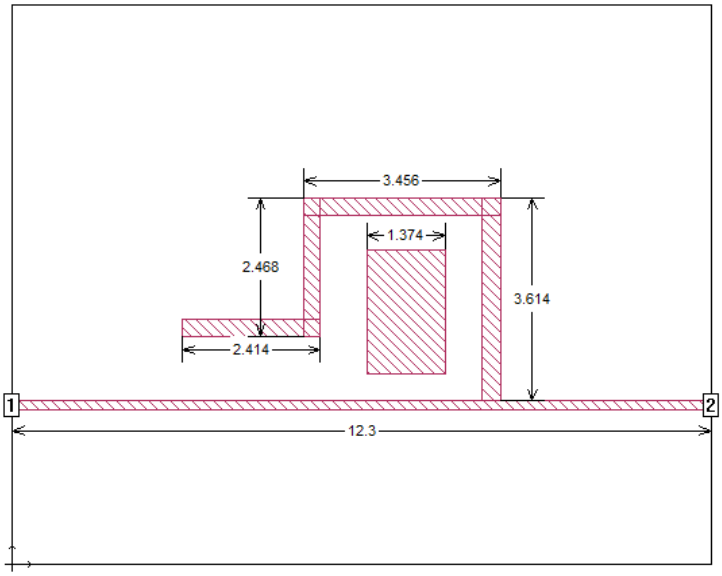

Fig. 1. Top view of the designed filter

As we can see in the picture above, we have 6 parts of the filter with dimensions first part 2.4x 0.3mm, second part 0.3 x2.4mm third part 3.4x0.3mm fourth part 0.3x 3.6mm fifth part 12.3x0.3 and last rectangular shaped 1.37x 2.21 mm. We changed dimensions of first, second and last part and what we can see in tables below. We did change spacings between microstrip lines.

TABLE I. FILTER SIZE CHANGE

Size (mm x mm)	S12	S11 (dB)
2.4 x 0.3	2.56 GHz	-10.11

3.45 x 0.3	2.44GHz	-9.96
1.8 x 0.3	2.66 GHz	-9.95

TABLE II. VARIATION OF SECOND PART OF FILTER

Size (mm x mm)	S12	S11 (dB)
0.3 x 2.4	2.55 GHz	-10.37
0.3 x 2.9	2.52 GHz	-10.04
0.3 x 1.73	2.62 GHz	-10.25

TABLE III. VARIATION OF FLOATING RECTANGULAR PATCH

Size (mm x mm)	S12	S11 (dB)
1.37 x 2.21	2.55 GHz	-10.36
1.03 x 2.21	2.75 GHz	-10.90
1.37 x 1.69	2.36 GHz	-10.30

Simulated results of the resonator are presented in Fig. 2. This results show that there is a transmission zero at 4.4 GHz with -43 dB attenuation. The value of insertion loss in the range of DC to 2.5 GHz is less than 0.1dB that indicates to a low passband ripple.

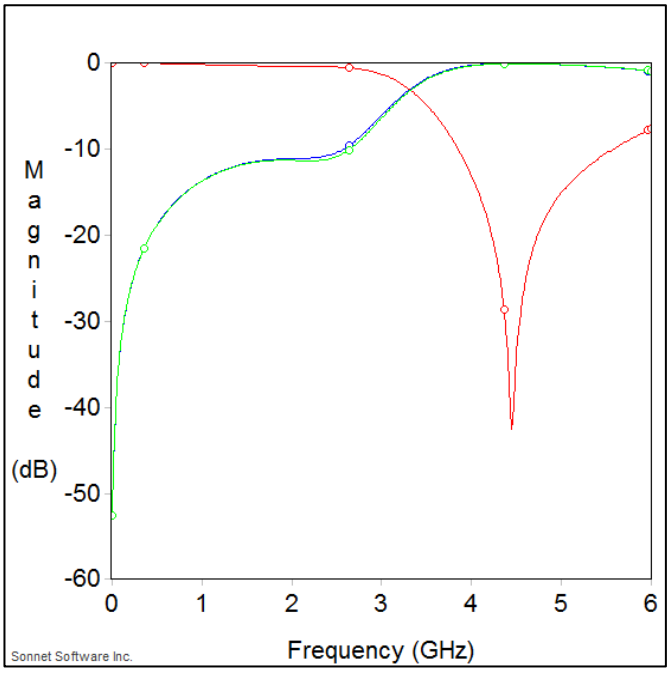

Fig. 2. Response of the filter.

III CONCLUSION

In this paper, we have tried to propose a new topology and a new way of implementing low pass filters.With different shapes of our microstrip components we get low pass filter with floating rectangular patch. Changing dimensions of some part of filter gives extremely good results in terms of the funcionality of the filter, which was our aim.

REFERENCES

[1] S. Shirin and C. H. R. P. Kumar, “Implementation of Nth Order Bandpass filter,” vol. 3, no. 3, pp. 4359–4361, 2012.

[2] Jia-Sheng Hong, “Microstrip Filters for RF / Microwave Applications, 2nd Edition,” *Book*, vol. 7, p. 656, 2011.

[3] W. Che, K. Deng, L. Xu, D. Wang, and L. Geng, *Improved spiral compact microstrip resonance cell low -pass filt stopband characteristics*, vol. 49. 2007.

[4] J. Gu and X. Sun, *Compact low-pass filter using spiral compact microstrip resonant cell*, vol. 41. 2005.

[5] S. Majidifar, S. V. A. D. Makki, A. Ahmadi, and S. Alirezaee, “Compact microstrip lowpass filter using stepped impedance spiral resonator,” *Proc. - 4th Int. Conf. Comput. Intell. Commun. Networks, CICN 2012*, no. May 2014, pp. 23–26, 2012.

6dB Hybrid Microstrip Coupler

Merjem Begovic, Lilian Bonus Nombo
Department of Electrical and Electronics Engineering
International University of Sarajevo,
Sarajevo, Bosnia and Herzegovina
Istanbul Sehir University, Istanbul, Turkey

Abstract- This work is based on designing and testing 6dB hybrid microstrip coupler. Combining the best solution for thickness, dielectric constant and dimensions we obtained the design using planar 3D electromagnetic software [1]. The frequency band was from 4.5 up to 7 GHz where we were mostly concerned with the frequency of 6 GHz. Simulation results are showed and represented through S-parameters, tables with different parameters and Cartesian graphs.

Keywords—coupler, 6dB, hybrid coupler, microstrip

I. INTRODUCTION

In the frequency range of 100 MHz to 1000GHz general radio frequency and microwave, engineering is operating. In that scope, the range of 3 to 300 GHz frequency is reserved for microwave engineering [2]. Couplers have wide usage possibilities in the microwave applications as well as in radio frequency through devices like power amplifiers, antenna feeders and balance mixers [3]. They are designed to achieve coupling at desired frequency range such that they separate and transmit radio frequency signals into two output ports [4,5]. We can divide couplers into 3-port and 4-port couplers. Hybrid couplers are in the group of 4-ports couplers which are employed either to split power into two parts or to combine signals [4]. They differ from directional couplers in power splitting. hybrid couplers provide non-equal power splitting of input signals [6]. Microstrip devices are the most usable ones because of their low cost, planar structure and their easiness of integration [5].

II. DESIGN STEPS

The procedure for designing 6dB hybrid microstrip coupler consisted of two parts. In the first step we chose the right geometry for the coupler and defined its dimensions. This can be seen in the top view of the design, including the dimensions we have used, Figure 1. Our design has 3 parts: a bottom substrate, an upper substrate with one part of the metal and third substrate with the second part of metal.

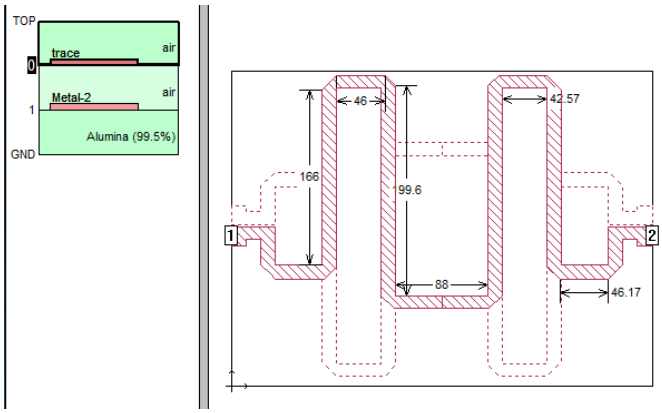

Figure 1. Top view of the geometry (dimensions are in mils)

The second step was choosing the right parameters. For the bottom substrate, we chose Aluminum (99.5%), for the upper ones air is chosen (Ɛr = 9.9, Dielectric Loss Tan = 0). The thickness of the first layer, Aluminum, was changed from 5 mils to 4 mils for the efficient simulation. 3D of our design can be seen in Figure 2.

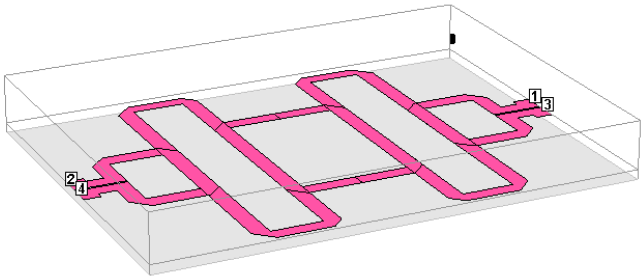

Figure 2. 3D representation of the geometry

III. SIMULATION RESULTS

In the following figure, Figure 3, we can see the simulation results in the frequency range of 4.5 to 7 GHz. It is, actually, the representation of S-parameters, where S11 is reflection, S12, S13 and S14 represent the coupling throughout the frequency range, from ports 2, 3, 4 to port 1. We can see that the center frequency is 5.8 GHz. At 6 GHz S12 is approaching the exact value of 6 dB, with a value of -6,27 dB.

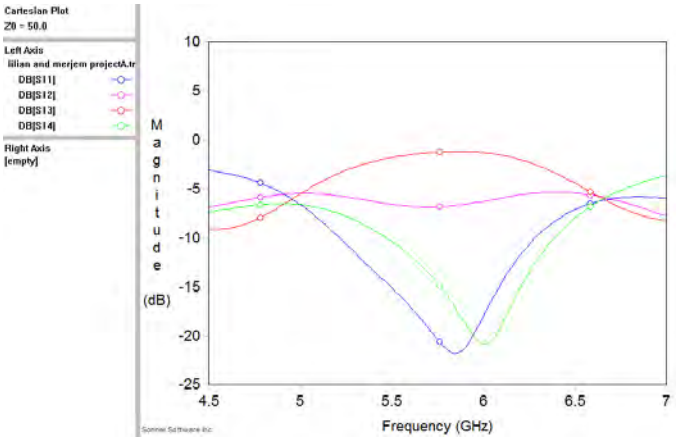

Figure 3. Simulation results

Taking into consideration the overall range we can see that operational range is fairly wide, with bandwidth from 4.8 to 6.58 GHz, 800Mhz, which can be seen in Figure 4. When we close up at coupling 6 dB we have 0.7 amplitude balance.

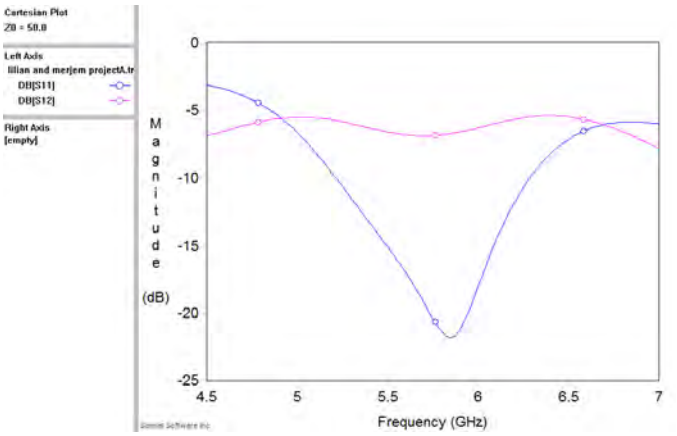

Figure 4. Close up on coupling 6 dB

Looking for the responses on the variation we have simulated the circuit changing the thickness of the most upper level and permeability of the Aluminum and got the results in the tables below. Table 1 is describing changes of the S11 and S12 during modifications of the thickness of air substrate on the top of the geometry. We can see that as we increase the thickness the bandwidth is decreasing and the lowest points of the S11 and S12 are changing and as such decreasing the amplitude balance.

TABLE I. AIR THICNKESS CHANGES

Thickness	S12 @ 6 dB	S11 @ 6dB	Bandwidth (GHz)	S12 lowest point	S11 lowest point
18	-6.3582	-18.7802	4.64 – 6.5	-6.9195	-22.0852
19	-6.3102	-18.3190	4.64 – 6.5	-6.8919	-21.9043
20	-6.2736	-17.9399	4.8 – 6.58	-6.8376	-21.7869
21	-6.2447	-17.6072	4.82 – 6.58	-6.8467	-21.6734
22	-6.2068	-17.3086	4.82 – 6.56	-6.8294	-21.5399

TABLE II. PERMITTIVITY OF ALUMINUM CHANGES

Ɛr	S12 @ 6 dB	S11 @ 6dB	Bandwidth (GHz)	S12 lowest point	S11 lowest point
9.7	-6.4289	-19.7117	5.04 – 7.5	-6.8431	-21.4363
9.8	-6.3586	-19.0453	4.84 – 6.68	-6.8185	-21.6928
9.9	-6.2736	-17.9399	4.8 – 6.58	-6.8376	-21.7869
10	-6.1518	-16.9473	4.78 – 6.5	-6.8495	-21.8692
10.1	-6.0892	-15.9628	4.76 – 6.56	-6.8279	-22.1121

IV. CONCLUSION

In this aricle we have designed the 6 dB hybrid microstrip coupler and have seen its behaviour under some changes. Increasing the thickness will increase the coupling and decreasing will decrease it with slightly changes in center fequency. Furthermore, changes made on the permittivity would also cause minor changes in the coupling as well as in the bandwidth frequency.

REFERENCES

[1] Sonnet Software, version 16.54, www.sonnetsoftware.com

[2] Pozar, D.M. (1998). Microwave Engineering[] (2nd ed.). USA: John Wiley & Sons

[3] K.C. Dalar, M. Yildirim, M. A. Aydin, Ş. T. Imeci, “3 dB Hybrid Coupler”, 28th Annual Review of Progress in Applied Computational Electromagnetics, April 10-14, 2012 - Columbus, Ohio

[4] S..S. Pai, M. Kumar , K. Singh, “Design and Performance Analysis of lumped and distributed 6-dB micro strip coupler topologies at S-band”, International Journal of Advanced Research in Electronics and Communication Engineering (IJARECE) Volume 6, Issue 5, May 2017REZAEI, A.

[5] Rezaei, A and Noori, L. Microstrip Hybrid Coupler with a Wide Stop-Band Using Symmetric Structure for Wireless Applications. J. Microw. Optoelectron. Electromagn. Appl., 2018, vol.17, n.1, pp.23-31

[6] https://www.markimicrowave.com/assets/appnotes/microwave_power_dividers_and_couplers_primer.pdf

A Compact Multi-Slot Microstrip Patch Antenna

Burhan Uzun, Mert B. Öçalan, Osman V.Koç,
Vedat A. Akün
Dep. of Electrical and Electronics Engineering, Istanbul Commerce University, Istanbul, Turkey

Taha İmeci
Dep. of Electrical and Electronics Engineering, Istanbul Commerce University, Istanbul, Turkey
Azra Yıldız
Dep. of Electrical and Electronics Engineering, International University of Sarajevo, Sarajevo, BiH

***Abstract*— In this work, design, simulation, fabrication and test of a compact multi-slotted microstrip patch antenna is studied. The antenna operates at 11 GHz. Radiation pattern of electric field phi-polarized gains is 4.70 dBi. Simulation and measurement results are presented with good agreement. The aim of our study was making a small size antenna which has multi-slots. The antenna has eleven rectangular slots thereby achieving easy fabrication and multi-resonance performance over previously published similar works in literature.**

Index Terms — multi-slot antenna, patch, compact

I. INTRODUCTION

The paper presents a compact patch antenna design supported by simulation. Simulations are obtained from the software called Sonnet Suites which uses Method of Moments as an electromagnetic solution technique [1]. Aperture antennas have been widely used as radiating elements. They are also used frequently as coupling elements for a variety of applications such as to excite a microstrip patch antenna [2]. These kind of antennas appear to be quite useful in various fields of application because of cost, size and weight [3]. Various features such as compactness, simple geometry and low cost makes the antenna suitable for recent wireless communication systems. The fundamental parameters of the antenna such as reflection coefficient, Voltage Standing Wave Ratio, radiation pattern, gain, directivity and efficiency are obtained for the proposed antenna [4] . The use of high permittivity microwave substrate in designing the antenna is an effective way to reduce the size of microstrip antenna at fixed operating frequency [5] . However, it degrades the radiation efficiency and bandwidth of the antenna. Thus, numerous techniques have been reported during the past few decades to reduce the size of MSA's [6]-[7]. These methods include shorted patch, meandered patch, meandered ground plane, meta-material loading or combination of mentioned techniques. Enclosing the patch in a metallic cavity is an another effective way for achieving miniaturization along with advantages like enhanced bandwidth, suppression of surface wave, enhanced gain etc. [8]-[9].

II. DESIGN AND SIMULATION RESULTS

In this work, a patch antenna was designed by feeding it from bottom-center. Several symmetric slots added to both sides of the antenna in order to meet the design specs. This resulted with having more gain and input matches are much better. We obtained resonance at 11 GHz. Highest gain and the lowest input match were obtained at 11.06 GHz. However, cross polarization of this frequency is higher than zero.In the final design, dielectric constant is 6.5 and dielectric thickness is 1.28 mm. The substrate that we used is Rogers RT3006. The resonance point seen at 11.625 GHz has low gain. The resonance frequencies were radiated in different planes. Radiation pattern of 11 GHz was on the x-z plane (Etheta). Figure 1 shows the dimensions that was shown for parametric study in Table 1.

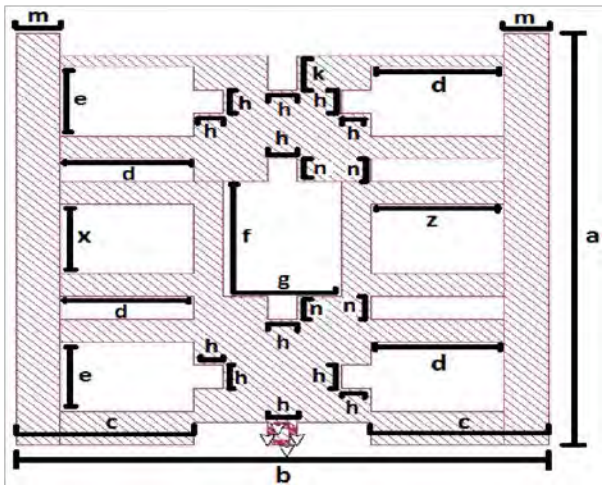

Fig. 1. Final design parameters.

TABLE I. PARAMETRIC STUDY

Length(mm)			**11 GHz**	
e	***F***	***n***	***Gain (dBi)***	***S11 (dB)***
6	10	2	4.701	-8.935
6.2	10	2	3.862	-6.160

5.8	10	2	3.443	-6.338
6.4	10	2	4.326	-6.400
6	10.2	1.8	4.114	-7.155
6	9.8	2.1	4.701	-8.934

III. IMPLEMENTATION

Fabricated antenna is seen in Figure 2. Simulated and measured S11 were shown in Figure 3, radiation pattern is in Figures 4. In Figure 4, measured and simulated radiation pattern were showed nearly same curve but 20° phase shifted. Almost same shift occured in S11 graph and the reason for that is errors in fabrication process.

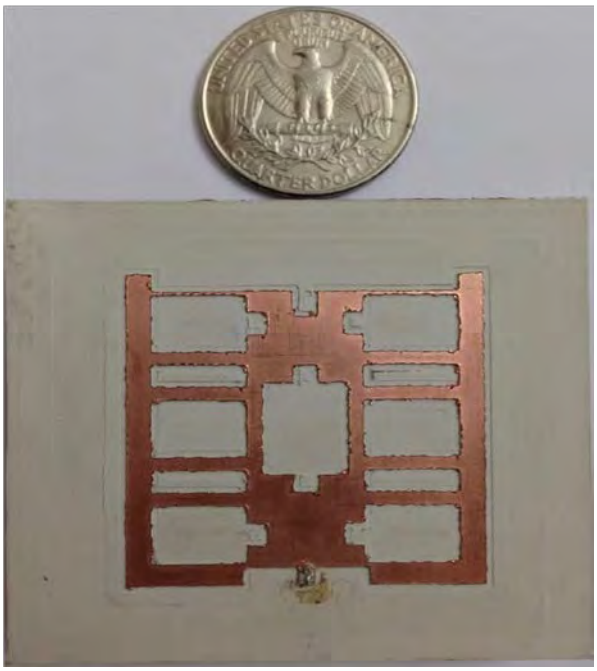

Fig. 2. Top view of the fabricated antenna

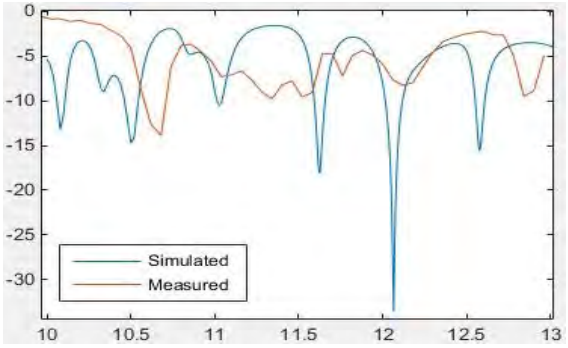

Fig. 3. Simulated and measured S11

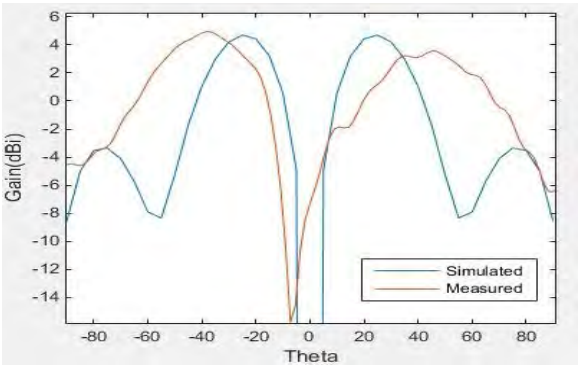

Fig. 4. Simulated and measured Gain at 11 Ghz

IV. CONCLUSION

In this work, a compact multi-slot patch antenna is designed, simulated, built and tested. Design was modified by making an optimization and a parametric study of slots on geometry. Simulated and measured results are found to be in good agreement. Next step is to improve the gain of the antenna.

REFERENCES

[1] M. Biswas, J. Y. Siddiqui, D. Guha and Y. M. M. Antar. "Effect of a cylindrical cavity on the resonance of a circular microstrip patch with variable air-gap," *Antennas and Wireless Propagation Letters, IEEE*, 5(1):418-420, 2006.

[2] C. Chen, W. E. McKinzie and N. G. Alexopoulos. "Spectral domain analysis of microstrip line fed arbitrarily-shaped aperture antennas," In *Antennas and Propagation Society International Symposium*, 1994. AP-S. Digest, volume 1, pages 158-161. IEEE, 1994.

[3] Y. Yoshimura. "A microstrip line slot antenna(short papers)," *Microwave Theory and Techniques, IEEE Transactions* on 20(11):760-762. 1972.

[4] N. Gunavathi and D. S. Kumar. "A compact coplanar waveguide-fed slot antenna for uwb applications," In *Electronics and Communication Systems (ICECS), 2014 International Conference* on, pages 1-4. IEEE, 2014.

[5] K. Wong and Y. Lin. " Microstrip-line-fed compact microstrip antenna with broadband operation," In *Antennas and Propagation Society International Symposium*, 1998 . IEEE, volume 2, pages 1120-1123. IEEE, 1998.

[6] A. A. Deshmukh and G. Kumar. "Compact broadband c-shaped stacked microstrip antennas," In *Antennas and Propagation Society International Symposium, 2002.* IEEE, volume 2, pages 538-541.IEEE, 2002.

[7] Y. Dong, H. Toyao and T. Itoh. "Design and characterization of miniaturized patch antennas loaded with complementary split-ring resonators," *Antennas and Propagation, IEEE Transactions* on,60(2):772-785, 2012.

[8] J. L. Volakis and J. M. Jin. "A scheme to lower the resonant frequency of the microstrip patch antenna," *IEEE microwave and guided wave letters*, 2:292 , 1992.

[9] A. Sharma, S. Kumar, B. K. Kanaujia and M. K. Khandelwal. "Truncated compact circular microstrip antenna loaded with asymmetric slits," In *Microwave and Photonics (ICMAP), 2013 International Conference* on, pages 1-4, Dec 2013.

Truncated Triangular T-Slotted Microstrip Patch Antenna

Faruk Bešlija
Department of Electrical and Electronics Engineering
International University of Sarajevo
Sarajevo, Bosnia and Herzegovina
fbeslija@ius.edu.ba

***Abstract* — A design of a triangular microstrip patch antenna (MPA) is presented. The patch is designed on an FR-4 substrate of a relative permittivity of 4.4 and thickness of 0.6 mm. The desired behavior of an antenna was achieved by utilizing single-edge truncation and a T-slot within the patch and increasing the length of the feeding probe. Several inherent disadvantages of the MPAs were addressed, most notably, the narrow impedance BW. The resonant frequency of an antenna occurs at 4 GHz, with over -30 dB input match available. The total available impedance bandwidth of 1.02 GHz, or 25.5% for the proposed antenna, is achieved. The Voltage Standing Wave Ratio (VSWR) is less than two throughout the entire bandwidth. The gain of 6.45 dB is obtained at 4 GHz, with a stable radiation pattern.**

Keywords* — *MPA, triangular patch, t-slot, probe-fed, impedance bandwidth, input match, VSWR

I. Introduction

Microstrip patch antennas are widely used due to their properties, such as low cost, high efficiency, simplicity of manufacture and easy integration to circuits [1]. As the market demands in personal communication systems, mobile satellite communications, direct broadcast and wireless local area networks increase rapidly, it is obvious that the demand for microstrip antennas will increase further [2, 3]. Although many design options are available, the triangular patch (especially with additional slots) is particularly interesting, due to its high gain and low input mismatch [4]. The MPA to be presented in this paper utilizes the triangular slotted patch to achieve the input match of at least -10 dB, gain of at least 5 dB and VSWR as close as possible to 1, values desirable for the antenna operation. The design to be presented also addresses one of the inherent disadvantages of the MPAs, the narrow impedance bandwidth [1], resulting in a significant impedance BW.

II. Antenna Design

There are two techniques to consider when achieving a reasonably low resonant frequency and a wider impedance BW, and those are: increasing the length of the probe feed and using a dielectric of an increased thickness with the low dielectric constant [1, 5, 6]. However, these dielectrics are more costly, and we aim to keep the low production costs. Thus, an FR-4 substrate of 0.6 mm thickness and 4.4 dielectric constant is used, and an additional 6 mm layer of air is added between the ground level and the substrate. The patch is designed on an FR-4 substrate of 150x150 mm. The initial design shape is a single-end truncated triangle. The feeding point is a circular via, centered vertically at 25.5 mm and aligned horizontally 22.5 mm away from the leftmost side. Experimentally, it has been found that adding a T-shaped slot on the left from the feeding point results in significant both the input match and the impedance bandwidth. Indentation on the truncated edge slightly increases the resonant frequency, but it additionally improves the performance. Also, it has been found that, for this design, the performance of the antenna improves as the circular via is optimized to be closer to the edges. The design of the patch is given in Figure 1 (2D patch view) and Figure 2 (3D layers view).

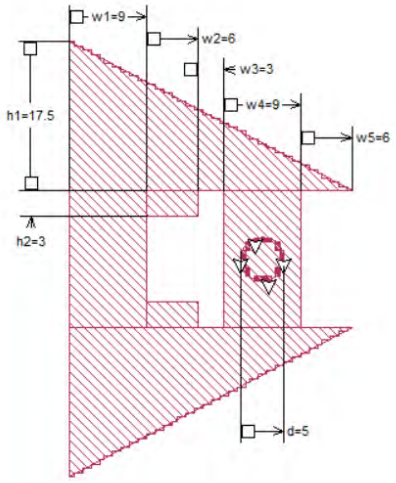

Fig. 1 Patch Design (all dimensions specified in mm)

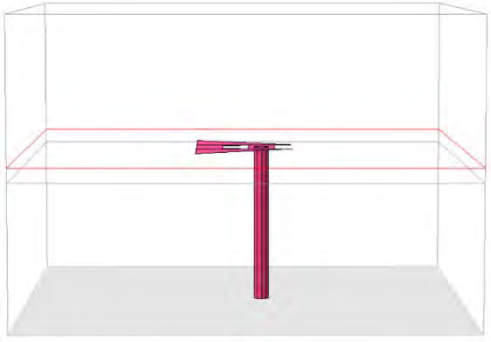

Fig. 2 3D Layers View (GND: air, 0: FR-4. 1: air)

III. Results

The simulation results show that the antenna behaves as previously described. The input match of an antenna available at 4 GHz is -30.19 dB. Also, the impedance bandwidth (considering S_{11} less than -10 dB) is significant, as the antenna appears to be effective from 3.54 GHz at lowest up to 4.56 GHz at highest, which allows for 1.02 GHz of the available impedance bandwidth, or 25.5% for the proposed antenna. From this, it can be concluded that the proposed MPA design is a good solution to the inherent narrow impedance bandwidth. Frequency response of the antenna is given in Figure 3.

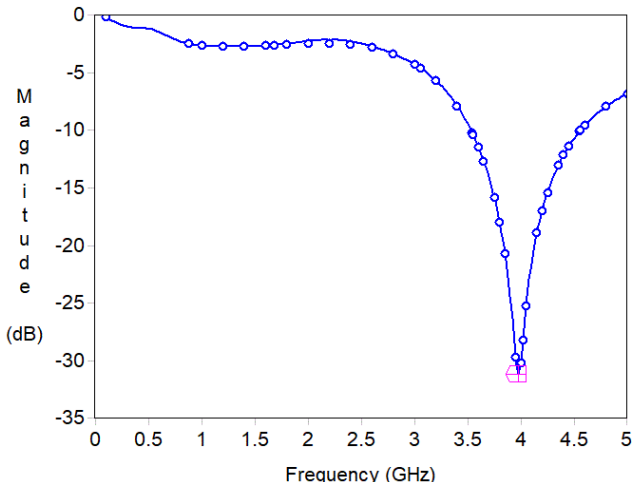

Fig. 1 Input match in dB

In terms of the VSWR, the antenna exhibits the desired behavior for the entire impedance bandwidth. At 4 GHz, the VSWR value is as low as 1.06, whereas, at the border frequencies, 3.54 GHz and 4.56 GHz, the VSWR values are 1.895 and 1.93, respectively. Therefore, the antenna has a good match for the given resonant frequency and the impedance bandwidth, as seen in Figure 4.

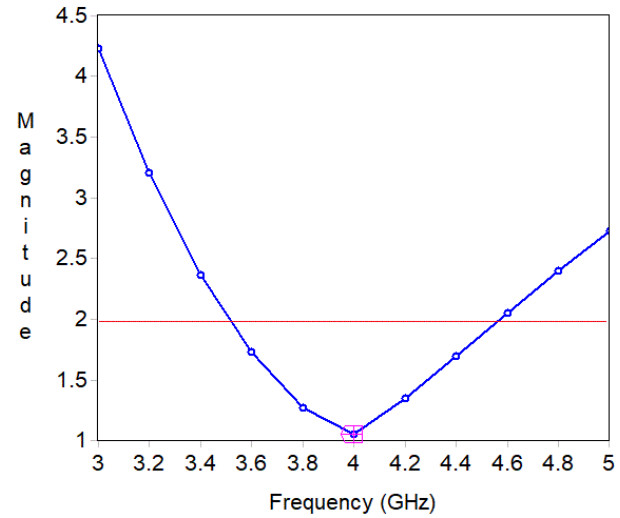

Fig. 4 VSWR

In terms of gain, the antenna appears to be working properly in the entire bandwidth, with the lowest E (Phi) of 6.11 dBi and the highest E (Phi) of 6.56 dBi. At 4 GHz, the value of the gain is 6.45 dBi.

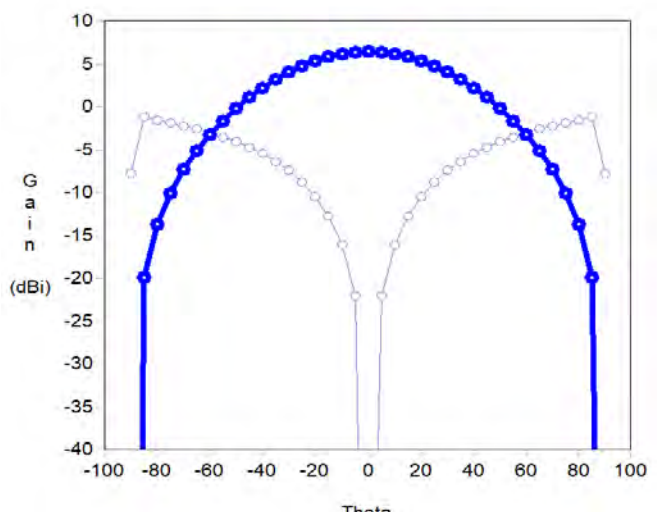

Fig. 5 E (Phi) in dB (Cartesian)

IV. Conclusion

A microstrip patch antenna design utilizing truncated triangular T-slotted patch and an extended length probe feed was presented. The following antenna has a resonant frequency at 4 GHz and a significant impedance bandwidth of 25.5%. The VSWR value reaches 1.93 at highest and 1.06 at the resonant frequency, whereas the E_{Phi} is constantly over 6.11 dBi, and 6.45 dBi at the resonant frequency. These results indicate that the proposed antenna is suitable for applications in the given bandwidth. The patch of the antenna was mounted on a low-cost, small-dimension FR-4 substrate, making the production of this antenna less expensive in comparison with the same types of antennas utilizing the high-end substrates.

V. References

[1] Bhomia, Yogesh, Ashok Kajla, and Dinesh Yadav. *"V-slotted triangular microstrip patch antenna."* Int. Journal of Electronics Engineering 2, no. 1 (2010): 21-23.

[2] Ćosić, Said, Yusuf Alper, and Mahir Čengić. *"Design, Optimization and Parametric Assessment of a Diamond-Hammer-Shaped Microstrip Patch Antenna."* Computational Methods and Telecommunication in Electrical Engineering and Finance, 2018.

[3] D. G. Fang. *"Antenna Theory and Microstrip Antennas."* 1st ed. Boca Raton, FL: CRC Press, 2010, pp. 85-110.

[4] Medhi, Mayurakshi Roy. *"Performance Analysis of Truncated Triangular Microstrip Patch Antenna."* International Journal of Advanced Research in Education & Technology (IJARET) 5, no. 2 (April 2018): 29-31.

[5] James, J.R, and P.S Hall. *"Handbook of Microstrip Antennas."* London: Peter Peregrinus, 1989.

[6] Balanis, Constantine A. *"Antenna Theory: Analysis and Design."* Hoboken, NJ: Wiley, 2016.

Square Slotted Microstrip Low-Pass Filter At 10GHz

Aldin Bekto
Electrical and Eelectronics Enginering
International University of Sarajevo
Sarajevo, Bosnia & Hercegovina
Aldinbekto5@gmail.com

***Abstract*—This paper will present a compact microstip low pass filter in a square slotted design using microstrip filter. The model combines an outer square resonator and an inner box with a square-shaped patch attached to each of its inner walls. After research on Square slotted designs, a structure was drafted, improved on and this final design was made. The compact design's area is 30x14mm2 and the cut-off frequency is at 10GHz.**

Keywords— compact, microstrip, filter, low pass, square slotted, SRR

I. INTRODUCTION

As technology advances, it also demands advances in all other areas as well. Developments in wireless communication systems such as in mobiles brought an obstacle in the design of microwave components such as filters and antennas. To overcome the obstacle the components design led to them becoming much smaller, cheaper and made the process of designing and fabricating simpler.

Microstrip technology has been widely used in several and various wireless circuits and systems due to its ease fabrication, integration and compatibility with the planar device. The demand for the compact size of microstrip low pass filters has increased and intensified, particularly when these filters are used in the monolithic microwave integrated circuits (MMIC). To achieve a compact filter circuit and high-performance, diverse technical methods were proposed in the research. Among them, defected ground structures were applied to have a low pass filter with wide stopband, high dielectric constant substrate, stepped-impedance resonator and metamaterials [1].As compared to waveguide filters, microstrip filters have smaller sizes, but in several applications very compact microstrip filters are required. Currently, radar, mobile and satellite communication systems are application examples which necessitate miniature filters as imperative components [2].

II. DESIGN STEPS

Due to the rapid advancement in the microwave field and modern communication systems, the demand for compact size and high electrical performances has been extensively increased in the design of microwave planar filter. These features and characteristics are unavailable by using the conventional and classical methods [3]. For the first draft of the design, a basic model of a low-pass filter was used. That model is the beginning basis for this prototype. After implementing a base model, research on SRR characteristics and requirements was done to be able to modify and expand on our existing base model. The square SSR composed of two concentric enclosed loops with splits in them at opposite sides.

The SRR unit cell has a magnetic response owing to the presence of artificial magnetic dipole moments by the ring resonator. At a resonant frequency band, these artificial magnetic dipole moments are larger than the applied field. This phenomena gives rise to the presence of the real part of negative effective permeability at the resonant frequency range of the resonator [4].

After obtaining more knowledge we modified our design. We tried to achieve the best frequency characteristics by experimented with the outer and inner squares. Numerous attempts, modifications and simulations were made in order to achieve the desired goals. We used 4.4 for our Dielectric constant and we set the dielectric constant of air to be 1 to make it a complete and valid system. The dimensions and symmetrical shape of our filter was coming a lot good. We had to add four microstrip blocks on each side of the inner box to improve the frequency characteristics and the gain. . Graphical values of S21 and S22 of the filter we designed are shown in figure 1. A novel compact miniature microstrip low-pass filter based on square SRR and dumbbell shape DGS is proposed, studied and fabricated. The two resonators have been added to improve the electrical performances and to achieve a small compact circuit area [5].

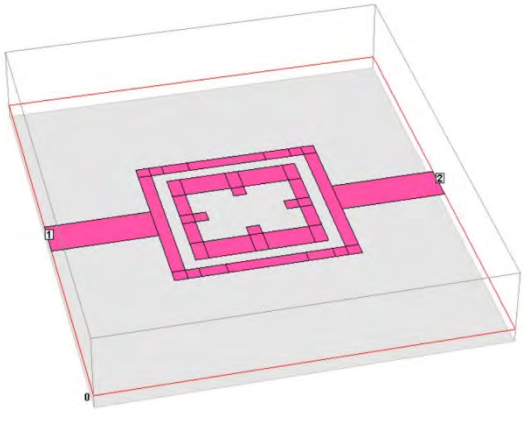

Figure 1. 3D View of the simulated LPF

III. SIMULATION RESULTS

After experimenting with different properties of the filter design, all of the results have been shown in table I and II below. As anticipated, the required S11 and S12 results were achieved with the dielectric constants (ε_r) of 1 and 4.4, before modification. The filter was simulated between 0.01 Hz and 12GHz. Figure 2 shows that the cut-off frequency falls at 10GHz.

TABLE I
FILTER BOX AND SPACING CHANGES

Dielectric Thickness / constant	Box Width / Coupled line Spacing	S11(dB)	S12(dB)
1.075 / 4.4	0.9/0.9	10.1GHz / -28.589556	10.1GHz / -6.013500
1.0 / 4.4	0.8/0.8	10.05 GHz / -7.9274914	10.05 GHz / -2.2534412
0.975 / 4.4	0.7/0.7	9.85 GHz / -13.053291	9.85 GHz / -0.2205130
0.85 / 4.4	1.0/1.0	9.95 GHz / -7.4403693	9.95GHz / -0.8633788
1.1 /4.4	**1.1/1.1**	**9.85 GHz / -11.433348**	**9.85 GHz / -0.3240029**

TABLE II
FILTER DIELECTRIC CHANGES

Air (mm)/ Dielectric constant	S11(dB)	S12(dB)
1.0 / 4.4	10 GHz / -9.7318000	10 GHz / -1.5806401
0.85/4.4	9.95 GHz / -7.4403693	9.95GHz / --0.8633788
0.975 / 4.45	9.75 GHz / -12.168045	9.75 GHz / -0.2719612
1.075 / 4.45	10.1 GHz / -8.2824858	10.1 GHz / -0.6981970

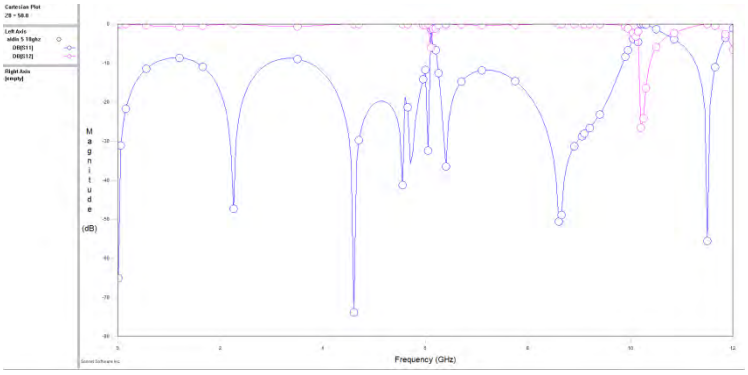

Figure 2. Simulated S11 and S12 of the filter

IV. CONCLUSION

Everything regarding this low-pass filter was designed and simulated in Sonnet Suites, 3D planar electromagnetic simulations software. The filter still needs some improvements and adjustments. For example, there is a glitch at 6 GHz, and it might be a simulation error. After it has been improved up to satisfaction, it will be fabricated and its characteristics will be measured and tested in real-life conditions.

REFERENCES

[1] L. Ge ,J. P. Wangand Y-X Guo, "Compact microstrip lowpass filter with ultra-wide stopband," Electronics Lett., vol. 46, no. 10, pp. 689 – 691, May 2010

[2]. Nasiri, B. (2019). A Novel Design of A Compact Miniature Microstrip Low pass Filter Based On SRR. Retrieved from https://www.researchgate.net/publication/317248194_A_novel_design_of_a_compact_miniature_microstrip_low_pass_filter_based_on_SRR

[3] Ahmed ES. Dual-mode dual-band microstrip bandpass filter based on fourth iteration T-Square fractal and shorting pin. Radio Engineering Journal.2012; 1 (2): 617–623

[4] J. Wang, H. Cui, G. Zhang, ''Design of compact microstrip lowpass filter with ultra-wide stopband", Electronics Letters, Vol. 48, Issue 14, pp. 854–856, July 2012.

[5] Nasiri, Badr & Ahmed, Errkik & ZBITOU, JAMAL & Tajmouati, Abdelali & El Abdellaoui, Larbi & Latrach, Mohamed. (2018). A Compact Miniature Microstrip Low pass Filter Based on Dumbbell DGS and SRR Unit Cell. International Journal of Microwave and Optical Technology. 131.

[6] Sonnet Suites, www.sonnetsoftware.com, ver. 16.54

Design of Compact Dual-Band Microstrip Bandpass Filter

Haris Basarić & Sadžida Halvadžić
Department of Electrical Engineering
International University of Sarajevo
Sarajevo, Bosnia and Herzegovina

Abstract

In this paper, we proposed Compact Dual-Band Microstrip Bandpass Filter with its projection, design, simulations and final analysis. The aim of the project is to introduce a new configuration of microstrip filter design. This filter combines a conventional two open stubs BPF and an optimum BPF. Simulations show this filter generates two passbands around 3.5 GHz and 6.3 GHz without increasing the circuit size much, compared with the conventional BPF. We have S11 for first frequency -31.55dB and for second -20.21dB. For S21 we have -.236dB for first and -0.885dB for second frequency.

Keywords **- Bandpass Filter, Open Stub, Optimum Bandpass Filter, Federal Communication Commission (FCC)**

I. INTRODUCTION

Microstrip bandpass filters are being widely used in microwave systems. A wide number of different topologies allows obtaining specific responses for a wide range of applications. We compared our work to Microstrip Bandpass Filter at 3.2 GHz [1]. They used similar technology with one passband at 3.2Ghz. We, on the other hand, have two passbands at 3.5Ghz and 6.3Ghz. We used similar methods and simulation software to test this filter. Various techniques have been developed to design and synthesize these BPFs [2]. Designing dual-band filters using loaded stub open-loop resonators is a common practice [3]. This structure has a return loss of more than 3 dB in two bands. Dual-band bandpass filters have also been provided using spiral stepped-impedance resonators [4]. In [5] dual-band filters have been designed using defected ground structure resonator and a dual-mode open-stub loaded stepped impedance resonator. Dual-band bandpass filters are highly desired in many applications for their two separate passbands at two different frequencies. Conventionally, a dual-band BPF can be obtained by cascading two different BPFs. The side effects are the high insertion loss in the passband and increased circuit size. In this paper, a dual-band BPF is formed by combining a conventional two open stubs BPF and an optimum BPF. By inserting an optimum BPF between the two open stubs of a conventional BPF, one can obtain a second passband without increasing the overall circuit size much. The proposed BPF is simulated on the Sonnet Suite software[6].

II. DESIGN STEPS AND DIMENSIONS

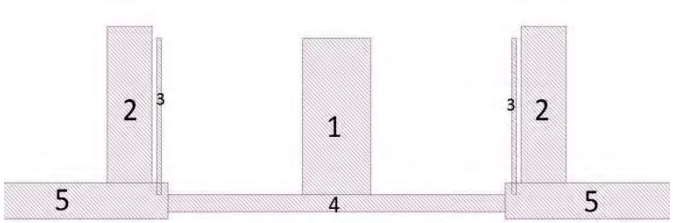

Figure 1. – Top view of the filter

Figure 1 has the top view of the filter and below in Table I are dimensions in milimeters. Below on Figure 2 is also 3D view of the model. Total size of the filter shows us that its size is compact.

TABLE I. FILTER DIMENSIONS

ID	Length	Height
1 - Central Box	30 mm	65 mm
2 – L Side Boxes	20 mm	65 mm
3 – S Side Boxes	2 mm	65 mm
4 – Bottom Box	150 mm	7 mm
5 – Bottom Side Box	75 mm	15 mm

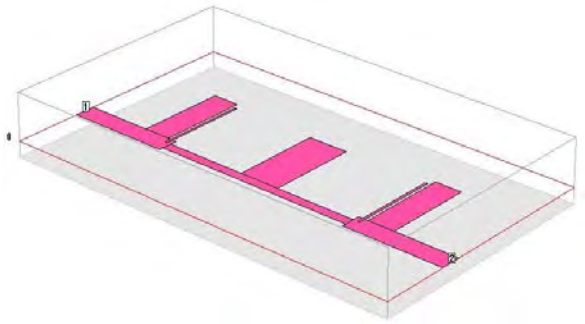

Figure 2. – 3D view of microstrip filter

III. Analysis and Parameters

The data below shows how parameters change (such as frequency) if we change dimensions of the filter. We have S11 and S21 parameters. Important thing is that frequencies stay the same as much as possible for these changes, which is true for our filter and it's shown below.

TABLE II. TESTING THE FILTER BY CHANGING DIMENSIONS

		Test 1	Test2	Test 3	Test 4	Test 5
Dimension 1		30 x 65	35 x 65	50 x 65	15 x 65	25 x 65
Dimension 2		20 x 60	20 x 60	20 x 60	20 x 60	20 x 60
Dimension 3		5 x 65	5 x 65	5 x 65	5 x 65	5 x 65
Dimension 4		150 x 5	150 x 5	150 x 5	150 x 5	150 x 5
S11	F1	3	3	3	2.9	3
	F2	5.6	5.5	5.3	6.7	5.9
S21	F1	3	3	3	2.9	3
	F2	5.6	5.5	5.3	6.7	5.9
S11	DB1	-34	-26	-25.9	-25.8	-25
	DB2	-18.84	-20	-17.9	-14.3	-15.7
S21	DB1	-0.17	-0.18	-0.21	-0.2	-0.2
	DB2	-0.93	-0.8	-0.7	-1.5	-1.1
Frequency on -10 for S21	F1	2.52	2.6	2.68	2.4	2.44
	F2	3.48	3.55	3.6	3.38	3.42

The table above shows the first five tests. For all these five tests first, bandpass frequency almost does not change. However, frequency 2 changes more when Dimension 1 is cut by half in test 4. This is reasonable because it's a drastic change in length of Dimension 1. In manufacturing, there won't be such mistakes and for small changes filter behaves perfectly as the simulated version.

TABLE III. TESTING THE FILTER BY CHANGING DIMENSIONS

		Test 6	Test 7	Test 8	Test 9	Test 10
Dimension 1		30 x 55	30 x 75	30 x 90	30 x 65	30 x 65
Dimension 2		20 x 60	20 x 60	20 x 60	20 x 60	20 x 60
Dimension 3		5 x 65	5 x 65	5 x 65	5 x 65	2 x 65
Dimension 4		150 x 5	150 x 5	150 x 5	150 x 7	150 x 7
S11	F1	3	3	3	3.4	3.5
	F2	6	5.4	5	6.3	6.3
S21	F1	3	3	3	3.4	3.5
	F2	6	5.4	5	6.3	6.3
S11	DB1	-34	-33	-31.8	-28.7	-31.5
	DB2	-17	-20.5	-18	-18.1	-20.2
S21	DB1	-0.17	-0.17	-0.17	-0.2	-0.24
	DB2	-1.05	-0.85	-0.78	-0.97	-1.28
Frequency on -10 for S21	F1	2.5	2.52	2.5	2.9	3
	F2	3.46	3.48	3.5	3.86	4

The second table shows the next five tests of the microstrip filter. By changing dimensions until the test 8, frequency 1 stays always 3Ghz, but in the last two tests, it jumps a little by 0.5Ghz. Frequency 2 changes more often, from approximately 5Ghz to 6.7Ghz. Chosen frequencies are with final dimensions. This is all normal and considerable if we look at the change in dimensions. It is important that small changes don't influence changes in frequencies that much.

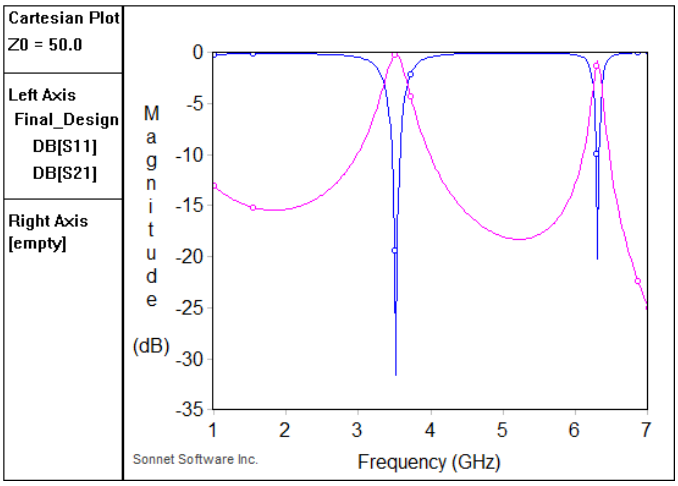

The picture shows the final output of the signals from the filter with passbands. We have two passband frequencies at 3.5Ghz and 6.3Ghz. We have S11 for the first frequency -31.55dB and for second -20.21dB. For S21 we have -0.236dB for first and -0.885dB for second frequency. This is great result for this filter.

IV. Conclusion

Dual pass microstrip bandpass filter using open stubs is designed and simulated. The simulation results are found to be very satisfactory. In order to shift the closest harmonic, we changed the dimension for the bottom box. Using that structure the proposed optimization is provided. In the final structure of the filter, the frequency of the first and second passbands are 3.52GHz and 6.30 GHz respectively. The proposed BPF is simulated on Sonnet Suite software.

References

[1] Mudrik Alaydrus, Designing Microstrip Bandpass Filter at 3.2 GHz, *International Journal on Electrical Engineering and Informatics - Volume 2, Number 2, 2010*

[2] J. S. Hong, Microstrip Filters for RF/Microwave Applications, John Wiley and Sons Inc., 2011.

[3] Mondal, P., Mandal, M. K. Design of the dual-band bandpass filter using stub-loaded open-loop resonators, *IEEE Transactions*

[4] Guo, L., Yu, Z., Zhang, Y. A dual-band band-pass filter using stepped impedance resonator. *Microwave and Optical Technology Letters*, 2011, vol. 53, no. 1, p. 123–125. DOI: 10.1002/mop.25648

[5] Wang, L., Guan, R. Novel compact and high selectivity dual-band bandpass filter with wide stopband. *Radioengineering*, 2012, vol. 21, no. 1, p. 492–495.

[6] Sonnet Software Suite, http://www.sonnetsoftware.com/

3 Element Coupled Line Bandpass Filter

Ahmed Nurović, Haris Kovačević
Department of Software Engineering
International University of Sarajevo
Sarajevo, Bosnia and Herzegovina
Ahmed.nurovic@hotmail.com , haris_kovacevic1@hotmail.com

Abstract- In this project we proposed a bandpass filter with its projection, design, simulations and final analysis the aim of the research was to make a working bandpass filter in the sonnet application which is made for analyzing and testing. Our bandpass filter is of a simple design it had three lines connected to two ports, each on one side. The bandpass filter is simulated band between 0.01 to 4.0 GHz, where S11 = - 36.44 dB and S12 = - 0.14 dB .

Keywords- Three element coupled line Bandpass filter, Band Pass filter (BPF), Sonnet suites.

I. BAND-PASS FILTER INTRODUCTION

A band-pass filter or BPF, is a device that passes frequencies within a certain range and rejects frequencies outside that range. Bandpass is an adjective that describes a type of filter or filtering process; it is to be distinguished from passband, which refers to the actual portion of affected spectrum. Hence, one might say "A dual bandpass filter has two passbands." A band pass signal is a signal having a band of frequencies ranging from some non zero value to another non zero value, such as a signal that comes out of a bandpass filter. There are various different structures. For implementing DGS [1]. By applying these different DGS structures filters, power splitter, power amplifier etc. Our main goal was to have an transmission for at least 0,5 GHz which we achieved in the long run. An ideal bandpass filter should have a flat passband, and would completely attenuate all fequnecies outside the passband. In addition, the transition out of the passband would have brick wall characteristics. Talking in practical terms, there is no ideal bandpass filter. The filter can't attenuate all frequencies outside the desired frequency range completely. [2]Simulation was conducted in a 3D planar high frequency electromagnetic software called Sonnet. The most important characteristic of this design is to find the best possible filter in order to obtain ideal results and get good response for nowadays BDF with modified ground structure [3],[4].

II. DESIGN AND SIMULATION RESULTS

In fig. 1 you can see how our bandpass filter looks from the top view. It has 3 coupled lines which are separated by 0,5 mm. The ones on the edges are the same size while the middle is the longest reaching their midpoints.

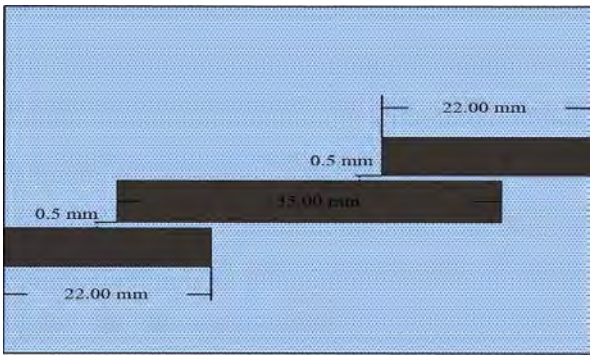

Figure 1. – Top view of the BPF

Table 1 shows the dimensions for our coupled line bandpass filter, and the names of the lines.

TABLE I. FILTER MEASUREMENTS

Name	Length	Width
Left piece	22.00 mm	4.0 mm
Coupled lines	35.00 mm	3.0 mm
Feedline Box	22.00 mm	4.0 mm
Spacing		0.50 mm

Table 2 repesents our parameters which we used to conduct the tests on the coupled line bandpass filter.

TABLE II. FILTER PARAMETERS

Parameters	Values
Dielectric thickness (Ɛr)	2.5
Cell size	0.5 mm
Box size	59 x 50 mm
Frequency	0.01 – 4.0 GHz

III. PARAMETRIC STUDIES

Table 3 shows frequencies we got after we changed dielectric thickness and air. Every change in dielectric thickness and air changed our frequency for a bit but its slight change that shows how frequency change every time.

TABLE III. CHANGING OF DIELECTRIC THICKNESSES AND AIR SPACE

Dielectric Thickness / Air (mm)	S11 (dB)	S12(dB)
1.2 / 7.0	2.80 GHz / -20.10	2.82 GHz / -0.28
1.4 / 7.0	2.74 GHz / -20.16	2.78 GHz / -0.73
0.8 / 8.0	2.72 GHz / -36.44	2.72 GHz / -0.14
0.6 / 8.0	2.72 GHz / -23.13	2.72 GHz / -0.23

Figure 2 shows the variation of the magnitude of (s11) with the frequencies

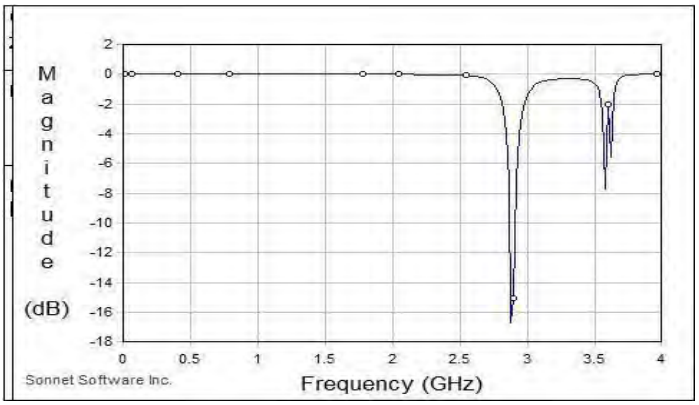

Figure 2. S11(Return loss)

Figure 3 illustrates how the magnitude of (S21) changes with the frequecies.

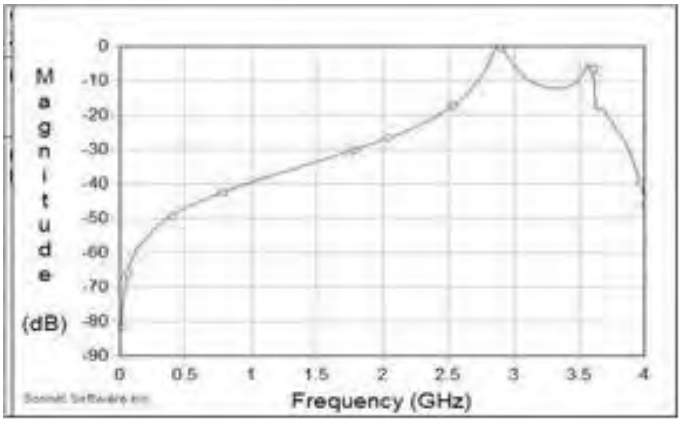

Figure 3. S21(Insertion loss)

Figure 4 shows us the combine view of both S11 and S21.

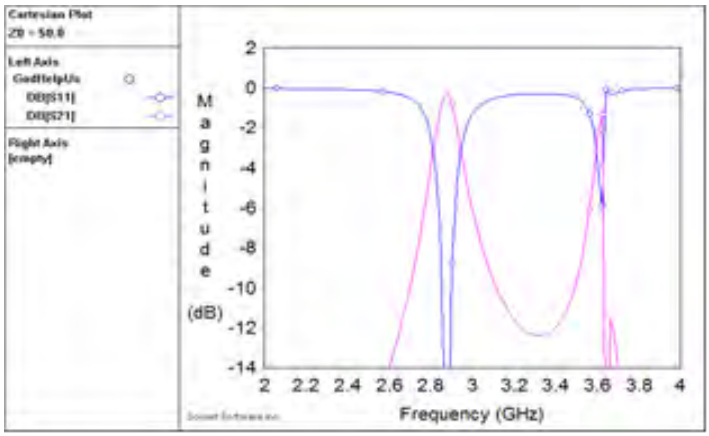

Figure 4. S11 and S21 combined

IV. CONCLUSION

This paper presented an approach to design a band pass filter. Several simulations was carried out for the design. The simulation reveals that the seperation must be 0.5mm. The filter that meets the design creteria was suceffully designed. Our paper was a simple design of an Band pass filter, we had three elements which where separated by 0,5 mm and our main goal was to achieve a trassmition which would last at least 0.5 GHz which we achieved in after a lot of testing and making mistakes which we didn't realize in the beginning . Regarding the whole project we feel satisfied by the results of our testing and our final design, thought we would have been more happy if our transmission was at least more than 1 GHz which would be compared to a professionally made Band Pass filter it looks good. We did simulations between frequencies 0.01 GHz and 4 GHz and implement all necessary components we needed for our simulation. After the testing, results were compared with similar ones found in the literature that are in good agreement with desired ones with acceptable difference.

V. REFERENCES

[1] L. H. Weng, Y. C. Guo, X. W. Shi, and X. Q. Chen "An Overview On Defected Ground Structure," PIER B", Vol. 7, pp. 173– 189, 2008

[2] Sonnet Suites, ver. 16, Sonnet Software Inc., Syracuse

[3] K. Bahal "Design and Analysis of Band Pass Filter using Modified Ground Structure," IJCCER", Vol. 3, No 4, 2015

[4] L. Barpete, B. Garg "Design And Analysis of High Pass Filter With Modified Ground T-Shape Structure for L Band Telecommunication User For 1800-1900MHz,"IJERT",Vol 7 Issue 09, pp. 89-91,2018

Directivity Enhancement of 60 GHz Inset-fed Patch Antennas Using Fabry-Perot Resonators

Müberra Arvas* and Mohammad Alsunaidi†
*Department of Electrical Engineering, Istanbul Medipol University, Istanbul, Turkey
†Electrical and Electronics Engineering Department, Marmara University, Istanbul, Turkey

***Abstract*—Channel loss in the 60 GHz communications band pose a very serious problem for long distance links. Consequently, methods for compensation must be developed. One way to partially overcome the channel loss is to improve the directivity of the antenna. In this paper, a patch antenna design that incorporates a dielectric Fabry-Perot resonator is presented. The antenna characteristics were studied using a commercial software. Simulation results show that the Fabry-Perot coupled antenna exhibits a high increase in the directivity without compromising antenna bandwidth and gain.**

***Keywords*— antenna directivity; patch antenna; 60 GHz band; Fabry-Perot resonator; 5G communications.**

I. INTRODUCTION

The 60 GHz frequency band presents a huge opportunity for high bandwidth and high rate communications. Besides being unlicensed and underutilized, a lot of potential for secure and high data rate communication links exist in this band and can hold the future of wireless systems. The most important challenge to wireless communications in this band is the significant absorption loss that reaches over 15 dB/km at 60 GHz [1]. Consequently, the successful adoption of 5G communications using the 60 GHz frequency band for wireless and radio communications is largely dependent on the introduction of novel antenna designs and communication strategies to overcome the channel loss. One direction that can lead to partial compensation of channel loss is antenna directivity enhancement. Several reports have used metasurfaces and electromagnetic bandgap structures and superstrates to manipulate antenna radiation properties [2-3]. Antenna designs based on the Fabry-Perot concept have also been reported [4-5].

In this paper, a novel dielectric Fabry-Perot resonator (DFPR)-coupled antenna design for 60 GHz operation is presented. The aim is to improve the directivity of the basic single patch antenna. The antenna radiation mode is coupled to the FP cavity mode, resulting in the focusing of the far field radiation. The DFPR is constructed separately and assembled on top of the antenna substrate, making device fabrication simple and straightforward. The resulting enhancement in the antenna directivity is significant with no compromise in the antenna bandwidth and gain. To the best of our knowledge, this is the first report of directivity enhancement of basic patch antennas using the DFPR technique in the 60 GHz frequency band.

II. BASIC DESIGN OF THE 60 GHZ ANTENNA

A basic patch antenna is used as a reference as shown in figure 1. The basic antenna dimensions are set for resonance in the 60 GHz frequency band and is fed using an inset. The antenna is printed on a 0.254 mm thick substrate with dielectric constant of 3.38. The design parameters, including the inset dimensions are given in table 1. The operation of the antenna was simulated using COMSOL Multipyhsics commercial software. Several studies have been performed to characterize the antenna, including return loss, directivity and radiation patterns. It was found that this reference inset-fed antenna has a return loss of -22.2 dB at a resonance frequency of 58.80 GHz, as shown in figure 2. Consistent with the fact that the directivity of a standard patch antenna is between 5-7 dB, the directivity obtained for the reference antenna was found to be 6.87 dB.

TABLE I. BASIC ANTENNA PARAMETERS.

Parameter	Value
Antenna Length (L)	1.24 mm
Antenna Width (W)	1.68 mm
Stub Width	0.15 mm
Stub Length	0.25 mm
Feed Line Width (W_f)	0.54 mm
Substrate Thickness	0.254 mm
Substrate Dielectric constant	3.38

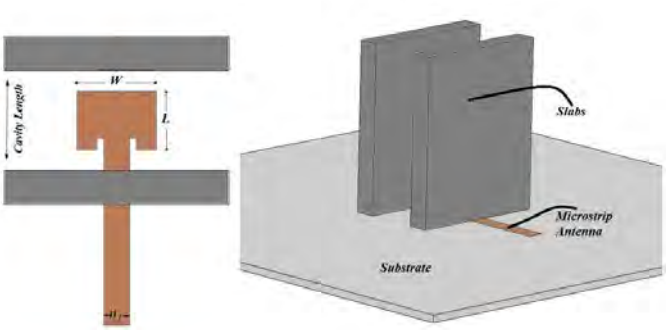

Fig. 1. Top view of antenna with DFPR (left) and the DFRR-coupled patch antenna(right).

III. FABRY-PEROT COUPLED PATCH ANTENNA

A DFPR structure consists of two dielectric slabs of a certain thickness and dielectric constant. The space between the slabs forms a cavity whose effective width together with the

cavity medium determine the mode resonances. This DFPR structure is shown in figure 1. In this work, the DFPR structure is placed on top of the substrate such that the patch antenna is contained within the space of the cavity and the radiating edges are parallel to the resonator slabs. A high dielectric material was used for the resonator slabs for effective confinement of the cavity modes within the resonator dimensions. Each of these dielectric slabs has a thickness of 0.7 mm, width of 4.7 mm and height of 5.75 mm. The dielectric constant of the slabs is 11.7 and the cavity medium is air. Figure 2 shows the return loss of the DFPR-coupled antenna for a cavity length of 2.1 mm. The cavity length is varied, and the resulting characteristics are studied. Table 2 shows the directivity of the DFPR-coupled antenna as a function of the effective cavity length. The resonant mode wavelength calculation of the DFPR is based on partial penetration of the mode profile inside the cavity walls. Figure 3 shows the directivity of the DFPR-coupled antenna versus the wavelength fraction of the cavity effective length. The directivity peaks at around λ/2. This result confirms that the radiated field from the patch antenna at resonance couple to the fundamental mode of the DFPR.

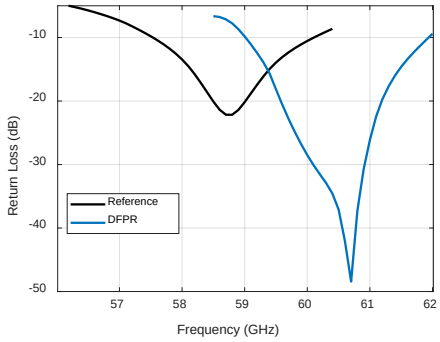

Fig. 2. Return loss of the reference antenna and the DFPR-coupled antenna.

TABLE II. DIRECTIVITY OF THE DFPR-COUPLED ANTENNA VERSUS CAVITY EFFECTIVE LENGTH.

DFPR cavity length (mm)	Directivity (dB)
2.16	10.386
2.46	12.735
2.8	12.379
3.0	12.299
3.2	11.352

It should be remarked that the enhancement in the directivity does not compromise other important antenna parameters such as bandwidth and gain. Finally, figure 4 shows a 3D view of the radiation pattern of the DFPR-coupled antenna for a cavity length of 2.1 mm.

I. CONCLUSION

We have presented a dielectric Fabry-Perot resonator-coupled patch antenna design that exhibits significant directivity enhancement. Directivity enhancement is very essential for effective communications in the 60 GHz frequency band due to the huge channel loss. The design concept is based on coupling the antenna radiation field to the fundamental mode of the FP cavity, resulting in a favorable manipulation of the antenna far-field radiation. The dielectric cavity structure is assembled on top of the antenna substrate such that the fabrication of the antenna structure is simple and straightforward. Experimental verification is underway, and more variations of the cavity design are attempted.

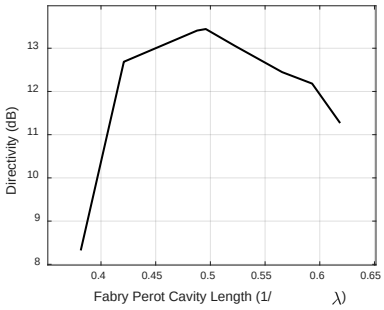

Fig. 3. Directivity of the DFPR-coupled antenna as a function of cavity length.

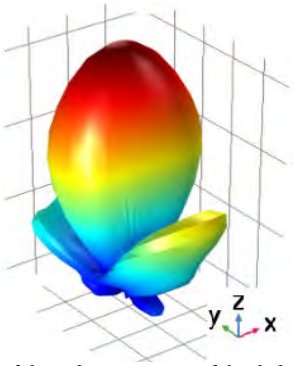

Fig. 4. A 3D view of the radiation pattern of the dielectric Fabry-Perot resonator-coupled antenna.

REFERENCES

[1] D. S. Makarov, M.Yu. Tretyakov, P.W. Rosenkranz, "60-GHz oxygen band: Precise experimental profiles and extended absorption modeling in a wide temperature range," *Journal of Quantitative Spectroscopy & Radiative Transfer*, 112, pp. 1420–1428, 2011.

[2] Olivier Roncière, Ronan Sauleau, Kouroch Mahdjoubi, "An EBG resonator antenna with a controllable directivity", *11th International Symposium on Antenna Technology and Applied Electromagnetics [ANTEM 2005]*, 2005.

[3] Hayat Errifi, Abdennaceur Baghdad, Abdelmajid Badri, Aicha Sahel, "Directivity enhancement of aperture coupled microstrip patch antenna using two layers dielectric superstrate", *Proceedings of 2014 Mediterranean Microwave Symposium (MMS2014)*, 2014.

[4] Z.G. Liu, "Fabry-Perot Resonator antenna", *Journal of Infrared Millimeter and Terahertz Waves*, Vol. 31, No. 4, pp. 391-403, 2010.

[5] Jian Yang, Feng Xu, Siyuan Yao, Shui Liu "A high directivity fabry-perot antenna based on metamaterial substrate" *2018 IEEE MTT-S International Wireless Symposium (IWS)*, pp. 1-3, 2018.

FPGA-Based Real Time Wide Band Radar Waveform Simulator

Gökhan Kara & Gamze Taşyürek
TÜBİTAK
Bilgem,İltaren
Ankara, Turkey
{gokhan.kara & gamze.tasyurek}
@tubitak.gov.tr

İlteriş Demirkıran
Embry-Riddle Aeronautical University
Department of Electrical, Computer,
Software & Systems Engineering
Daytona Beach, USA
ilteris.demirkiran@erau.edu

***Abstract*— In this paper a real time FPGA-based wide band radar signal simulator is presented. In many electronic support (ESM), electronic attack (EAS) and electronic countermeasure systems (ECM), a radar signal simulator is needed for developing algorithms and testing system capabilities. As the capabilities of modern electronic support or attack systems develop, a more comprehensive radar simulator becomes imperative. A simulator that can emulate all possible modern threats is optimal. The outputs and capabilities of such a radar simulator is presented in this study.**

Keywords—digital pulse compression waveform; non-linear frequency modulation wideband radar simulator, multiple channel, noise generator

I. INTRODUCTION

In many complex electronic countermeasure, attack and support systems, a wide variety of threats should be analyzed for the electronic system to accomplish its mission. While developing more capable systems, a more comprehensive radar simulator is needed. The simulator may be implemented as an analog system or a digital system as in [1]. While designing a wide band radar simulator, a primary criterion is its ability to emulate a variety of threats as in the real world. This is also the most challenging part of electronic support measurement (ESM) systems [2]. Accordingly, among the most important aspects of a radar simulator are its ability to model a wide selection of channels, various patterns, pulse repetition intervals, frequency repetition types, and the like. Also the simulation of noise with a wide band is an added capability of the work in this study.This study is implemented on ApisSys AV104 board that uses a Virtex-7 core and 2.5 GSPS DAC.

In this study, the basic properties of a radar simulator are presented first. For example, pulse repetition interval (PRI) patterns, pulse width (PW) patterns, frequency patterns, and amplitude modulations are simulated. After that, a noise generator is simulated so that real time environment simulation is achieved. In this paper, sinusoidal waveform generator, the details about PW and PRI patterns, the frequency pattern, noise and amplitude modulation processes are presented respectively. Finally, source utilization and future works are provided in the conclusion sections.

II. THEORETICAL BACKGROUND

1. Pulsed Radars

The main purpose of this research effort is to build cost effective and highly efficient pulsed radar simulator. Fig. 1 illustrates the block diagram of this simulator at intermediate frequency (IF) [3].

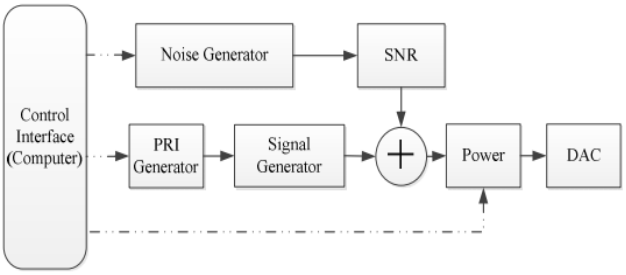

Fig. 1: Pulsed Radar Simulator Block Diagram

As seen in the block diagram, the main part of the simulator is the waveform generator. Notice that there are sinusoidal and noise generators in Fig. 1. By controlling and shaping the output of the signal generator block, a pulsed radar simulation in intermediate frequencies can be achieved. Once the simulator generates the desired waveform, the desired signal is corrupted by interference generated by the noise generator block. The SNR block enables a user to change the interference power. The power block in the diagram is utilized to amplify or attenuate the received signal.

III. REAL TIME IMPLEMENTATION

Each block in this simulator works in parallel on the FPGA and is implemented independently.

A. Sinusoidal Waveform Generator

In this research effort a direct digital synthesizer (DDS) compiler is used to generate sinusoidal waveforms. The DDS provides quite good frequency resolution and allows direct implementation of frequency, phase and amplitude modulations. The DDS unit on the Virtex-7 generates a sinusoidal waveform according to input frequency and phase values. The output of this core is given by

This work is supported by TUBITAK 1007 program within project number 114A001.

$$s(t) = \cos(2\pi f_c t + \phi(t)) \quad (1)$$

where fc is the carrier frequency and ϕ(t) is the phase of the signal. The resolution is 1/fs, where fs is the sampling frequency of 2.5 GHz. The waveforms can be generated at any desired frequency provided that the frequencies are in the first or second Nyquist zone. The input frequencies to the DDS core are provided as a 32 digit unsigned binary number. When all bit values are high (i.e: 232-1), then the core generates a 156.25 MHz sinusoidal wave. However, by using the 16 channel structure, the output can be up to 2.5 GHz if the multiple outputs are used. The phase and frequency input values for the DDS compiler of each channel are determined as follows:

$$frequency = mod\ (f, 156.25\ MHz) \quad (2)$$

$$phase = \frac{f\ x\ (2^{32}-1)}{2.5\ GHz} \quad (3)$$

Where f is the desired frequency and mod is the modulus function (i.e. mod(200,156.25) = 43.75).

B. Pulse generator

At the second stage, a pulse train is generated with the desired pulse width and pulse repetition interval. In this block, both PWs, PRIs patterns are the same but can be changed by a user. Both PW and PRI patterns are same but work independently. The simulator that we built is capable of generating the constant, staggering, sliding, random, and sinusoidal patterns.

C. Frequency Pattern Generation

For each pulse in the pulse train, the frequency is controlled and modulated according to a pattern. As such, frequency is controlled in two ways: Intrapulse or Interpulse Modulation.

1. Intrapulse Frequency Modulation

In this simulator the frequency is modulated linearly. As in Eq. (1), by changing the ϕ(t), a linearly frequency modulated (LFM) signal is achieved. The phase of the sinusoidal wave form is given by $2\pi(f_c t + kt^2/2)$ where k is the LFM coefficient. During the pulse, if the frequency of a waveform is linearly increased, it is called up-chirp LFM. If decreased, it is called down-chirp LFM. Also, if the frequency increases linearly for the first half of the pulse width, and then decreases for the second half, it is called up-down-chirp LFM. These LFM types are also used for continuous wave (CW) signals.

2. Interpulse Frequency Modulation

In this kind of modulation, while the frequency of a single pulse does not change, the frequency over several pulses changes according a defined pattern. The same patterns as those in the PW or PRI are also used for these frequency repetition patterns. Since only one Nyquist zone is used in this scenario, the user can define a pattern for frequency up to 1.25 GHz bandwidth. With the use of this type of modulation, an agile or frequency hopping pulsed radar waveform can be simulated as well.

D. Noise Generator

Interference is generated and simulated by a noise generator in the simulator. The simulator is designed to produce two types of noise: Uniform and Gaussian. Uniformly distributed noise is implemented by using a 32-bit linear feedback shift register (LFSR). A Gaussian noise generator, which is based upon the Box-Muller method is also realized.

E. Amplitude Modulation Generator

ESM or ECM systems are designed not only for tracking radars but also for search radars. Due to this fact, this simulator is designed in a such way that it is able to produces a search radar pattern called Amplitude Modulation Over Pulses. Two types of amplitude modulation as search pattern and conical pattern are implemented.

F. Multiple Pulsed Radar Waveform

For ECM or ESM systems, many radar signals might occur simultaneously, therefore this simulator is designed to be able generate up to 8 different radar signals. Since there is only 1 DAC channel, they are all summed and routed to the DAC output. When any pulse intersects with another pulse of a neighboring waveform, they are generated by time sharing. This saves source utilization on the FPGA.

IV. RESULTS

In this work, an approach to simulate radar signals is presented. The approach made use of an FPGA board. The Virtex-7 core of AV104 board is utilized. The hardware on the board enables one to generate radar signals with a high degree of flexibility. Total source utilization is given in Table 1.

Table 1: Source Utilization

Resource	Utilization	Available	Utilization %
FF	108182	866400	12,49
LUT	59818	433200	13,81
Memory LUT	2178	174200	1,25
I/O	373	600	62,17
BRAM	192,50	1470	13,10
DSP48	464	3600	12,89

Although our design has many advantages, it has also some drawbacks. For example, due to hardware limitations on the FPGA board, a simulation with a maximum bandwidth limited to 1.25 GHz is possible. The number of threats is also limited to eight. Though our FPGA-based radar simulator prototype provided high level performance with limited hardware there is still room to improve the design. Hence, in the next phase of this research effort a VP430 board made by Abaco is to be utilized. This board will enable the user to simulate wider bandwidth signals and more threats. In addition, on the new board, there are 8 ADC and DAC channels. This will enable direction finding algorithms to be implemented by using eight different phase shifters.

REFERENCES

[1] M. I. Skolnik, "Radar Handbook," 3rd edition, McGraw Hill, 2008.

[2] N. Levanon and E. Mozeson, "Radar Signals," Wiley and Sons, 2004.

[3] A. Orduyilmaz, G. Kara, M. Serin, A. Yildirim, M. Efe, "FPGA-based match filter implementation in frequency domain using an overlap-add method," IEEE 22nd Signal Processing and Communication Applications Conference (SIU), Trabzon, 23-25 April 2014.

Coupled Line Microstrip Bandpass Filter with slots

Farah Memić, Suada Čomor
Department of Electrical Engineering
International University of Sarajevo
Sarajevo, Bosnia and Herzegovina

Abstract *– Topic of this paper is Microstrip Bandpass Filter with its projection, design and analysis. This paper introduces configuration of Bandpass Filter design which is containing five parallel rectangle shapes with spaces between them. They are connected to two ports, one on each side. Microstrip bandpass filter has a bandwidth of 5.28 to 5.30 GHz, where S11=-30.460486 dB and S21=-0.296486 dB.*

Keywords: *Microstrip Filter, Sonnet Suites software, CBMF*

I. INTRODUCTION

Filter which can pass a certain range of frequencies and reject those who are outside of given range is a type of filter called bandpass. The process of designing a filter can be in one of the many interesting fields of microwave engineering. A wide number of different topologies allows to obtain specific responses for a wide range of applications. Inductive filters constitute a strategy of special interest due to their simplicity and easy manufacturing processes associated with these configurations [1]. There are many filters available in the market but due to some reasons, it has a certain disadvantage. "The lumped-element filter will not be a good choice if sharp rejection is needed because of its limited "Q" value. Helical filters are the best, as they provide excellent performance but suffer from big size, assembly and tuning problems". Surface acoustic wave filters provide excellent performance but their shortcoming is lousy. The demand in high-speed communication has led to the design and development of wideband filters to support applications such as UWB technology that promises communication speed of up to 1000 Mbps. [2]. As a type of microwave filter, microstrip BPF has been researched thoroughly. Each microstrip is a short portion of parallel capacitance and series inductance, while parallel coupled line consits of coupled inductances and capacitors. [3].For a filter to operate successfully it will require large bandwidth, but there are many applications where very narrow bandpass filter can be successfully used, such as use as laser line, laser cleanup and laser excitation filters in both medical and laser applications..

II. CBMF (COUPLED-LINE BANDPASS MICROSTRIP FILTER)

Figure 1. shows the dimensions of the filter. It consists of five parallel rectangle shapes with symmetrical slot size which are connected to two ports, one on each side. Figure 2. shows magnitude vs. frequency graph, with S11 going up to -30.460486 dB and S21 to -0.296486 dB. S12 and S22 are symmetrical to S11 and S21. Bandpass frequency range is from 5.28 GHz to 5.30 GHz.

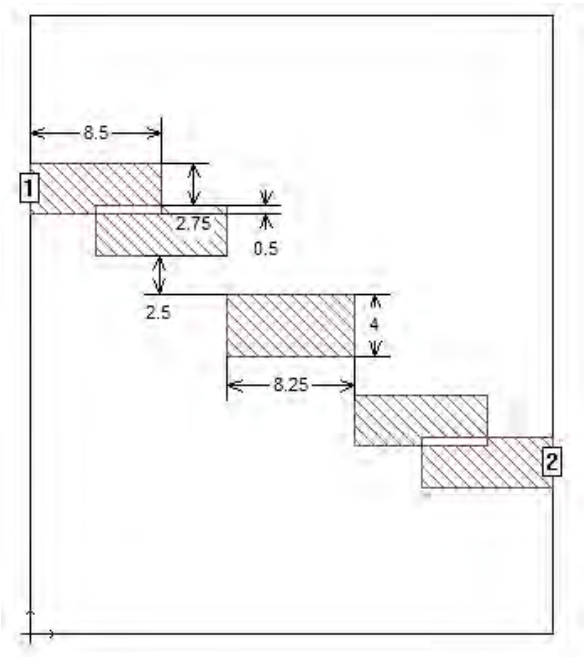

Figure 1. Dimensions of CBMF

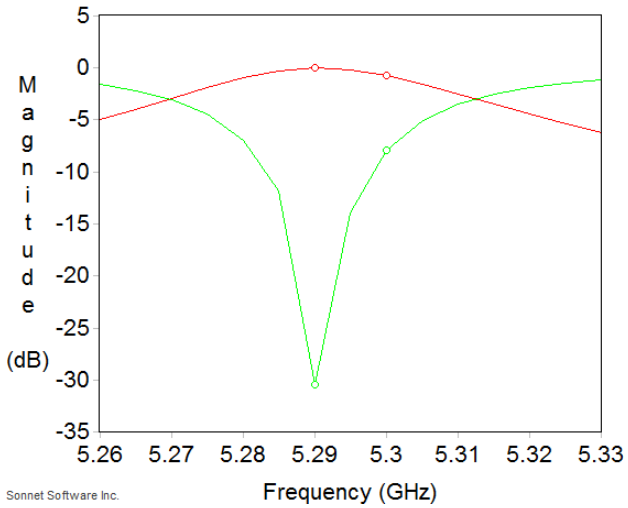

Figure 2. Magnitude vs. Frequency graph

TABLE 1. PARAMETERS

Parameters	Values
Dielectric thickness (Ɛr)	3
Cell size	0.25

Box size	33.75 x 40.00 mm
Frequency	5.28– 5.30 GHz

III. PARAMETRIC STUDIES

In table 2. below we can see how a change of dimension of space between symmetrical slots and central slot, which are different dimension themselves influences the change between S11 and S21. The original dimension between them is 2.50 mm, and changes by 0.25 mm going up to 3.50 mm. The range of frequency stayed same, but values of S11 decreased from -30.460487 dB to -22.014188 dB, and values of S21 decreased from -0.296486 up to -0.010306 dB, with other changes shown in table 2.

TABLE 2. CHANGE OF DIMENSION BETWEEN SYMMETRICAL SLOTS AND CENTRAL SLOT

y (mm)	S11 (dB)	S21 (dB)	Frequency (GHz)
2.50	-30.460487	-0.296486	5.27-5.31
2.75	-27.361926	-0.153703	5.27-5.31
3.00	-26.252082	-0.010306	5.27-5.31
3.25	-25.296982	-0.012844	5.27-5.31
3.50	-22.014188	-0.027081	5.27-5.31

The change was made with the dimension of the symmetrical slots and dimension between them, each increasing by 0.25 mm. Again, the range of frequency stayed the same, from 5.28 to 5.30 GHz, and the values of S11 and S21 decreased. The dimension between symmetrical slots and central slot stayed at 2.50 mm. Changing values of S11 and S21 are shown in table 3.

TABLE 3. CHANGE OF DIMENSION OF SLOTS

Width (mm)	Length (mm)	Space (mm)	S11 (dB)	S21 (dB)
8.50	3.25	0.50	-30.460487	-0.296486
8.75	3.25	0.75	-24.591802	-0.015113
9.00	3.25	1.00	-20.217031	-0.041506
9.25	3.25	1.25	-19.806342	-0.028742
9.50	3.25	1.50	-18.899564	-0.056312

Table 4. shows the comparison of S11 and S21 values from the varying dimensions of distance between symmetrical slots and central slot, and values from the variation of the dimension of symmetrical slots, which now we call S11.1, S21.1, S11.2 and S21.2 for clearer understanding. Values of S11.2 decreased more than S11.1, so increasing of the dimensions of symmetrical slots has a higher impact on the decrease of the value of S11. For S21 values from one variation of dimensions to another didn't change with big difference, so the changes didn't have as high impact as they had on S11.

TABLE 4. COMPARISON OF S11 AND S21 VALUES

S11.1 (dB)	S11.2 (dB)	S21.1 (dB)	S22.2(dB)
-30.460487	-30.460487	-0.296486	-0.296486
-27.361926	-24.591802	-0.153703	-0.015113
-26.252082	-20.217031	-0.010306	-0.041506
-25.296982	-19.806342	-0.012844	-0.028742
-22.014188	-18.899564	-0.027081	-0.056312

IV. CONCLUSION

This paper presents a Coupled Line Microstrip Bandpass Filter with the narrow bandpass frequency range. Filters are circuits through which we can select certain frequency or frequency band among other frequencies. Each filter has a frequency range including a set of frequencies that can pass through the filter. A microwave filter has 2 ports that are used in a communication system in order to control frequency response [4]. By changing the dimension of symmetrical coupled lines, and dimension of distance between symmetrical coupled lines and central box, we concluded that changing of dimension only changed the values of S11 and S21 but not the frequency range, which stayed the same throughout every change, from 5.28 to 5.30 GHz. Our research was a combination of dimension adjusting, analysis of the sensitivity of specific parameters which showed us how Coupled Line Microstrip Bandpass Filter responds to changes of its parameters. Simulation was done in a 3D planar high-frequency electromagnetic software, Sonnet Suites [5]. The response of this Coupled Line Microstrip Bandpass filter was the decrease of S11 and S21 by the increase of specific dimensions.

V. REFERENCES

[1] S. Member *et al.*, "Design of Bandpass Elliptic Filters Employing Inductive Windows and Dielectric Objects," *IEEE Trans. Microw. Theory Tech.*, vol. 55, no. 11, pp. 2393–2398, 2007.

[2] Federal Communications Commission, "Commission's Rules Regarding Ultra-Wideband Transmission Systems," Washington, D.C. 20554, 2002.

[3] S. Agarwal, R. K. Garg, and R. Tomar, "Microstrip band pass filter design," no. July, pp. 379–382, 2015.

[4] M. Taghizadeh, G. Moloudian, and A. R. Rouzbeh, "Design and Simulation of Band-Pass Filter using Micro-Strip Lines," *Int. J. Comput. Sci. Mob. Comput.*, vol. 4, no. 11, pp. 331–337, 2015.

[5] "Sonnet Suites." .version 16.54, www.sonnetsoftware.com

T-Shaped Patch Antenna with a Slit and a Slot

Ajla Sokol
Computer Science and Engineering Department
International University of Sarajevo
Sarajevo, Bosnia and Herzegovina
ajla.sokol@hotmail.com

***Abstract* — A slotted, compact microstrip patch antenna design suitable for X-band application is proposed. Antenna operates in the frequency range of 7.0 – 8.3 GHz. Design, which consists of rectangular patches making rectangular slot, is made with a circular shaped feeding input with diameter of 1 mm on FR-4 dielectric substrate with the permittivity of 4.4. The gain of the design at the frequency of 7.6 GHz is 7.26 dB. Simulation is done using Sonnet software.**

Keywords — microstrip patch antenna, slotted antenna, rectangular patches

I. INTRODUCTION

Idea behind microstrip patch antennas exists for over 70 years, and the trend of advancing the technology behind it continuously grows. The characteristics of microstrip patch antennas are the ones to make them very appealing and the reason why a lot of researches, as well as implementations and proposed designs, are being released on this topic [1].

Another reason why the popularity of microstrip patch antennas has been increasing over time is the growth of wireless communications. Together with it, the necessity of having low profile, wide-band antennas that can operate on a multiple frequency for variety of applications has changed. Since the antenna is the basic element of the communication system and its key component, it is important to track design and performance to satisfy some main criteria and requirements that are set [2].

Creating antennas with slotted spaces increase resonating frequencies, according to researches, and they are considered to have a high value of return losses, which make them good for satellite communication as well [3]. Except for wireless and satellite communication, the antenna with rectangular patches is playing big role in the radar systems that use ultrawideband system communication. Microstrip rectangular patches antenna has been commonly used as the UWB antenna because of its ease of fabrication and integration with microwave integrated circuits [4]. The antennas with the broad frequency range of 3.1 GHz to 10.6 GHz have been essential in UWB systems [5].

One of the most common designs of microstrip patch antenna is using rectangular patches. The geometry of this type of antenna consists of length, width, substrate thickness and relative permittivity [6]. In this paper, antenna design is made using rectangular patches. This antenna design is suitable for X-band frequency operation All the geometry and design measurements, as well as analysis, are presented in the next sections.

II. ANTENNA DESIGN

This antenna is designed on the FR-4 dielectric substrate material with a 1 mm thickness and with permittivity of 4.4. Layer below, as well as the layer above FR-4 dielectric substrate, consists of air with 3 mm and 5.5 mm thickness respectively. The top view of the antenna designed, together with all the measurements of antenna, can be seen in the Fig. 1., while 3D view of antenna design can be seen in Fig.2.

Antenna itself consists of four different rectangular patches that, combined, form a rectangular shaped slot. Feeding input is found in the corner of the antenna.This feeding input is in a shape of circle with diameter of 1 mm, and goes through layer of FR-4 dielectric substrate and layer below, that consists of air, until the ground. Antenna measurements are 49 mm x 50 mm, which makes it almost a squared microstrip patch antenna made from several smaller rectangular patches.

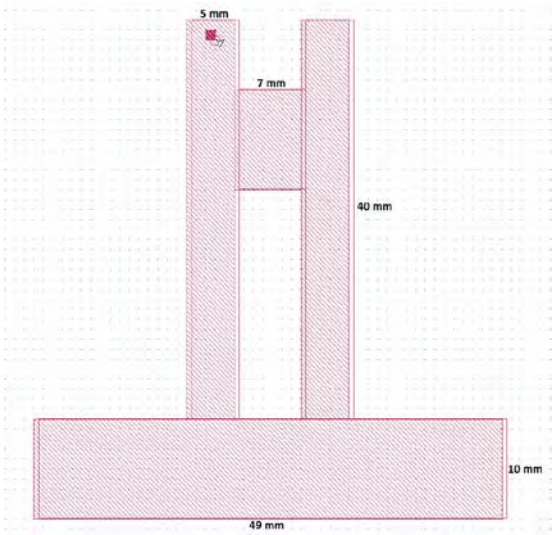

Fig. 1. Antenna Design Top View

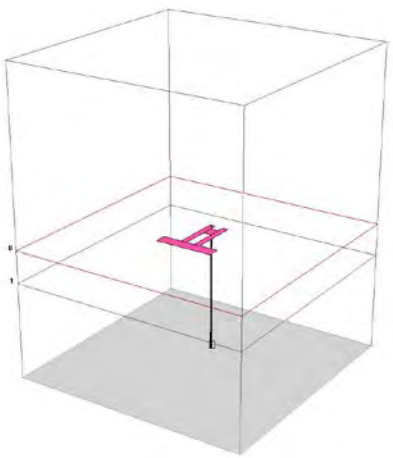

Fig. 2. Antenna 3D Design

III. Design Results and Analysis

The analysis and design were done using Sonnet software. The S11 diagram of the antenna is shown in the Fig. 3. As we can see, the area where S11 > -10dB, and θ > 0dB is found in range of 7.0 GHz and 8.3 GHz, which means that the frequency range of operation of this antenna is found in this section. The bandwidth calculated is 1.3 GHz, or 17.10% of its peak value at 7.6 GHz.

Polar view of gain distribution is shown in Fig. 4. The antenna design has a peak gain of 7.26 dB at 7.6 GHz frequency. Current distribution can be seen in Fig.5.

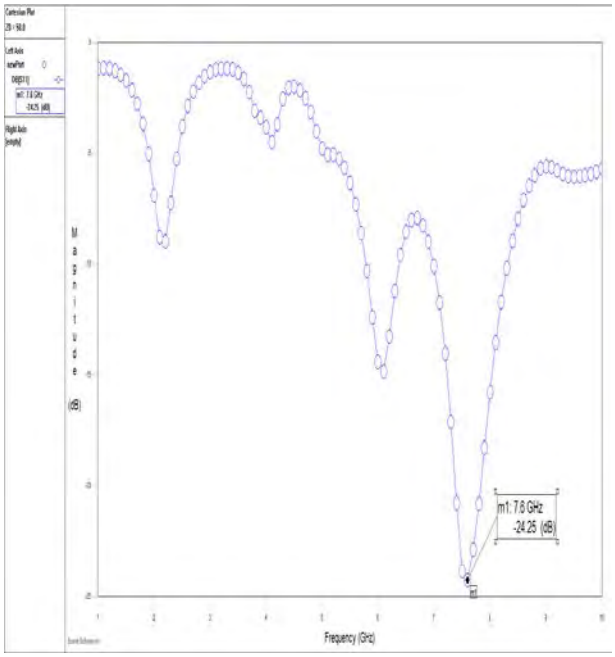

Fig. 3. S11 Distribution

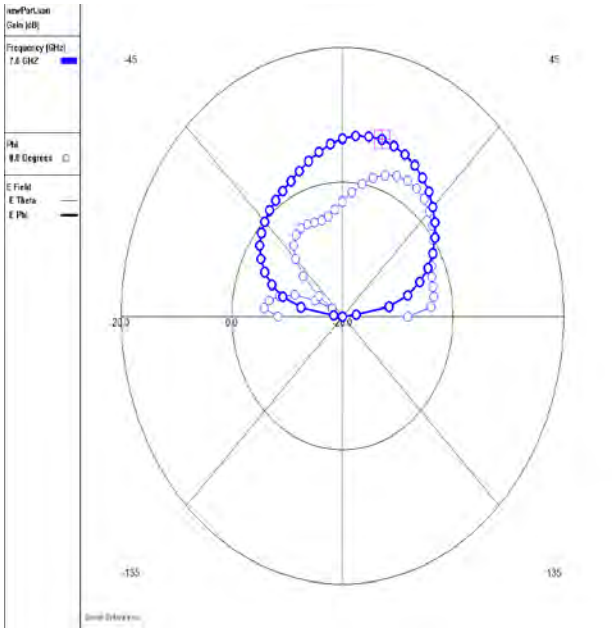

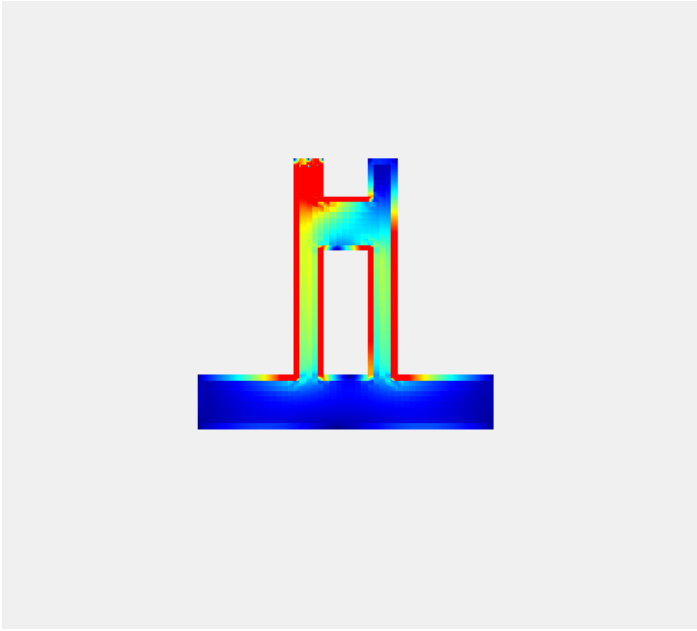

Fig. 5. Current Distribution

Conclusion

In this paper, microstrip patch antenna with rectangular patches and rectangular slot area is presented. Design is made in the Sonnet software, together with all the analysis and measurements. Dielectric substrate used is FR-4 of 1 mm thickness. This antenna has satisfied the initial requirements with the gain of 7.26 dB at the frequency of 7.6 GHz. The range of the antenna operating is in between of 7.0 GHz and 8.3 GHz, which can be seen in the figures. Antenna is suitable for use in X-band applications.

References

[1] D. M. Pozar, “Microstrip Antennas”, Proceedings of the IEEE, vol. 80 (1), 1992, pp. 79-91

[2] M. N. Srifi, M. Meloui and M. Essaaidi, “Rectangular Slotted Patch Antenna for 5-6 GHz Applications”, International Journal of Microwave and Optical Technology, vol. 2 (5), 2010, pp.52-57

[3] S. Das and S. Gokhroo, “Microstrip Patch Antenna at 7 GHz for Satellite Communication”, International Journal of Engineering Technology Science and Research, vol. 2 (11), 2015, pp. 9-11

[4] H. Werfelli, K. Tayari, M. Chaoui, M. Lahiani and H. Ghariani, “Design of Rectangular Microstrip Patch Antenna”, International Conference on Advanced Technologies for Signal and Image Processing”, 2016

[5] D. Sarkar, K. V. Srivastava and K. Saurav, “A Compact MicrostripFed Triple Band-Notched UWB Monopole Antenna”, IEEE Antennas and Wireless Propagation Letters, vol. 13, 2014, pp. 396-399

[6] K. F. Lee and K. M. Luk, “Microstrip Patch Antennas”, Imperial College Press, 2011

Fig. 4. Polar Distribution

Coupling Characterization of A Single Sided Cross-Shape Magnetic Coupler Pair

Emre Orta[1], Alper Kaya[1] and Seyit Ahmet Sis[1]
[1]Balikesir University, Electrical-Electronics Engineering Department, Balikesir, Turkey

***Abstract*— Cross-shape coupler structure employs two parallel connected rectangular subunit coils which are 90° rotated to one another around the center of both. Such a configuration slightly improves the overall misalignment tolerance of the coupler structure as the coupling coefficient of rectangular coil pairs are less sensitive to misalignment along its longer side. This is a major advantage in wireless power transfer applications; because, system efficiency and transferred power level is strongly dependent on the magnetic coupling coefficient between the couplers. In this paper, electromagnetic simulation results for single sided cross-shape coil structure are presented. Self-inductance and coupling coefficient of single-sided couplers are presented as a function of vertical distance and lateral misalignments.**

Keywords—wireless power transfer, magnetic coupler, misalignment.

I. INTRODUCTION

Wireless power transfer (WPT) systems are commonly implemented via magnetically coupled primary and secondary coils or so called couplers [1]. The couplers are resonated out by series or parallel connected capacitors for increasing the power transfer distance [2]-[4]. One of the major challenges in magnetic resonance based WPT systems is that the efficiency and the transferred power level of the system is strongly dependent on the coupling between the primary and secondary couplers. Therefore, quite a few works have been published on increasing WPT system's tolerance to misalignment and distance variations [5]-[11]. These works are usually based on either impedance tuning techniques or on changing the parameters of high frequency power or voltage sources such as voltage level, power level, frequency and duty cycle. These techniques provide an adaptivity to coupling variations. In addition to these adaptive solutions, significant efforts have been dedicated to designing couplers with high tolerance of coupling coefficient (k) to misalignment [12]-[15].

In [15], a novel double-sided cross-shape coupler structure with improved lateral misalignment tolerance and high coupling coefficient is proposed. In this work, we further analyze the cross-shape structure with a ferrite layer on one side of the windings. The added ferrite layer will make the cross-shape structure exhibit a single-sided flux distribution. Single-sided couplers have the advantage of lower electromagnetic interference (EMI) as compared to double-sided couplers.

II. CROSS-SHAPE COUPLER STRUCTURE

The cross-shape coupler structure is formed by two rectangular sub-unit coils. The rectangular coils exhibit lower tolerance to lateral misalignment along its longer side. Therefore, when these two electrically connected sub-unit rectangular coils are vertically oriented to one another on the horizontal plane, the constituted cross-shape coupler exhibit improved misalignment tolerance as compared to sub-unit rectangular coils. The sub-unit rectangular coils are electrically parallel connected for keeping the overall self-inductance small. A ferrite layer is added at one side of the coupler for ensuring a single-sided flux distribution. Fig. 1 shows a schematic drawing for a coupled single sided cross-shape coupler pair.

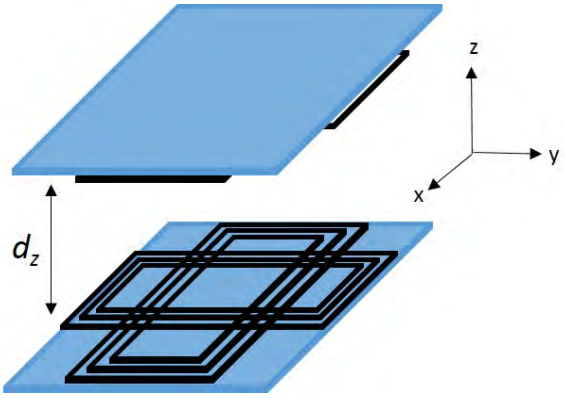

Fig. 1. Schematic drawing for a single sided cross-shape coupler pair.

III. SIMULATION RESULTS FOR CROSS-SHAPE COUPLERS

Coupling parameters for a coupled single-sided cross-shape coupler pair, each one employing 100 cm by 70 cm rectangular coil, is simulated using via an EM simulator, Maxwell 14.0. The thickness of the ferrite layer is 27 mm. Fig. 2 shows the picture of a simulation model. The simulated self-inductance (L_1, L_2) of the coupler is 51 μH. Mutual inductance (M) between couplers are simulated for various separation (d_z) and misalignment (d_x, d_y) between couplers. Coupling coefficient (k) between couplers is calculated as follows:

$$k = \frac{M}{\sqrt{L_1 L_2}} \tag{1}$$

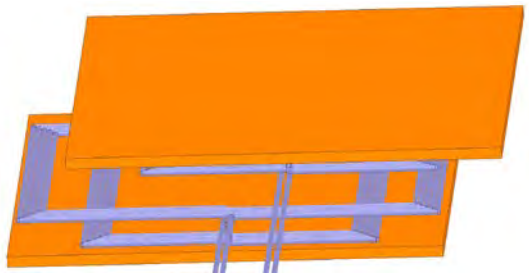

Fig. 2. Simulation model for a single sided cross-shape coupled pair.

Fig. 3 shows simulated *k* as a function separation between couplers. *k* changes from 0.79 to 0.26 when the separation between couplers varies from 5 cm to 35 cm. Fig. 4 shows *k* as a function of misalignment when the vertical separation between couplers are 20 cm. As seen in Fig. 4, the coils are highly tolerant to misalignment especially up to 15 cm misalignment. *k* only changes from 0.45 to approximately 0.40 (11% variation) when lateral misalignment is 15 cm. The *k* reduces to 0.27 when misalignment is 30 cm.

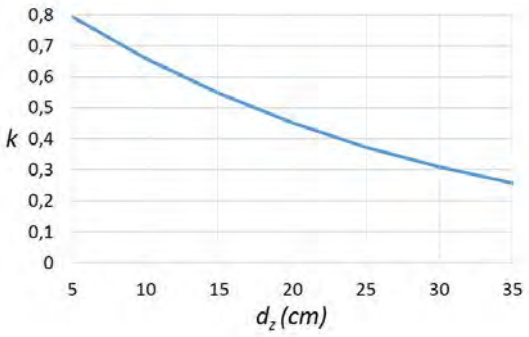

Fig. 3. Simulated *k* as a function of separation between couplers when couplers are perfectly aligned.

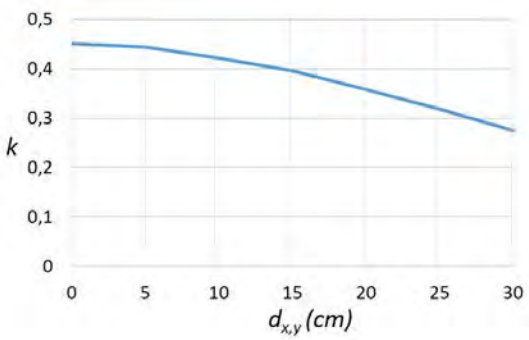

Fig. 4. Simulated *k* as a function of lateral misalignment between couplers when couplers have a vertical separation of 20 cm (d_z = 20 cm)

CONCLUSION

EM simulation results for a cross-shape coupler pair is presented. The simulated structure employs a ferrite layer on one side of the windings to form a single sided flux distribution. Simulation results show that the cross-shape couplers not only exhibit high coupling coefficient but also have high tolerance to lateral misalignment between the couplers.

ACKNOWLEDGEMENTS

This work is supported by the Balikesir University Scientific Research Projects Coordination Unit (Project Number: 2018/161)

REFERENCES

[1] Fernández, C.; Garcia, O.; Prieto, R.; Cobos, J.A.; Uceda, J., "Overview of different alternatives for the contact-less transmission of energy," in *IECON 02 [Industrial Electronics Society, IEEE 2002 28th Annual Conference of the]* , vol.2, no., pp.1318-1323 vol.2, 5-8 Nov. 2002

[2] Sample, A.P.; Meyer, D.A.; Smith, J.R., "Analysis, Experimental Results, and Range Adaptation of Magnetically Coupled Resonators for Wireless Power Transfer," in *Industrial Electronics, IEEE Transactions on* , vol.58, no.2, pp.544-554, Feb. 2011

[3] Thomas, E.M.; Heebl, Jason D.; Pfeiffer, C.; Grbic, A., "A Power Link Study of Wireless Non-Radiative Power Transfer Systems Using Resonant Shielded Loops," in *Circuits and Systems I: Regular Papers, IEEE Transactions on* , vol.59, no.9, pp.2125-2136, Sept. 2012

[4] Tierney, B.B.; Grbic, A., "Planar Shielded-Loop Resonators," in *Antennas and Propagation, IEEE Transactions on* , vol.62, no.6, pp.3310-3320, June 2014.

[5] S. Bıçakçı, S. A. Sis, "Design Of A Resonance Frequency Tracking System For Rf Applications", GU J Sci, vol. 5, no. 2, pp. 211-221, 2017.

[6] Sis, Seyit Ahmet, and Sabri Bicakci. "A resonance frequency tracker and source frequency tuner for inductively coupled wireless power transfer systems." *2016 46th European Microwave Conference (EuMC)*. IEEE, 2016.

[7] Heebl, Jason D., et al. "Comprehensive analysis and measurement of frequency-tuned and impedance-tuned wireless non-radiative power-transfer systems." *IEEE Antennas and Propagation Magazine* 56.4 (2014): 44-60.

[8] Li, Hongchang, et al. "A maximum efficiency point tracking control scheme for wireless power transfer systems using magnetic resonant coupling." *IEEE Transactions on Power Electronics* 30.7 (2015): 3998-4008.

[9] Kennedy, Henry, et al. "A Self-Tuning Resonant-Inductive-Link Transmit Driver Using Quadrature Symmetric Delay Trimmable Phase-Switched Fractional Capacitance." *IEEE Journal of Solid-State Circuits* 53.6 (2018): 1694-1706.

[10] Xu, Dong, Dongqing Wang, and Jiadong Li. "Transmitter Current Tracking Method of Improving Power-Transfer Efficiency for Two-Coil Wireless Power Transfer System." *2018 Chinese Automation Congress (CAC)*. IEEE, 2018.

[11] Sis, Seyit Ahmet, and Selcuk Kavut. "A frequency-tuned magnetic resonance-based wireless power transfer system with near-constant efficiency up to 24 cm distance." *Turkish Journal of Electrical Engineering & Computer Sciences* 26.6 (2018): 3168-3180.

[12] Budhia, M.; Covic, G.; Boys, J. A new IPT magnetic coupler for electric vehicle charging systems. In Proceedings of the IECON 2010—36th Annual Conference on IEEE Industrial Electronics Society, Glendale, AZ, USA, 7–10 November 2010; pp. 2487–2492.

[13] Budhia, M.; Boys, J.T.; Covic, G.A.; Huang, C.Y. Development of a Single-Sided Flux Magnetic Coupler for Electric Vehicle IPT Charging Systems. *IEEE Trans. Ind. Electron.* **2013**, *60*, 318–328.

[14] Jonah, O.; Georgakopoulos, S.V.; Tentzeris, M.M. Orientation insensitive power transfer by magnetic resonance for mobile devices. In Proceedings of the 2013 IEEE Wireless Power Transfer (WPT), Perugia, Italy, 15–16 May 2013; pp. 5–8.

[15] Sis, S.A.; Orta, E. A Cross-Shape Coil Structure for Use in Wireless Power Applications. *Energies* **2018**, *11*, 1094.

Dual Bandpass Microstrip Coupled line Filter

Rauf Can Ozturk
Department of Electrical Engineering
International University of Sarajevo
Sarajevo, Bosnia and Herzegovina
raufcanozturk@gmail.com

***Abstract* – In this paper, dual band microstrip coupled line filter is designed and the simulated. As an electromagnetic simulation tool, planar 3 dimentional software program, Sonnet Suites was used . The microstrip filter is simulated from 0.01 to 4 GHz, where S11 = -18.159528 dB, S12 = -0.0668606 dB at 3.2Ghz and, where S11= -22.004872 db and S12= -0.0274580 dB at 3.48 GHz.**

***Keywords* - Dual-bandpass filter Microstrip Filter.**

I. INTRODUCTION

Sonnet's suites of high-frequency electromagnetic (EM) Software are aimed at today's demanding design challenges involving predominantly planar (3D planar) circuits and antennas. Predominantly planar circuits include microstrip, strip line, coplanar waveguide, PCB (single and multiple layers) and combinations with vias, vertical metal sheets (z-directed strips), and any number of layers of metal traces embedded in stratified dielectric material [1]. There are a number of different types of filters being used for numerous different applications. Each filter has specific characteristics such as to either allow or block a certain range of frequencies from passing. A Microwave Band Pass Filter (BPF) is the key component in wireless communication systems. It is a two port reciprocal, passive device which attenuates undesirable signal frequency, thereby facilitating the transmission of desired signal frequencies. The practical band pass filters have small non – zero attenuation in pass band and a small signal output in stop band due to the presence of resistive losses in reactive elements and propagating medium [2]. There are applications where a particular band, or spread, or frequencies need to be filtered from a wider range of mixed signals. Filter circuits can be designed to accomplish this task by combining the properties of low-pass and high-pass into a single filter. The result is called a band-pass filter. What emerges from the series combination of these two filter circuits is a circuit that will only allow passage of those frequencies that are neither too high nor too low [3]. This design works well in the area of wireless telecommunications. The frequency boundary between RF and microwaves is somewhat arbitrary, depending on the particular technologies developed for the exploitation of that specific frequency range. Therefore, by extension, the RF/microwave applications can be referred to as communications, radar, navigation, radio astronomy, sensing, medical instrumentation, and others that explore the usage of frequency spectrums in the range, for example, 300 kHz up to 300 GHz. [4]

Design and simulation of CBMF (Coupled-line Band pass Microstrip Filter)

Figure 1 has the coupler of the filter. This shows the odd and even strips that were implemented in this design. Filter has central box, coupled line and feed line box. All of them have dimensions on table I. Also I used dielectric thickness, box size, cell size and frequency in table II.

Filter measurements

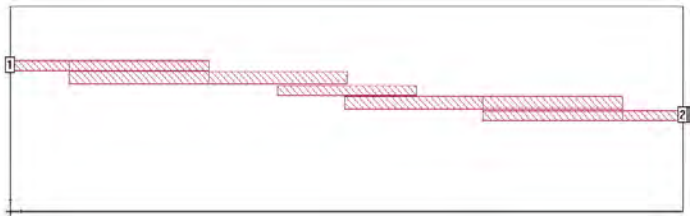

Figure 1- 2-poles band-pass filter

TABLE I. DIMENSIONS OF FILTER

Name	Length	Width
Central Box	23.5mm	1.5 mm
Coupled lines	23.8mm	2.00 mm
Feed line Box	23.8 mm	2.00 mm
Spacing		0.20 mm

TABLE II. FILTER PARAMETERS

Parameters	Values
Dielectric thickness (Ɛr)	1.00
Cell size	0.10 mm
Box size	114.9 x 9.3 mm
Frequency	0.01 – 4 GHz

This band pass filter is made out of odd and even poles of coupled microstrip lines, which we specifically modeled to improve the characteristics of the filter. With the dimensions from table I and set parameters from table II, we get the graphical output that shows the band pass region of our filter. Thus, curves of gain versus frequency and phase versus

frequency are commonly used to illustrate filter characteristics, and most widely used mathematical tools are based on the frequency domain. [5]

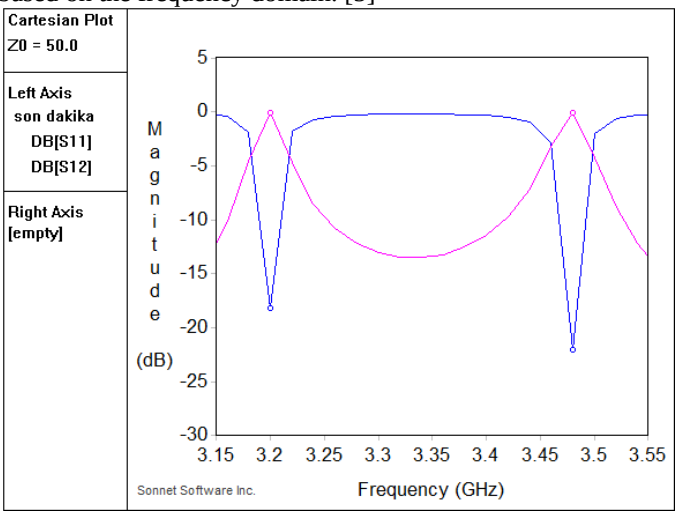

Figure 2. – Simulated S-parameters graph

II. PARAMETRIC STUDIES

In this section, we observed how the frequencies are changing while changing different dielectric. We observe the return losses (gamma) S11 and S12 to make it ideal as possible.

TABLE III. CHANGING OF DIELECTRIC THICKNESSES AND CONSTANT

Dielectric Thickness / constant	S11 (dB)	S12(dB)
1.075 / 4.4	3.2 GHz / -7.3734107	3.2 GHz / -0.8782451
1.05 / 4.4	3.2 GHz / -9.3328375	3.2 GHz / -0.5384494
1.0 / 4.4	3.2 GHz / -18.159528	3.2 GHz / -0.0668606
0.95 / 4.4	3.2 GHz / -16.427036	3.2 GHz / -0.1000166
0.9/ 4.4	3.2 GHz / -7.5794411	3.2 GHz / -0.8333800

Table IV is representing S11 and S12 while changing air (mm) and Dielectric constant with spacing between coupled lines.

TABLE IV. CHANGING COUPLED LINE SPACING AND DIELECTRIC CONSTANT AND AIR SPACE

Air (mm)/ Dielectric constant	Coupled line Spacing	S11(dB)	S12(dB)
1.0 / 4.4	0.2	3.2 GHz / -18.159528	3.2 GHz / -0.0668606
1.0 / 4.4	0.3	3.24GHz / -18.14602	3.24GHz / -0.0670704
1.0 / 4.45	0.3	3.22 GHz / -11.370666	3.22 GHz / -0.3288961
1.0 / 4.45	0.2	3.18 GHz / -15.013256	3.18 GHz / -0.1391221

Table V shows how changing some of the parameters has an effect on the other parameters, most importantly S11 and S12. We experimented with the Dielectric Constant and the Coupled line Spacing. After each modification was made, a new simulation was made and the changes were noted down. Numerous iterations were made, the final and most efficient combination of the parameters has been found and it is noted in the last column which written in bold.

TABLE V.

CHANGING: DIELECTRIC THICKNESS AND AIR SPACE TOGETHER WITH COUPLED LINE SPACING AND CENTRAL BOX WIDTH

Dielectric Thickness / constant	Box Width / Coupled line Spacing	S11(dB)	S12(dB)
1.075 / 4.4	1.5/0.2	3.54GHz / -16.697653	3.54GHz / -0.0939087
1.0 / 4.45	2.0/0.2	3.2 GHz / -25.048643	3.2 GHz / -0.0136019
0.95 / 4.4	1.5/0.3	3.24 GHz / -6.4367929	3.24 GHz / -1.1190713
1.0 / 4.48	2.0/0.1	3.14 GHz / -7.8272052	3.14 GHz / -0.7827313
0.9 /4.4	**1.5/0.2**	**3.2 GHz / -7.5794411**	**3.2 GHz / -0.8333800**

III. CONCLUSION

Microstrip filters are widely used in many different areas and in almost aspects of our lives. In this paper, we have designed and simulated a dual band pass filter with odd and even microstrip lines to produce the desired results. The results of the simulation represent the characteristics of this type of filter nicely. Last results are S11 is -18.159528 dB and S12 is dB, S12 = -0.0668606 dB at 3.2 GHz. The design will be further for best results and a prototype design will be fabricated to analyze the results in real-life environment.

IV. REFERENCES

[1] Sonnet Suites. (n.d.). Retrieved from http://www.sonnetsoftware.com/products/sonnet-suites/
[2] D.M Pozar, “Microwave Engineering”, 2nd edition, 1998 John-Wiley&sons.
[3]Allaboutcircuitscom.(2019).https://www.allaboutcircuits.com/textbook/alternating-current/chpt-8/band-pass-filters/
[4] Jia-Shen Hong,M.J Lancaster,“Microstrip Filters for RF/Microwave applications”, 1st edition 2001, pg. 1.
[5] S.A. Pactitis,Active Filters-Theory and Design”,2007, pg. 1.

Dual Resonance Patch Antenna Array Design at 11.40 GHz and 17.50 GHz

Sevkuthan KURAK
Electrical and Electronics Engineering
International University of Sarajevo
Sarajevo, Bosnia and Herzegovina
sevkuthan@student.ius.edu.ba

***Abstract*— In this paper, a microstrip patch antenna array has been designed for X-Band monopulse tracking radar application. The presented antenna was designed on an FR-4 substrate and operates at 11.40 GHz and 17.50 GHz with the gain of 10.09 dBi and 10.33 dBi, respectively. Reflection Coefficients are -25.52 dB and -10.51 dB, and were included to dBi measurements. 11.40 GHz center frequency has % 3.05 bandwidth. Obtained design can be used in a monopulse tracking radar solution.**

Keywords — X-Band Tracking Radar, Microstrip Patch Antenna, Dual-Band Patch Antenna.

I. INTRODUCTION

Monopulse Radars are used to provide accurate directional information. The name refers to its ability to extract range and direction from a single signal pulse. The three main angle-sensing techniques for Monopulse Radars are Amplitude Comparison, Phase Comparison and Combination of the Amplitude and Phase Comparisons.

Amplitude comparison monopulse radar uses four antennas (or quadrants of a single antenna). The target is illuminated by all four quadrants equally (Figure 1). A comparator network is used to "calculate" four return signals.

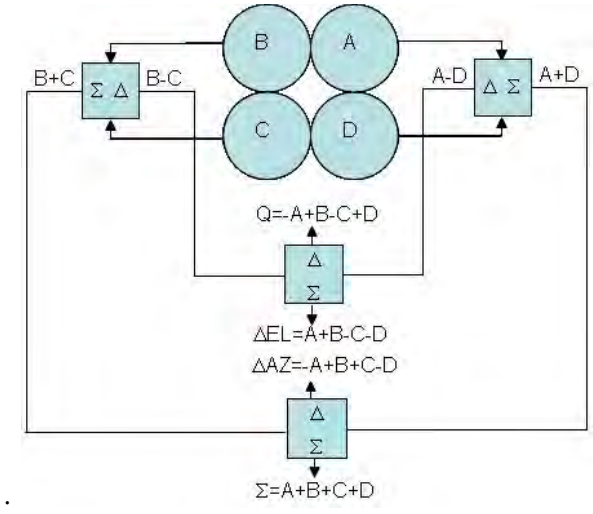

Figure 1, Amplitude Comparison Monopulse Antenna

The sum signal has the same pattern in receive as transmit, a broad beam with the highest gain at boresight (the axis of maximum gain (maximum radiated power) of a directional antenna); the sum signal is used to track target distance and perhaps velocity. The elevation difference signal is formed by subtracting the two upper quadrants from the two lower quadrants and is used to calculate the target's position relative to the horizon. The azimuth difference signal is formed by subtracting the left quadrants from the right quadrants and is used to calculate the target's position to the left or right.

In traditional monopulse radar systems, Cassegrain parabolic antennas or lens antennas are commonly applied. The monopulse comparator in such systems is usually very complicated and heavy. Therefore, a lightweight and low-cost microstrip structure has been developed for pulse antennas [1].

The signals at the antenna outputs are coherently added and subtracted by using a π-hybrid. When the π-hybrid is used for adding and subtracting two signals it is often called Σ-Δ hybrid [2].

The X band and Ku-Band defined by an IEEE standard for radio waves and radar engineering with frequencies that range from 8.0 to 12.0 GHz and 12.0 to 18.0 GHz respectively. The X-Band is used for short-range tracking, missile guidance, marine, radar and airborne intercept. Especially it is used for radar communication ranges roughly from 8.29 GHz to 11.4 GHz. The Ku-Band is used for high-resolution mapping and satellite altimetry. Especially, Ku-Band is used for tracking the satellite within the ranges roughly from 12.87 GHz to 14.43 GHz [3].

[4] provides an example of the usage of multiple patch elements. Artificial neural networks were used in [5] to obtain high transmission gain (dBi, decibel isotropic) gain and low reflection coefficient (S_{11} in dB). In that paper, the developed neural network can offer to design a multi-band microstrip antenna in accordance with the user's setting resonance frequencies and their return losses. In [6] circularly polarized microstrip patch array is introduced for the X-Band applications. The antenna employs a dual-ring array structure in which the radiating elements are fed by non-radiating slots with sequential phase excitations to generate circular

polarization. Thus, two novel features are introduced: firstly, two concentric ring sub-arrays of linearly polarized elements are used to improve the axial ratio and, secondly, development of a new model for power distribution to ensure that all the elements radiate the same power, thus ensuring pattern symmetry and high-quality circular polarization.

In this work, 2by2 patch element is prepared for a monopulse microstrip antenna array design. The operating frequency was aimed at 11.40 GHz as per X-Band requirements. In such a design, multiple usages of patch elements will increase the integrated antenna gain. Antenna design described in Section II and Section III gives the conclusions.

II. ANTENNA GEOMETRY

The geometry of the prepared rectangular patch antenna is shown in Figure 1. The size of the antenna is 23×14.8 mm. The antenna is designed on an FR-4 dielectric substrate whose thickness and permittivity are 0.4 mm and 4.4, respectively.

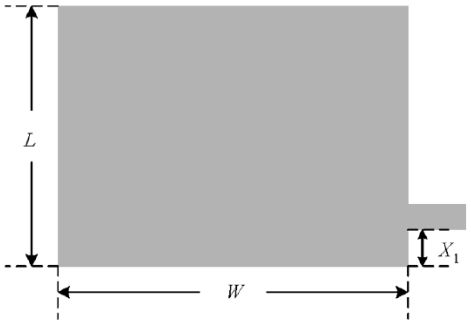

Figure 2, Dimension of the one of the four microstrip patch. W=8mm, L=6mm, X1= 0.4mm.

III. CALCULATIONS FOR ONE PATCH

Design Parameters:

$$f_0 = 11.40\ GHz$$
$$\varepsilon_r = 4.4$$
$$h = 0.4\ mm$$
$$c = 3e8\ m/s$$

Step 1: Calculation of Width (W)

$$W = \frac{c}{2f_0\sqrt{\frac{(\varepsilon_r + 1)}{2}}} = \mathbf{8.002}\ [\boldsymbol{mm}]$$

Step 2: Calculation of Effective Dielectric Constant (ε_{reff})

$$\varepsilon_{reff} = \frac{(\varepsilon_r + 1)}{2} + \frac{(\varepsilon_r - 1)}{2}\left(1 + 12\frac{h}{W}\right)^{-\frac{1}{2}}$$

$$\varepsilon_{reff} = 4.044\ [unitless]$$

Step 3: Calculation of Effective Length (L_{eff})

$$L_{eff} = \frac{c}{2f_0\sqrt{\varepsilon_{reff}}} = 6.538\ [mm]$$

Step 4: Calculation of the Length Extension (ΔL)

$$\Delta L = 0.412\ h\ \frac{\left(\varepsilon_{reff} + 0.3\right)\left(\frac{W}{h} + 0.264\right)}{\left(\varepsilon_{reff} - 0.258\right)\left(\frac{W}{h} + 0.8\right)} = 0.1842\ [mm]$$

Step 5: Calculation of Actual Length of Patch (L)

$$L = L_{eff} - 2\,\Delta L = \mathbf{6.170}\ [\boldsymbol{mm}]$$

According to simulation results, patch size was set as 8 $[mm]$ x 6 $[mm]$ for the dielectric thickness is 0.4 mm.

Table 1, Dielectric Thickness vs. Patch Sizes

Dielectric Thickness (mm)	$f_0\ (GHz)$	Dielectric Constant (ε_r)	W (mm)	L(mm)
0.40	11.40	4.4	8.002	6.170
0.70	11.40	4.4	8.002	6.032
1.00	11.40	4.4	8.002	5.870
1,55	11.40	4,4	8.002	5.544

Step 6: Calculation of the ground plane dimensions (X_g, Y_g)
The transmission line model is applicable to infinite ground planes only. However, for practical considerations, it is essential to have a finite ground plane. It has been shown that similar results for finite and infinite ground plane can be obtained if the size of the ground plane is greater than the patch dimensions by approximately six times the substrate thickness all around the periphery.

Table 2, Feeding Point Location Effects

Feeding Point $X_1(mm)$	Air Thick. (mm)	Dielectric Thickness (mm)	Reflection Coefficient S_{11} (dB)	Resonance Frequency (GHz)	Max Gain (dBi)
0.5	5	0.40	-17.06	11.35	10.04
0.6	5	0.40	-18.63	11.35	10.06
0.7	5	0.40	-20.68	11.35	10.07
0.8	5	0.40	-23.19	11.35	10.09
0.9	**5**	**0.40**	**-25.52**	**11.35**	**10.09**
1.0	5	0.40	-24.76	11.35	10.08

Feeding Point $X_1(mm)$	Air Thick. (mm)	Dielectric Thickness (mm)	Reflection Coefficient S_{11} (dB)	Resonance Frequency (GHz)	Max Gain (dBi)
0.5	5	0.40	-11.71	17.50	10.37
0.6	5	0.40	-11.29	17.50	10.35
0.7	5	0.40	-10.95	17.50	10.34
0.8	5	0.40	-10.69	17.50	10.33
0.9	**5**	**0.40**	**-10.51**	**17.50**	**10.33**
1.0	5	0.40	-10.39	17.45	10.33

Step 7: Determination of feed point location (X_f, Y_f)

The feed point must be located at the point on the patch, where the input impedance is 50 ohms for the resonant frequency. Hence, a trial and error method is used to locate the feed point. For different locations of the feed point, the reflection coefficient was compared and that feed point, $X_1 = 9\ [mm]$, is selected where the reflection coefficient is second most negative.

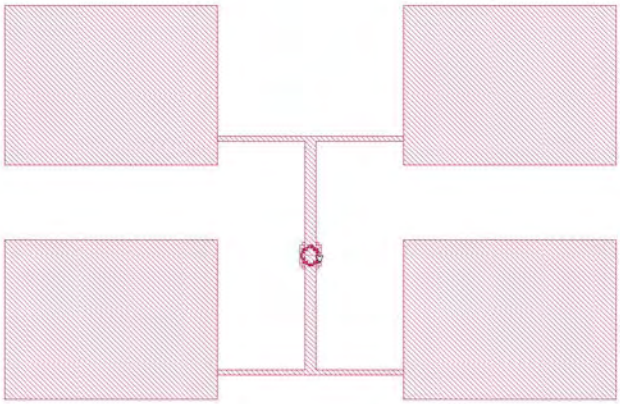

Figure 3, Patch Array Design with 0.9 mm Feeding Point

IV. Analysis Results

The antenna has modeled and analyzed using the Sonnet software program. The reflection coefficient (S_{11}) of the antenna is shown between 9 GHz and 21 GHz in Figure 2. 11.35 GHz and 17.50 GHz have minimum peak reflection coefficients as -25.52 dB and -10.51 dB, respectively. Reflections were included in dBi measurements in Figure 5 and Figure 6.

Figure 4, Reflection Coefficient of The Antenna, between 9 - 21 GHz.

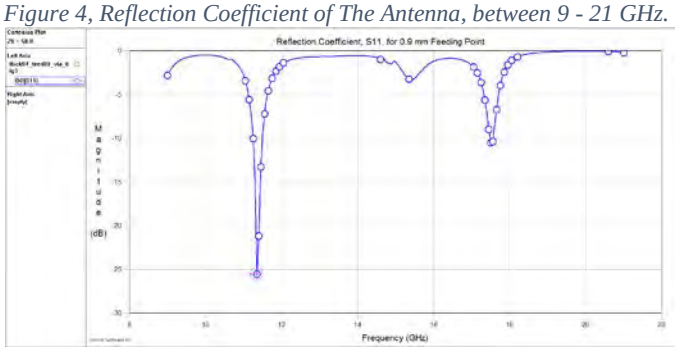

Table 4, Antenna Parameters for Different Dielectric Thicknesses for 11.40 GHz

Air Thickness (mm)	Dielectric Thickness (mm)	Reflection Coefficient S_{11} (dB)	Resonance Frequency (GHz)	Max Gain (dBi)
5	0.39	-25.03	11.40	10.11
5	**0.40**	**-25.52**	**11.35**	**10.09**
5	0.41	-34.26	11.35	10.09

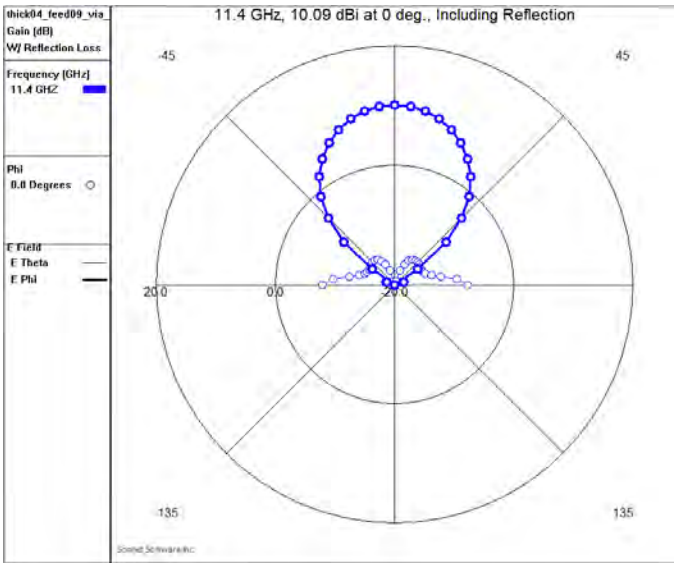

Figure 5, Isotropic Antenna Gain 10.09 dBi at 11.40 GHz, Including Reflection

Table 4 and Table 5 give information about different dielectric thicknesses vs. S_{11} and dBi values.

Table 5, Antenna Parameters for Different Dielectric Thicknesses for 11.40 GHz

Air Thickness (mm)	Dielectric Thickness (mm)	Reflection Coefficient S_{11} (dB)	Resonance Frequency (GHz)	Max Gain (dBi)
5	0.39	-10.60	17.55	10.39
5	**0.40**	**-10.50**	**17.50**	**10.33**
5	0.41	-10.70	17.50	10.24

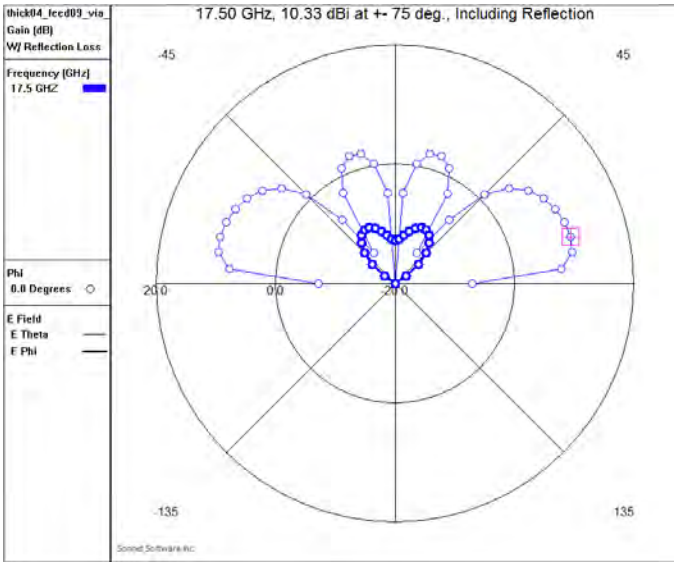

Figure 6, Isotropic Antenna Gain 10.33 dBi at 17.50 GHz and +/- 75 Degrees, Including Reflection

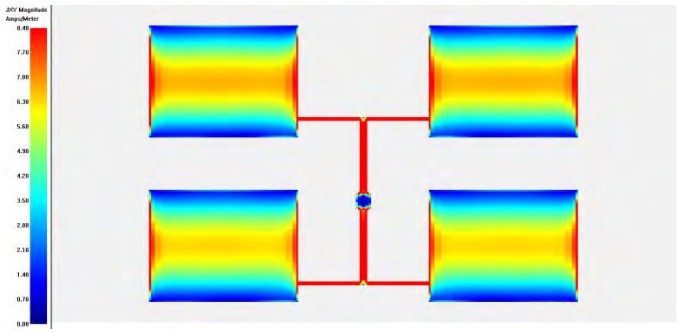

Figure 7, Current Distribution of Patch Antenna. f=11.40 GHz. Thickness = 0.4

Figure 7 and Figure 8 give information about current distributions.

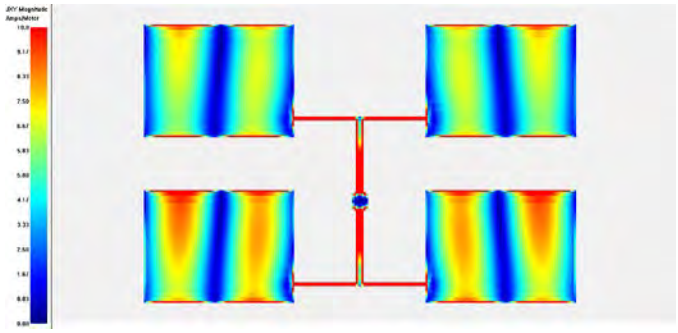

Figure 8, Current Distribution of Patch Antenna. f=17.50 GHz. Thickness = 0.4

V. CONCLUSION

In this paper, dual resonance patch antenna array has been designed by considering an FR-4 ($\varepsilon_r = 4.4$) with the substrate height of 0.4 mm. According to simulation results, designed antenna has center frequencies at 11.40 GHz and 17.50 GHz, gains of the antenna are 10.09 dBi and 10.33 dBi, respectively. Reflections were included at dBi measurements by using Sonnet Software options. At the 11.40 GHz center frequency, antenna bandwidth is % 3.05 with -10 dB reflection coefficient.

The specified antenna may be enhanced by using Genetic Algorithms. For further enhancement in the antenna gain, more elements can be combined as an 8x8 array, 16×16 array etc. Also, as future work, a comparator network can be designed.

REFERENCES

[1] Wang, H., Fang, D.-G., & Chen, X. G. (2006). *A Compact Single Layer Monopulse Microstrip Antenna Array. IEEE Transactions on Antennas and Propagation, 54(2), 503–509.* doi:10.1109/tap.2005.863103R. Garg, P. Bhartia, I. Bahl, A. Ittipiboon, Microstrip Antenna Design Handbook. 2001: Artech House.

[2] Bonefacic, D., & Jancula, J. (2006). *Laboratory Model of a Monopulse Radar Tracking System. Proceedings ELMAR 2006.*doi:10.1109/elmar.2006.329549

[3] A Printed Microstrip Antenna for RADAR Communication. IOSR Journal of Electronics and Communication Engineering (IOSR-JECE) ISSN: 2278-2834, ISBN: 2278-8735. Volume 3, Issue 5 (Sep-Oct. 2012), PP 01-04

[4] Thakur, S., Narkhede, S. S., & Bhuiya, T. (2013). *Microstrip patch antenna array for Rainfall RADAR. 2013 Fourth International Conference on Computing, Communications and Networking Technologies (ICCCNT).*doi:10.1109/icccnt.2013.6726722

[5] Ozkaya, U., & Seyfi, L. (2015). *Dimension Optimization of Microstrip Patch Antenna in X/Ku Band via Artificial Neural Network. Procedia - Social and Behavioral Sciences, 195, 2520–2526.* doi:10.1016/j.sbspro.2015.06.434.

[6] Min, C., & Free, C. E. (2009). *Dual-Ring Circularly-Polarized Microstrip Patch Array Using Hybrid Feed. IEEE Transactions on Antennas and Propagation, 57(6), 1825–1828.*doi:10.1109/tap.2009.2019984

[7] Gao, S., Li, L. W., Leong, M. S., & Yeo, T. S. (2003). *A broad-band dual-polarized microstrip patch antenna with aperture coupling. IEEE Transactions on Antennas and Propagation, 51(4), 898–900.* doi:10.1109/tap.2003.811080.

[8] Sharma, R., & Kumar, M. (2013). *Dual band microstrip antenna for C- and X band wireless applications. IMPACT-2013.* doi:10.1109/mspct.2013.6782108.

[9] *Compact and Broadband Microstrip Antennas.* Kin-Lu Wong Copyright_c 2002 John Wiley & Sons, Inc. ISBNs: 0-471-41717-3

Investigations on the Characteristic Mode Analysis Applied to Electrically Large Structures

Adem Yilmaz
Dept. of Electrical and Electronics Eng.
KTO Karatay University
Konya, Turkey
adem.yilmaz@karatay.edu.tr

Hulusi Acikgoz
Dept. of Electrical and Electronics Eng.
KTO Karatay University
Konya, Turkey
hulusi.acikgoz@karatay.edu.tr

Raj Mittra
EMC Lab.
University of Central Florida
Orlando, Florida
rajmittra@ieee.org

I. Introduction

In an ideal antenna design methodology, it is desired to achieve optimal antenna performance with very clear physical understanding, which is not easy most of the time. The Theory of Characteristic Modes (TCM), which is a modal analysis method, provides an optimization procedure in antenna design while giving the physical background clearly. The TCM was first described by Garbacz et al. [1] with scattering matrix, and reformulated by Harrington et al. in 1971 [2] with the impedance matrix of Method of Moment (MoM). Since then, it has been successfully applied to mobile handset, electrically small, and platform mounted antenna designs [3]. Characteristic modes (CM) are eigenmodes, which are numerically obtained for an arbitrary conducting object. They expands the currents and fields scattered or radiated by the conducting object. The radiation pattern of any object is a linear combination of modal patterns that are orthogonal to each other. The current distribution on the object can be decomposed into an infinite number of eigencurrents (or characteristic currents), which are also orthogonal to each other. The eigencurrents J_n can be determined from the following generalized eigenvalue equation [2]:

$$[X]J_n = \lambda_n[R]J_n \tag{1}$$

where R and X are the real and imaginary parts of the impedance matrix of the electric field integral equation (EFIE). λ_n is the nth eigenvalue associated with the nth eigencurrent J_n.

The TCM is a source-free analysis in which parameters of the characteristic eigenvalues, modal significance, and characteristic angle are considered. In general, an eigenvalue parameter provides a significant amount of information into the resonant and scattering properties of an object. If an eigenvalue has negative values the structure is said to be in capacitive mode, where the structure will store more electric than magnetic energy. At the point of resonance, a CM stores equal amounts of energy, and the object is a perfect radiator. If an eigenvalue has positive values the structure is said to be in inductive mode, where the structure will store more magnetic than electric energy. Furthermore, the smaller the magnitude of the eigenvalue is the more efficiently the mode radiates. An alternative parameter to measure the potential radiation contribution of each characteristic mode is the parameter of modal significance (MS), which represents the normalized magnitude of the eigenvalues of the characteristic modes. A mode is considered resonant when the MS of that mode attains a value of 1, and a mode is considered significant when the MS is greater than or equal to 0.707. The closer the value of MS is to 1 (the maximum value), the more effectively the associated mode contributes to radiation. Yet another parameter to evaluate characteristic modes is the characteristic angle. Characteristic angles are defined as:

$$\alpha = 180^0 - \arctan(\lambda_n) \tag{2}$$

Modes with characteristic angles close to 180^0 are effective radiators, while those with characteristic angles close to 90^0 or 270^0 are ineffective radiators. The characteristic angle gives the phase difference between an eigencurrent (λ_n) and the associated eigenfield (E_n). Characteristic angles also provide information on the phases of characteristic modes.

The present study aims to present the limitations of the TCM analysis and an alternative based on the use of the Characteristic Basis Function Method (CBFM) which was recently developped to reduce the computational cost while designing electrically large structures.

II. Numerical Study

As an example, the TCM is applied to a strip dipole. The first three dominant characteristic modes are considered here.

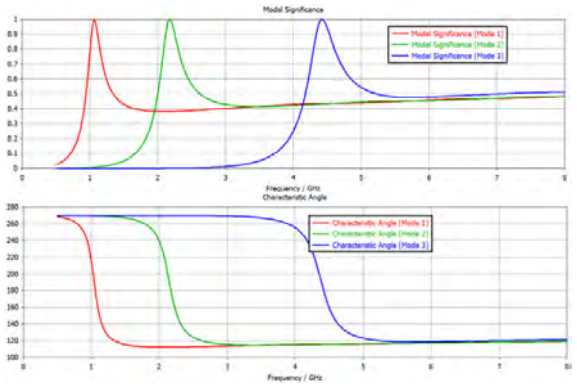

Fig. 1. Modal Significance of the strip dipole.

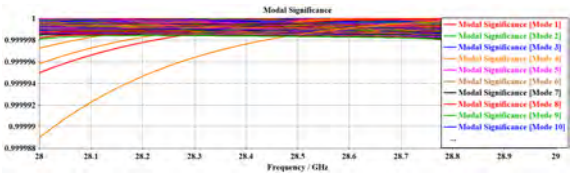

Fig. 2. Modal Significance of a PEC chassis.

It can be seen from Fig. 1 that the first mode has a MS of 1 at around 1.1 GHz. It can be deduced that the structure can radiate effectively at 1.1 GHz if it is properly excited. In addition, the first mode has a characteristic angle of $180°$ at 1.1 GHz. Once the characteristic values are calculated, the excitation scheme should be considered in order to excite the modes properly. In 1979, it is proposed that the structure should be excited at the location of its maximum current [4]. One should excite the strip dipole since it has its maximum current location in the middle of structure. In this basic example, the half-wavelength dipole behavoir is verified with the TCM. Beside all the advantages brought by the TCM in designing antennas, as pointed out by R. Mittra [5], there still exists major issues when it comes to deal with electrically large structures such as ships, airplanes and mobile phones at high frequencies. Such structures may exhibit hundreds of dominant modes, which leads to excessive time of calculations. Furthermore, usually only a small area is allowable for placing the antenna. Therefore, using maximum current location is not a practical approach for locating the excitation. In this manner, a perfect electric conductor (PEC), which has a dimension of 120×60 mm and mostly used as a chassis of a handset mobile phone, is chosen to apply the TCM at relatively higher frequencies (28 - 29 GHz). The first 100 modes are defined to be calculated. It can be seen from Fig. 2 that all 100 modes are dominant modes (MS $>$ 0.707) at operating frequencies. It is not clear how to handle the results with the TCM, and in general questions arose when studying such large structures. Those questions are for instance: In case of multitude significant modes, how to excite all of them at once? If only some of them should be excited, which one to choose? If multiple exciters are to be used, is there sufficient allocated room? These are questions that for TCM does not provide any good answers.

An alternative approach for the numerical analysis of large is to use Characteristic Basis Function Method (CBFM), which was proposed by R. Mittra [6] and succesfully developed since then [7]- [10]. The CBFM uses a set of high level basis functions called as characteristic basis function. In this method, the structure is divided into several subdomains (patches) in order to reduce the size of MoM-associated matrix. A low level basis functions, such as RWG (Rao-Wilton-Glisson) basis functions, can be applied to each subdomain. Since, the CBFM is a non-iterative method, it does not suffer from convergence problem. In addition, the CBFM calculates the self interaction (primary basis) of a patch within itself and and the mutual coupling with other subdomains (secondary basis).

III. Conclusion

In this short abstract, the TCM analysis and its shortcomings are presented briefly. Due to the larger number of dominant modes existing when dealing with electrically large structures, the TCM analysis fails to provide solutions on antenna design problems. Instead, the CBFM that consider the excitation right from the beginning of the analysis is a convenient way of solving electrically large structures. The work is ongoing for applying the CBFM to practical structures such as mobile phone chassis working at 5G frequency bands.

References

[1] Garbacz, R., Turpin, R. (1971). A generalized expansion for radiated and scattered fields. IEEE Transactions on Antennas and Propagation, 19(3), 348-358.

[2] Harrington, R., Mautz, J. (1971). Theory of characteristic modes for conducting bodies. IEEE Transactions on Antennas and Propagation, 19(5), 622-628.

[3] Chen, Y., Wang, C. F. (2015). Characteristic modes: Theory and applications in antenna engineering. John Wiley & Sons.

[4] Newman, E. (1979). Small antenna location synthesis using characteristic modes. IEEE Transactions on Antennas and Propagation, 27(4), 530-531.

[5] Mittra, R (ed.). (2018). Developments in Antenna Analysis and Design: Volume 1, Chapters 1-2.

[6] Prakash, V.V.S., Mittra, R. (2002). Characteristic Basis Function Method: A new technique for efficient solution of method of moments matrix equations. Microwave and Optical Technology Letters, 36(2), 95-100.

[7] Lucente, E., Monorchio, A., Mittra, R. (2008). An iteration-free MoM approach based on excitation independent characteristic basis functions for solving large multiscale electromagnetic scattering problems. IEEE Transactions on Antennas and Propagation, 56(4), 999-1007.

[8] Yagbasan, A., Tunc, C.A., Erturk, V.B., Altintas, A. and Mittra, R., (2010). Characteristic basis function method for solving electromagnetic scattering problems over rough terrain profiles. IEEE Transactions on Antennas and Propagation, 58(5), pp.1579-1589.

[9] Maaskant, R., Mittra, R., Tijhuis, A. (2008). Fast analysis of large antenna arrays using the characteristic basis function method and the adaptive cross approximation algorithm. IEEE Transactions on Antennas and Propagation, 56(11), 3440-3451.

[10] Li, C., Mittra, R. (2019). Characteristic Basis Function Method for Fast Analysis of 3-D Scattering From Objects Buried Under Rough Surfaces. IEEE Transactions on Geoscience and Remote Sensing.

A DEEP LEARNING BASED MICROWAVE TECHNIQUE FOR BREAST TUMOR DETECTION

Dervise Nur Gokalp
Dept. of Electrical and Electronics Eng.
KTO Karatay University
Konya, Turkey
dervise.nur.gokalp@ogrenci.karatay.edu.tr

Zeynep Gulbeyaz Demirdag
Dept. of Electrical and Electronics Eng.
KTO Karatay University
Konya, Turkey
zeynep.gulbeyaz.demirdag@ogrenci.karatay.edu.tr

H.Oktay Altun
Dept. of Electrical and Electronics Eng.
KTO Karatay University
Konya, Turkey
oktay.altun@karatay.edu.tr

Hulusi Acikgoz
Dept. of Electrical and Electronics Eng.
KTO Karatay University
Konya, Turkey
hulusi.acikgoz@karatay.edu.tr

I. ABSRACT

In this study, we use a microwave characterization technique combined with deep learning algorithm for detection of breast tumors. We first develop a 2D biological tissue model in a simulation environment with appropriate physical parameters. We assume a non-invasive technique based on the use of coaxial applicator for sending and receiving the electromagnetic signal. Then, we record the synthetic reflected signal from cancerogenous and non-cancerogenous tissues for different sizes and locations of the tumor to form the signal database in order to train various deep learning architectures for classification. We show the effectiveness of the proposed method by reporting its classification performance.

II. INTRODUCTION

Globally, breast cancer is the most common type of cancer among women. Each year, 1.1 million women are diagnosed with cancer, $\%23$ of them are breast cancer. Every year more than 411,000 women die from breast cancer, corresponding to $\%1.6$ of all deceased women [1]. Cancer is treateble when detected in early stage. People have better survivability rates when cancer detected earlier. Therefore since the 1960s, regular screening is thought to reduce the fatal effect on breast cancer. X-ray mammography is the primary method used for the detection and imaging of breast cancer. However, breast compression during imaging and low-power ionized X-rays are the major disadvantages of mammography. Although magnetic resonance imaging and ultrasound imaging are relatively better than mammography, they are not sufficient for small size tumor detection. An important consequence of these studies is that early detection of breast cancer significantly improves treatment outcomes and reduces the rate of death that justifies regular screening [2], [3].

III. DILECTRIC PROPERTIES OF BREAST TISSUE

The permittivity and conductivity values of the breast tissue are very important for cancer detection using microwaves. Permittivity (ϵ) and conductivity (σ) values differ as frequency values change. For example, the electrical properties of the breast and tumor tissues have different values at different frequencies [4]. At the same time, cancer tumors show different conductivity and permeability compared to their environment. This allows tumors to be distinguished from healthy tissues. Permittivity and conductivity values used in this project are given in table 1 [5] [6].

Table 1: Electrical properties of biological tissues [5]

Electrical Properties			
Tissue Type	Permittivity (ϵ)	Conductivity (σ)(S/m)	Permeability (μ)
Breast Tissue	9.8-46	3.7-34 (S/m)	1
Malignant Tissue	66.7-55.4	1.6-9.2 (S/m)	1

IV. DESIGN

The simulation was performed in COMSOL Multiphysics. As the model was symmetrical, the design was made as 2D axisymmetric. A 2D model of the breast tissue with tumor and the coaxial probe is shown in Figure 1. The designed coaxial cable operates at a frequency of 2.45 GHz.

It is very important to keep the S_{11} parameter under -10 dB. Coaxial cable is used as a non-destructive detection [7]. Firstly, the biological tissue parameters that are the permittivity and the conductivity modeled were entered. Tumors were added to the breast tissue to evaluate the results at different distances to the coaxial cable. The resulting S_{11} parameter was compared.

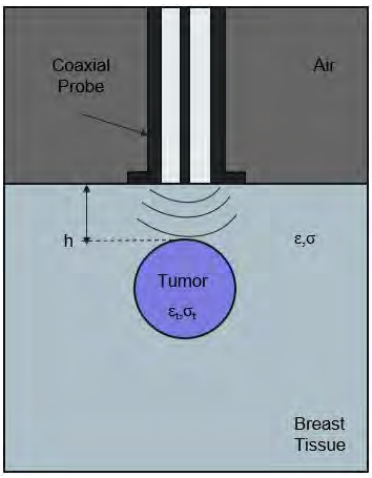

Fig. 1. Simulation design

V. Results

In this study, simulations were performed for 2 different coaxial cables. These cables are labeled as S15 and M25 [8]. The dimensions of the cables are given in Table 2. Simulations were performed for the same tissues for these two different coaxials selected [8].

Table 2: Diameters of coaxial cables [8]

Cable Properties			
Cable Type	Center Conduc. Diam. (mm)	Insulator Outer Diam. (mm)	Outer Coax. Diam. (mm)
S15	3	10	18
M25	5	15	21

The return loss (parameter S_{11}) obtained for the coaxial named M25 and S15 are as shown in the Figure.2 and Figure.3. The cancer tissue was modeled at different distances and simulation was performed for each distance.

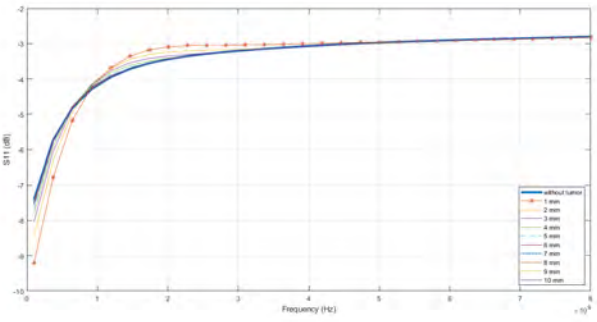

Fig. 2. M25 cable results

Figure 4 shows the change in the phase of the S_{11} parameter depending on the distance of the tumor. In the simulation, 1 W and 5 W values were used as input power and the differences were examined.

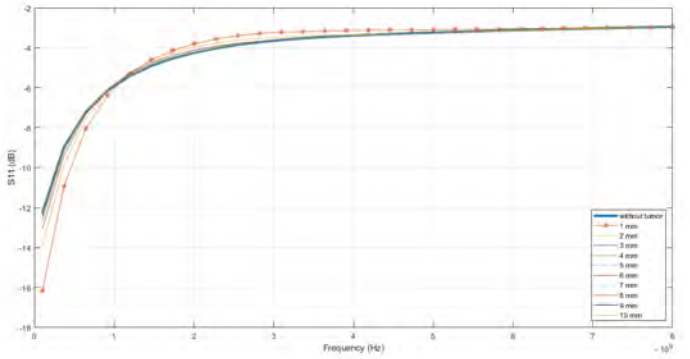

Fig. 3. S15 cable results

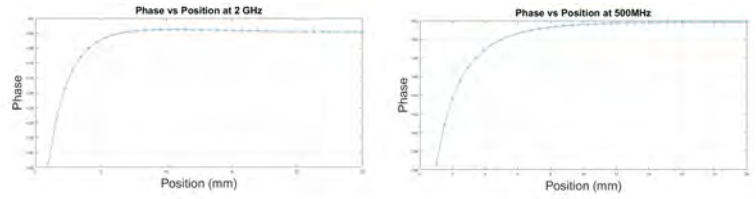

Fig. 4. Phase vs. position at 2 GHz and 500 MHz frequency

VI. Conclusion

Preliminary results suggest that it is possible to easily detect malignant tumors, especially the ones closer to the surface. It looks possible to locate the tumors by observing the phase of S_{11} reflection parameter. Low frequency microwave performs better against dielectric losses. In the future, time domain feature of the system will be examined and deep learning technique will be performed to estimate the shape and the location of the tumor.

References

[1] P. Boyle and B. Levin, "World cancer report," 2008.
[2] L. Tabar and P. B. Dean, "A new era in the diagnosis and treatment of breast cancer," 2010.
[3] L. Tabar, A. A. Gad, L. H. Holmberg, U. Ljungquist, and F. Pettersson, "Reduction in mortality from breast cancer after mass screening with mammography: Randomised trial from the breast cancer screeningworking group of the swedish national board of health and welfare," pp. 829–832, April 1985.
[4] Y. Cheng and M. Fu, "Dielectric properties for noninvasive detection of normal, benign, and malignant breast tissues using microwave theories," pp. 459–465, 2018.
[5] M. O'Halloran, M. Glavin, D. Byrne, and R. Conceicao, "Fdtd modeling of the breast: A review."
[6] M. Lazebnik, C. B. Watkins, S. C. Hagness, J. H. Booske, D. Popovic, L. McCartney, M. Okoniewski, M. J. Lindstrom, T. M. Breslin, J. Harter, S. Sewall, W. Temple, D. Mew, A. Magliocco, and T. Ogilvie, "The dielectric properties of normal and malignant breast tissue at microwave frequencies: analysis, conclusions, and implications from the wisconsin/calgary study," pp. 2172–2175, 2007.
[7] A. Jusoh, Z. Abbas, M. A. A. Rahman, and C. E. Meng, "Critical study of open-ended coaxial sensor by finite element method (fem)," pp. 343–360, 2013.
[8] P. M. Meaney, A. P. Gregory, J. Seppl, and T. Lahtinen, "Open-ended coaxial dielectric probe effective penetration depth determination," pp. 915–923, 2016.